Helical Piles as Complementary Foundation for Offshore Temporary Structures

A study into the effects of incorporating helical piles into monopile installation templates

P.H.N. Meijer

Delft University of Technology

TU Delft

Cover: Heerema Marine Contractors

Helical Piles as Complementary Foundation for Offshore Temporary Structures

A study into the effects of incorporating helical piles into monopile installation templates

by

P.H.N. Meijer

to obtain the degree of Master of Science
at the Delft University of Technology,
to be defended publicly on Tuesday September 26, 2023 at 15:00.

Student number:	4609190	
Project duration:	December 5, 2022 – September 26, 2023	
Thesis committee:	Dr. ir. P. van der Male,	TU Delft, chair of committee
	Ir. A.C.M. van der Stap,	TU Delft, committee member
	Ir. J.S. Hoving,	TU Delft, committee member
	Mr. P. Hagenaar,	Heerema Marine Contractors, company supervisor

TU Delft

MARINE CONTRACTORS

Preface

Before you lies the master thesis ”Helical Piles as Complementary Foundation for Offshore Temporary Structures”. This work has been undertaken to fulfil the requirements for graduation from the Offshore and Dredging Engineering programme at the Technical University of Delft. The thesis is written for readers with a basic understanding of offshore engineering. I was engaged in researching and writing this thesis from December 2022 to September 2023. Initiated by a literature review, the current study was set into motion.

I would like to thank my supervisor Pim Hagenaar from Heerema Marine Contractors for the guidance and support during the process. You have always challenged me and provided useful feedback. This has increased the learning opportunities, for which I am grateful. Furthermore, I would like to thank everyone from Heerema Marine Contractors who was involved, who made it possible for me to work in a pleasant work environment and provided me with any guidance I needed. I also want to thank Pim van der Male, my supervisor from the Technical University of Delft, for his guidance. Your feedback helped me to stay critical towards information and results. Additionally, I would like to thank my friend and colleague Isa van Tuyll for her support and encouragement during my graduation, which kept me motivated.

Finally, I want to thank my family and friends for being there for me throughout my complete study career, but particularly during my graduation process.

Philip Meijer
Amsterdam, September 2023

Summary

This study examines the effect of integrating helical piles to the foundation mechanism of monopile installation templates. A monopile installation template is a gravity-based structure, which is placed on the seabed. An illustration of the installation process of an offshore wind turbine utilising a template is depicted in the figure below. The installation template is utilised for the installation of monopiles, and to ensure its verticality during this installation. At this time, challenges arise due to the growing dimensions and mass of installation templates, which are essential for the safe and precise installation of expanding monopiles. The growth of the monopiles is driven by the increased demand for green energy. Challenges arise because the installation templates are often restricted in size and mass by the capabilities of the installation vessel.

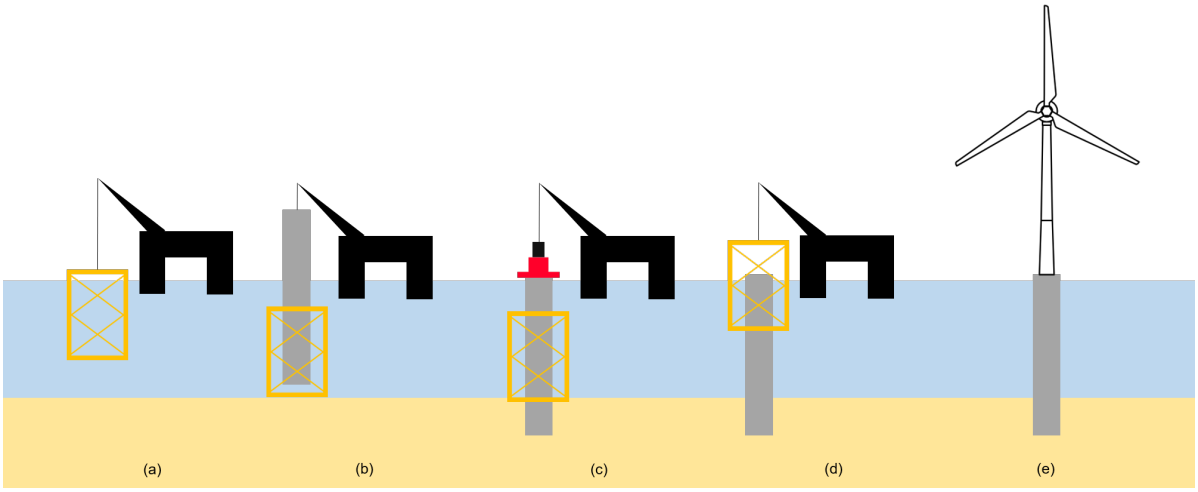

Monopile installation using a template: (a) template installation, (b) inserting monopile, (c) monopile driving, (d) template removal, (e) wind turbine installed

The installation templates generally use mud-mats as foundation system to ensure stability and prevent the template from excessive settling. The mud-mats cause significant dynamic effects, especially when taken through the water line. Moreover, the sliding capacity of mud-mats is often insufficient, leading to potential sliding failure of the template. Use is made of so called skirts, which penetrate the soil to enhance the sliding capacity. However, the skirts are often over-designed as the soil characteristics are difficult to predict. Additionally, challenges occur with the installation of the skirts, as the penetration generally varies per location within the template footprint and wind farm. Furthermore, use is made of clump weights if the mass of the template is restricted by the vessel. The weight is added to enhance the stability of the template. The clump weights are mounted on the template after it has landed on the seabed.

A literature review is conducted using different sources, such as reviews, offshore guidelines, research papers, and expert interviews, to investigate installation templates and different foundation mechanisms. The investigated foundation mechanisms are suction buckets, mud-mats, and (helical) piles. The complementary foundation mechanism must be integrated into the template design, to minimise additional installation and decommissioning time of the template. The literature review demonstrates that helical piles show greatest potential of being added to the mud-mat foundation. Therefore, solely helical piles are considered in the current study, and the following research question is answered:

How, and to what extent, does adding helical piles affect the footprint of the monopile installation template designed for the benchmark project?

The current study uses a project carried out by Heerema Marine Contractors as benchmark. All parameters of this project are used as input for the study. Findings of analytical analyses on the (environmental) loading and mud-mat capacity are validated with the benchmark project results. Subsequently, the helical pile geometry is optimised for maximum uplift capacity, using the methodology shown in the figure below. The capacity is optimised for uplift capacity, as it is assumed that the mud-mats can bear the compressive loading. Additionally, the lateral capacity would significantly increase by utilising piles, and therefore optimising for lateral capacity is not recommended. The obtained geometry, optimised for maximum uplift capacity, is then assumed to be constant and used to determine the uplift, compressive, and lateral capacity. The analysis shows a positive correlation between embedment depth and capacity (uplift, compressive, and lateral). The helical pile capacity is added to the mud-mat capacity. Consequently, effects on design variations are examined, such as reduction in template's mass and size, mud-mat size, and variations in helical pile geometry and soil parameters.

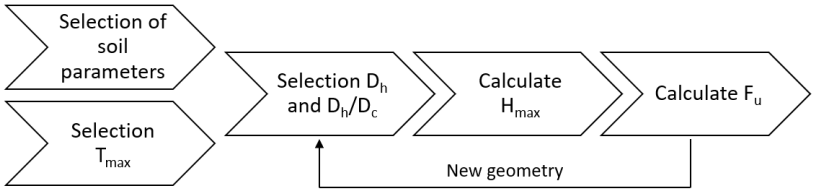

Visualisation of methodology for determination of uplift capacity helical pile

The analysis shows a significant improvement in capacity of the foundation, in both compressive and lateral capacity. The uplift capacity of the helical piles ensure no uplift of mud-mats occurs. This leads to a more evenly load distribution among the mud-mats, lowering the maximum factored load on the legs. Consequently, the mud-mat size and the template's mass and dimensions could be reduced. It can be concluded that a reduction in mud-mat size directly results in the potential of reducing the template dimensions. The reduction in both template and mud-mat size would automatically lead to a decrease in mass. However, the reduction in template mass could lead to a decrease in structural performance. This should be investigated in further studies. Variations in soil characteristics show that the performance is even more enhanced in denser sands.

Concluding, the helical piles have a positive influence on the template's overall capacity. The findings show that a reduction in the footprint of the template is possible, of maximum 13.6%. The mud-mat size must be reduced in order to achieve this, which is possible due to the additional capacity of helical piles. However, the behaviour of combined foundation, the mud-mats and helical piles, is unknown and therefore requires attention. Moreover, further analyses must show if the helical piles can be installed, as the installation requirements are significant.

Contents

Nomenclature

Abbreviations

Abbreviation	Definition
ALS	Accidental Limit State
API	American Petroleum Institute
ASM	Allowable Stress Method
CFD	Computational Fluid Dynamics
CPT	Cone Penetration Test
DNV	Det Norske Veritas
FEM	Finite Element Method
FLS	Fatigue Limit State
FPUT	Flanged Pile Upending Tool
GHP	Grouped Helical Piles
HES	Heerema Engineering Solutions
HFG	Heerema Fabrication Group
HMC	Heerema Marine Contractors
ISO	International Organization for Standardization
KC	Keulegan-Carpenter
LNG	Liquefied Natural Gas
LRFD	Load and Resistance Factor Design
MSL	Mean Sea Level
NTEW	Not-To-Exceeded-Weight
PFM	Partial Factor Method
SLS	Serviceability Limit State
SSCV	Semi-submersible Crane Vessel
STF	Storm Factor
SWP	Self Weight Penetration
ULS	Ulitmate Limit State
WSD	Working Stress Design

Symbols

Symbol	Definition	Unit
A	Reference area	m^2
A'	Effective area	m^2
a	Stress drop index	-
B	Width	m
C_d	Coefficient of drag	-
D	Diameter	m
D_c	Shaft diameter	m
$D_{eq,i}$	Equivalent diameter of tubular i	m
D_h	Helix diameter	m
D_i	Inner diameter	m
D_o	Outer diameter	m
D_r	Soil density	%
E	Young's modulus	Pa

Symbol	Definition	Unit
e	Eccentricity	m
F_b	Force of base	N
F_c	Current force	N
F_c	Force of shaft	N
F_{MM}	Force on mud-mat	N
F_{waves}	Wave force	N
F_{wind}	Wind force	N
F_g	Gravitational force of mass	N
F_h	Force of helix	N
F_l	Force on lower guide	N
F_s	Uplift factors	N
F_u	Force on upper guide	N
$F_{y,c}$	Crowd force	N
g	Gravitational acceleration	m/s^2
h_i	Vertical distance to section from seabed	m
H	Embedment depth	m
H	Wave height	m
H_{eff}	Effective shaft length	m
H_{max}	Maximum wave height	m
H_s	Significant wave height	m
I	(Area) Moment of inertia	m^4
K	Euler buckling condition	-
K_0	Initial coefficient of lateral earth pressure	-
L	Length	m
$M_{current}$	Current moment	Nm
M_{MP}	Moment due to inclined monopile	N
M_T	Moment due to tools	N
M_{wave}	Wave moment	Nm
M_{wind}	Wind moment	Nm
N_q	Bearing capacity factor	-
P_s	Perimeter of the pile shaft	m^2
Q_c	Compressive capacity	N
Q_u	Uplift capacity	N
Q_v	Bearing capacity	N
q	Distributed load	N/m
q_v	Unit bearing capacity	N
T	Torque	Nm
T_b	Torque of base	Nm
T_c	Torque of shaft	Nm
T_h	Torque of helix	Nm
T_p	Peak period	s
T_z	Zero-crossing period	s
$U_{surface}$	Current speed at the water surface	m/s
U_{wind}	Wind speed	m/s
z	Height above MSL	m
z_0	Surface roughness length	m
z_r	Reference height	m
α	Alpha factor for weather forecasting inaccuracies	-
β	Crane off-lead angle or monopile inclination angle	degrees
φ	Friction angle	degrees
φ_f	Filter layer friction angle	degrees
φ_p	Peak friction angle	degrees
δ	Interface friction angle	degrees
γ'	Effective unit soil weight	N/m^3

Symbol	Definition	Unit
ψ_p	Peak dilatancy angle	degrees
λ	Wave length	m
θ	Angle	degrees
σ_y	Normal stress	Pa
$\sigma_{eq,c}$	Von Mises stress of shaft	Pa
$\sigma_{eq,w}$	Von Mises stress of weld	Pa
σ_x	Stress of helix	Pa
τ	Shear stress	Pa
ρ_{air}	Density of air	kg/m^3
ρ_{water}	Density of water	kg/m^3

List of Figures

List of Tables

1 Introduction

1.1. Current practice offshore wind

The increasing global demand for green energy sources leads to an increase in demand for offshore wind turbines, resulting in both a growth in their number and size, as well as a trend towards exploring deeper waters for their installation. Consequently, the industry is dedicating significant efforts to develop and implement efficient installation methods of wind turbines. One of the big players on the market is Heerema Marine Contractors (HMC). HMC delivers innovative and sustainable solutions for the transportation, installation, and removal of offshore structures. More information about HMC is presented in Appendix A.

The installation stage of offshore wind turbines involves installation of the foundation, tower, nacelle, blades, and cables. Installation can be challenging, especially installation of the foundation, as it is a complex and critical stage which has unique requirements for each offshore wind farm and even for each wind turbine within such a farm [34, 40]. One popular foundation technique for offshore wind turbines is the monopile foundation, which involves driving, or occasionally drilling, a single large steel pile into the seabed to support the turbine. However, there are also alternative foundation methods that have been developed in recent years, such as tripods and jackets. These alternative methods are typically more expensive and only used when inevitable, for example for deeper water depths or specific soil types [34]. A recent study revealed that in Europe up to the year 2020, more than 80% of all installed wind turbines, including floating wind turbines, utilised monopiles as foundation technique [23].

The size of monopiles increases proportionally with the increasing size of wind turbines, which causes several challenges. For example, the structural engineering design challenges could lead to under-conservative designs with the potential for catastrophic consequences or, more commonly, costly over-conservative engineering approaches [53]. Additionally, the installation of these substantial monopiles presents another significant challenge. The verticality of the monopile is of critical importance as any deviation from vertical could jeopardise the stability and safety of the foundation. The monopiles should be installed within allowable tolerances, which typically is 0.5° (to the vertical). Specialised installation equipment is employed to achieve this precise installation using floating installation vessels. Currently, two types of monopile installation equipment are utilised: a monopile installation template and a gripper frame.

1.1.1. Monopile installation template

A monopile installation template is a subsea structure that is positioned on the seabed, specifically designed to ensure precise installation of monopiles. An illustration of the installation process is depicted in Figure 1.1. These templates are gravity-based structures and often utilise mud-mats to provide both horizontal and vertical support, while preventing the structure from excessive settling. However, challenges arise due to the increased size of monopiles and thus increased dimensions of templates. Larger monopiles and templates endure larger environmental loading which affects stability of the template, and thus potentially jeopardise the precise installation of the monopile. The template is restricted in size and weight by the available deck space and crane capabilities of the installation vessels. Ad-

ditionally, the considerable size of the templates result in large (dynamic) loads during lowering of the structure though the water level. These challenges lead to increased cost and CO2-emissions [6, 27, 49, 52].

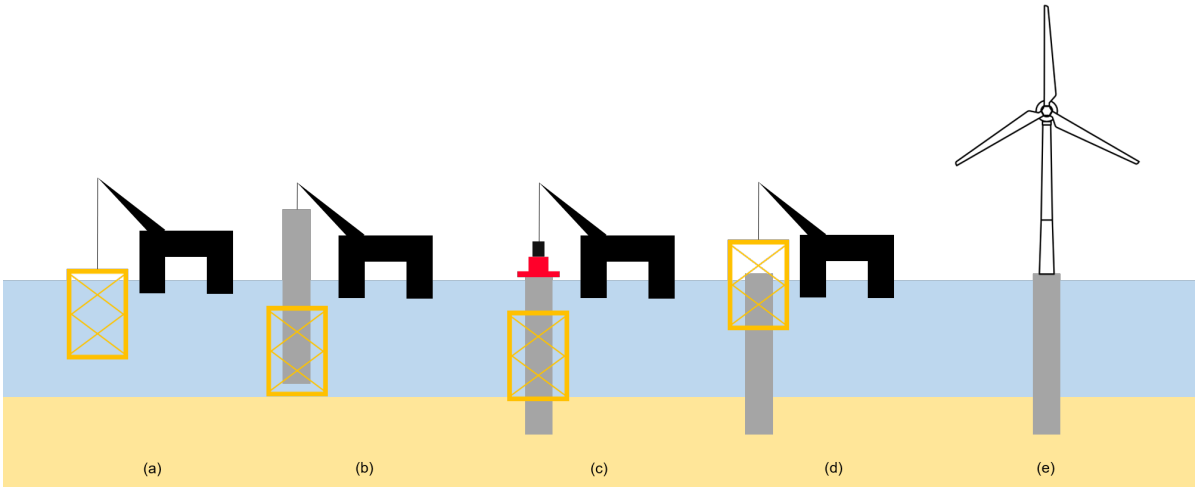

Figure 1.1: Monopile installation using a template: (a) template installation, (b) inserting monopile, (c) monopile driving, (d) template removal, (e) wind turbine installed

1.1.2. Gripper frame

An alternative installation method utilises a motion-compensated gripper frame, which is a hydraulic device that is designed to facilitate the installation of monopile foundations using floating vessels, see an example in Figure 1.2. The device is equipped with hydraulic cylinders and a gripping mechanism that enables it to securely hold the monopile. It is mounted on the floating vessel and utilises a motion-compensation system to offset the effects of wave and vessel motion, to ensure the monopile is installed within allowable tolerances. The device is used to lower and drive the monopile into the seabed while maintaining a stable and vertical position. Especially in Europe, the adoption of gripper frames instead of monopile installation templates is prevalent due to the excessive size of the current monopiles and thus the size of monopile templates [40]. On the one hand, the shift towards gripper frames could offer several benefits such as minimal installation time, easier handling, and the ability to use the mass moment of inertia of the installation vessel, as the gripper frame is positioned above sea level [49]. However, on the other hand, a gripper frame is an expensive tool and still an emerging technology in the offshore wind sector. A gripper frame can cost up to five times the amount of a monopile installation template [25, 27]. Furthermore, the maintenance of a template is simple as it contains little tools and technology. A gripper frame is significantly more complex and utilises state-of-the-art technology, consequently leading to higher maintenance costs [25].

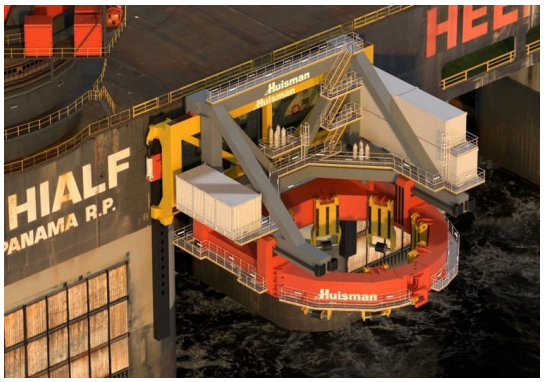

Figure 1.2: An example of a gripper frame mechanism, mounted on a vessel of HMC

1.2. Problem statement

One of the main challenges is the handling of monopile installation templates due to the growing dimensions and mass of these structures. The dimensions and mass of the template are now limited by the installation vessel its capabilities. The dimensions are limited by the available deck space and the mass is limited by the crane capabilities. As a result, ensuring stability of the template becomes more complicated which potentially compromises the precise installation of growing monopiles. Alternatives are not widely available, and currently the primary competitor is the gripper frame. This gripper frame is still an emerging technology and significantly more costly than installation templates. Therefore, expanding the application of the monopile installation templates could be promising. One potential concept could be to increase the capacity of the template's foundation. The addition of an integrated helical pile system to the existing (mud-mat) foundation is investigated. Each mud-mat would contain a helical pile, stabbed through the centre of the mud-mat. This could potentially lead to a redesign of the structure, resulting in reduction of the template dimensions and mass. The current study investigates this concept, and uses the following research question:

How, and to what extent, does adding helical piles affect the footprint of the monopile installation template designed for the benchmark project?

1.2.1. Approach

In this study, initially a comprehensive literature review was conducted to enhance understanding of various aspects related to monopiles, installation templates, and foundation methods such as mud-mats, suction buckets, and (helical) piles [40]. The review investigated which foundation mechanism had greatest potential to be added to the mud-mats. It showed that helical piles are the most promising, and therefore solely helical piles are investigated in the current study. It is assumed that the additional foundation mechanism is integrated into the design. This leads to minimal additional installation and decommissioning time of the installation template. In Figure 1.3 an illustration of a template including a helical pile foundation mechanism is shown.

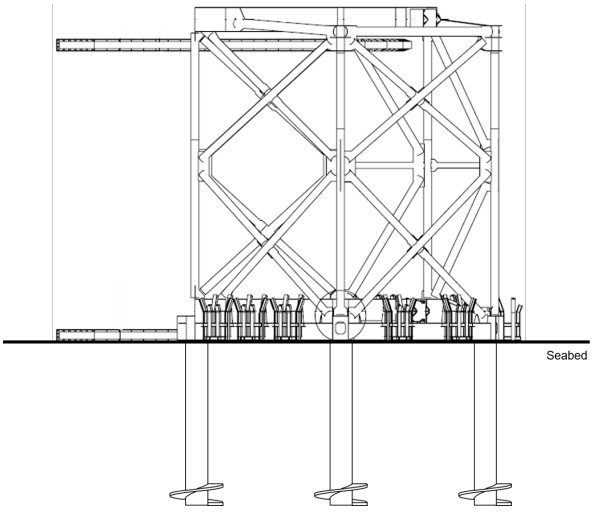

Figure 1.3: Template with helical piles incorporated in its design (not to scale)

Subsequently, a project is selected as benchmark, and an in-depth investigation is conducted into the design and calculations on a monopile installation template designed for this project (designed by HMC). The dimensions of the to be installed monopiles are substantial, the larger piles have a diameter of 8.9 meters. Moreover, the designed monopile template is restricted on its size and mass by the capabilities of the installation vessel. All parameters of this project are used as input, such as water depth, soil conditions, scour protection, environmental conditions, and the template design. Calculations are performed on, among others, the environmental loading and capacity of the mud-mats. The findings are validated against the results acquired by HMC, to ensure the correct analyses are performed. HMC assessed the environmental loading using software applications, whereas the

calculations are performed analytically in this study. As the benchmark project is situated in sandy soils, the current study focuses on sand soils only.

Stability of the template relies on the moment induced by the environmental loading being less than the righting moment exerted by the template's (submerged) mass. The restricted dimensions and mass of the template jeopardise its stability. Occasionally, use is made of clump weights to add mass to the template, which are mounted on the structure after landing on the seabed [27]. Figure 1.4 shows a simplification of the arrangement of the loads applied to and within the template. This load arrangement is utilised to determine the loading on the legs, and thus mud-mats, which is required for capacity calculations.

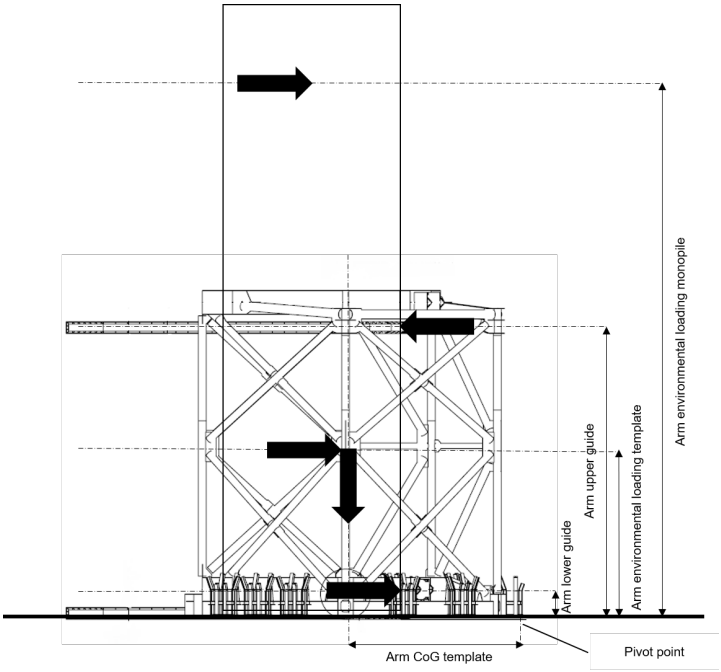

Figure 1.4: Illustration of stability analysis on the template

Next, to investigate the potential of adding helical piles to the existing mud-mat foundation, the uplift capacity of helical piles is determined. The method of a recent study carried out by the University of Dundee is adopted, which involved validation against offshore experiments [8]. This groundbreaking study signifies a significant milestone in the advancement of offshore helical piles, as it presents the first-ever up-scaled offshore validated experimental data. The helical pile geometry is optimised for maximum uplift capacity. The choice for maximising its uplift capacity rather than its compressive or lateral capacity is made because it is assumed that the mud-mats can be optimised for maximum compressive capacity. The lateral capacity is generally enlarged by adding skirts to the system. It is assumed that the addition of helical piles would already add sufficient lateral capacity to the system, and therefore optimisation for lateral capacity is not beneficial. The compressive and lateral capacity of the helical piles are determined using the geometry, which is optimised for maximum uplift capacity.

The integration of the helical piles into the template's design is not considered. However, the capacity of the helical piles is included in the overall capacity and design variations are performed. The helical pile geometry, mud-mat dimensions, template dimensions, and soil parameters are varied. These variations show their influence on helical pile capacity, its installation requirements, and mud-mat capacity. Finally, based on the findings obtained throughout the study, results are discussed, conclusive remarks are formulated and recommendations for future work are suggested. These suggestions aim to enhance the overall performance of monopile installation templates, and in specific the performance and application of helical piles.

1.3. Outline of the report

In Chapter 2, background information about monopile installation templates is provided. This section describes the installation procedure, the required equipment and tools within a template, and briefly describes its design process. In Chapter 3, background information about helical piles is introduced. More information about helical piles can be found in the literature review [40]. Additionally, this section provides information about the geometry and design of helical piles as well as the potential grouping effect when piles are installed close to each other.

Consequently, in Chapter 4 general soil behaviour is described, as well as utilised soil parameters. This study focuses on sandy soils and therefore solely provides information about parameters important for calculations in sand. Furthermore, different failure mechanisms of mud-mats and helical piles are described, and the soil-structure interaction is briefly explained.

The input of the benchmark project is described in Chapter 5. This section provides information about the equipment used, such as the monopile and template dimensions. Additionally, this section provides information about the environmental conditions and explains how they are determined. The considered load cases are described as well, which are used to determine the maximum loading on the template.

In Chapter 6 the foundation mechanisms are described. The derivations of both the mud-mat and helical piles are explained in detail and specifically the determination of the helical pile geometry is specified. The derivations for the bearing and sliding capacity of mud-mats is provided, based on offshore guidelines. Subsequently, the derivation of the uplift, compressive, and lateral capacity of the helical piles are described as well as installation and structural requirements.

Chapter 7 explains how the loading on the template is derived. It describes the environmental loading, such as wave loading, as well as the loading due to the inclination of the monopile. A method to determine the environmental loading on the template, called equivalent stick model, is presented in this chapter as well. Additionally, this section describes how the loading on the mud-mats is calculated. This is essential to understand the behaviour of the foundation mechanisms under such loading. This is done using an uncoupled and coupled method, where the soil-interaction is not considered in the uncoupled method and is considered in the coupled method.

The results of the benchmark project are introduced in Chapter 8. The findings of the environmental loading are presented, as well as specific loading per load case. Also, the results of the stick model are shown. The mud-mat capacity of the benchmark project is also presented, and is used later to compare results.

Then, in Chapter 9, the results of the helical pile calculations are shown. First, the optimised geometry of the helical pile is given. These findings are used subsequently to derive the uplift, compressive, and lateral capacity. Second, it is shown how these helical pile capacities influence the overall capacity of the template.

In Chapter 10, results of design variations are presented. The influence on the capacity and installation requirements of the helical pile is examined as well as the mud-mat capacity. Reduction of the template's mass and dimensions, and reduction of the mud-mat's size are evaluated. Additionally, the influence of the soil parameters is shown on both the mud-mat capacity and the helical pile capacity. Also, variations to the helical pile geometry are described.

The findings of the study are discussed in Chapter 11. This section provides a summary and interpretation of the results. Also, it shortly describes the limitations of the research. Conclusions are drawn in Chapter 12, and recommendations for further research is provided in Chapter 13. Recommendations for future work are suggested for helical piles, installation requirements and tools, the monopile installation template, and the soil.

2

Background Monopile Installation Template

This chapter provides an overview of the basic functions of a monopile installation template. It presents a brief explanation of the installation procedure, and introduces key equipment and tools that are integrated in the template's design. Subsequently, the design process of a monopile installation template is described. The design of an offshore structure generally has design targets, such as to minimise costs, maximise reliability, maximise workability, and minimise offshore handling time. Lastly, the applied limit states are presented, and differences between two methods are explained.

2.1. Functionality

A monopile installation template is a steel guide frame, that is positioned on the seabed. The structure often utilises mud-mats to provide horizontal and vertical support while preventing the structure from excessive settling. The basic functions of a monopile installation template are to support the monopile during installation and correct the monopile inclination and orientation as required, to assure the monopile is installed within the allowable tolerances. The use of templates also helps to minimise risks during the foundation installation process of offshore wind turbines [40].

2.2. Installation procedure

The installation procedure of a template involves multiple sequential steps. Initially, the rigging is attached to the template. The next step is to overboard the template, lower it through the splash zone and install it on the seabed. After the position of the template is confirmed the rigging can be retrieved. The mud-mats can be pre-loaded and the template is levelled. Visualisations of the overboarding process are shown in Figures 1.1 and 2.1.

Subsequently, a barge or heavy-transport vessel is positioned to hoist the monopile. If possible, the monopile is already on the vessel's deck. Before lifting, the sea-fastening needs to be cutted and the rigging should be connected to the monopile. The monopile is then lifted, upended, and positioned into the template. The rotator and centraliser systems subsequently ensure the correct orientation and position of the monopile. The monopile is then lowered to self-weight penetration depth. Consequently, the hammer is installed onto the monopile, which is then driven until target penetration depth. Finally, the rigging is reconnected to the template and the lifting tool is engaged for template removal. It might be necessary to lock the mud-mats, before going through the splash zone. The template may be retrieved on deck, or directly transported to the new location while suspended on the crane.

2.2.1. Duration

The procedure of installing the monopile installation template and subsequently the monopile, including the removal of the template is estimated to last at most 12 hours. A monopile installation template is therefore categorised as a temporary structure. Not all design recommendations do provide guidelines

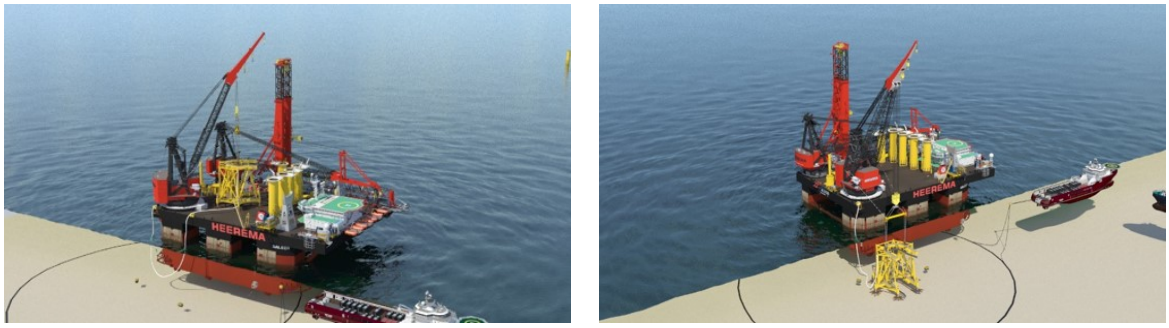

(a) Template on deck **(b)** Template on seabed

Figure 2.1: Visualisation of monopile template installation with a semi-submersible crane vessel

for temporary structures and solely provide generic safety factors for permanent offshore structures. This could potentially lead to over-designing of the template and its components.

After the template is landed on the seabed, a significant amount of time is required for the upending and lowering of the monopile. Therefore, it can be concluded that during this time, the helical piles can be installed on the template simultaneously. Contrarily, the retrieval of the helical pile foundation system may lead to additional time due to the relatively short duration required for template removal. The retrieval of the helical pile foundation system may require more time compared to the connection of the rigging and engaging the internal lifting tool for template removal. On the other hand, it might be possible to start the removal procedure of the helical piles during the driving of the final section of the monopile, as the functionality of the template at this moment is limited. This should, however, be investigated further for each project, as this depends on the vessels and equipment used.

2.3. Integrated equipment and tools

Multiple equipment and tools are incorporated into a template design, as illustrated in Figure 2.2. These mechanisms are assumed to be working properly throughout this complete study, as HMC has a significant track record of using these tools in their offshore (installation) projects, and are therefore not investigated.

Levelling system

The levelling system within a monopile installation template is typically used to ensure the correct alignment of the monopile during installation. It includes hydraulic jacks that can be adjusted to level the template and the monopile, for instance due to an inclination of the seabed. This system helps to ensure that the monopile is installed in a stable, vertical position.

Pile guide system

Generally bumpers are used to ensure quick and easy engagement of the monopile into the template, and ensure protection to the equipment, template, and the monopile itself. Furthermore, the use of rollers and guides are occasionally used to enhance the process of lowering the pile while assuring the protection of the equipment, template and monopile.

Framework

Generally tubular framework is integrated into the template design. It is designed to provide stability and support to the template. The tubular framework helps distribute the forces and loads encountered during the installation process. This framework is either designed to be stiff or soft, which depends on the design choice (see Section 2.4.2). Additionally, all the tools are connected to this framework.

Pile centraliser system

The centraliser system within a monopile installation template is used to centre the monopile within the template during installation. This system typically consists of a set of hydraulic cylinders that apply lateral pressure to the monopile to ensure that it is positioned precisely in the centre of the template. As a result, it can be ensured that the monopile is installed in a stable position within installation tolerances, which is critical for the long-term reliability of the foundation.

Pile rotation system

The template generally also includes a pile rotating system which is capable of accurately rotating the pile to the correct orientation for installation. The pile rotation system should be designed to work while the pile is still suspended from the crane of the installation vessel. The rotation system should also be able to rotate the pile within a small tolerance to allow for any rotation after driving the monopile. The correct orientation of the monopile is of essence for, among others, connection of the power cables.

Mud-mats

Mud-mats are typically used as foundation system for template structures and are designed to support the template on the seabed. Mud-mats are optimised to mobilise sufficient bearing and sliding capacity for all load cases. The offshore guidelines for foundation calculations do not include guidelines for temporary structures and this could result in conservatism in mud-mat design. Additionally, different areas within the wind farm may have various soil characteristics. To ensure the stability of the wind turbine in each location, this could lead to further conservatism [50].

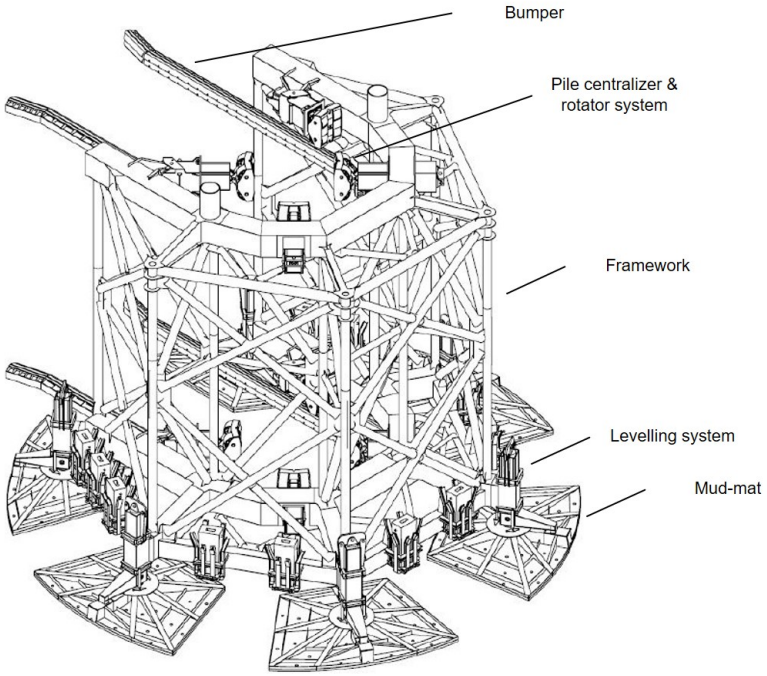

Figure 2.2: Monopile installation template components nomenclature

2.4. Design process

2.4.1. Design phases

Generally, multiple design phases are considered for offshore structures such as concept design, basic design, and detailed design. The concept design phase describes the main design parameters based on the performance requirements. The results give an indication of the feasibility of the project and provide a founded basis for the next phase. The basic design continues on the concept design phase and provides more detailed documents that can be used to get an initial price offer on the primary steel requirements, and invitation to tender. This phase is a sound basis for the detailed design. In the detailed design phase a package of documents and drawings are delivered in such an extent that the project can be realised. The benchmark project is in the basic design phase.

2.4.2. Design decisions

Design choices have a direct consequence on required hydraulic cylinder capacities, stability and required stiffness of the monopile template. For example the decision on the number of legs the template,

more legs might make the template more stable and increase its capacity, but it leads on the other hand to an increase in costs, weight and complexity.

The template can be designed either maximising or minimising the structure's stiffness. In case of a stiff template design, the template should be able to coop with first order wave loads. The natural period of the system, with the monopile present in the template, should be lower than the natural period of predominant wave period. During the hammering process, the soil provides additional stiffness, thereby shifting the natural period of the system further away from the wave periods. Consequently, if resonance occurs, it will likely occur at the initial stages of installation when the penetration depth of the monopile is minimal. Alternatively, if the template is designed to be soft, the initial natural period of the system can be significant, resulting in minimal wave loads. Resonance will not occur at the beginning of the installation process. However, as the monopile penetration depth increases, the stiffness of the system also increases, eventually reaching a point where the natural period aligns with the wave period. At this point, resonance may occur, leading to substantial motion and loading. Since most of the stiffness in this approach is derived from the soil, environmental loads are directly transferred to the seabed. Consequently, a comprehensive understanding of soil properties is required to accurately predict the behaviour of the monopile installation template under such circumstances. Generally, given the uncertainty associated with soil properties, it is common practice to design a monopile installation template using a stiff approach.

2.4.3. Global and local analyses

The structural behaviour and performance of offshore structures are typically evaluated through (numerical) analyses, which can be broadly classified into global and local analyses. Global analysis considers the overall response of the installation template, and is typically evaluated in the basic design phase. Such analyses provide a complete understanding of the system's behaviour, enabling the assessment of its overall stability, strength, and dynamic response. Conversely, local analysis of a structure concentrates on examining specific regions or individual components of the template in more detail, such as the weld connections, grouted interfaces, or local stress concentrations. Local analysis is generally considered in the detailed design phase. While local analyses can provide valuable insights into the localised behaviour of these components, they do not capture the complete system response.

2.5. Limit states and design methods

A limit state is a condition of a structure beyond which it no longer fulfils the relevant design criteria, related to load and resistance. Several important limit states can be distinguished within the offshore environment, among which the ultimate limit state (ULS), the serviceability limit state (SLS), the fatigue limit state (FLS), and the accidental limit state (ALS). The ULS corresponds to the maximum load-carrying capacity of a structure and is safety related. The SLS corresponds to the structural ability to perform daily use and is therefore operations related. The FLS corresponds to cumulative damage from repeated loading and is safety and operations related. Particular attention must be paid, when installing monopiles, to the hammering operation as the template will be exposed to a significant number of cycles. Finally, ALS corresponds to structural integrity due to an accident and is related to acceptable damage.

2.5.1. Working stress design

Working Stress Design (WSD) method is also known as the Allowable Stress Method (ASM). This is represented as the probability that the load does not exceed the resistance, using the probability density function of the load and resistance. The strength check is used in order to obtain a safety factor, which is determined by dividing the representative value of the resistance by the load.

2.5.2. Load and resistance factor design

The Load and Resistance Factor Design (LRFD) method is also known as the Partial Factor Method (PFM). This method uses partial load and resistance factors in order to compare the capacity of structural components with the determined loads and stresses. The main difference between WSD and LRFD method is that the WSD method uses a single safety factor regardless of load types, while the LRFD method uses a specific safety factor per load component. Therefore, higher safety factors can be applied to load components with greater uncertainties and vice versa.

3

Background Helical Piles

This chapter provides general information about helical piles, including information about its installation and application. Additionally, the geometry used in this research is presented. The helical piles are assumed to have a single diameter shaft and a single helix, and the pitch is taken as a constant. All other parameters are taken as variable, and can be optimised. To conclude this section, the effect of grouped helical piles is described.

3.1. General application

Helical piles, also called screw piles, are composed of one or several helices, typically made of steel, attached to a shaft. A helical pile is a type of foundation commonly used in onshore applications, for example for bridges, railroads and docks. Helical piles are currently not widely used for offshore applications, although there are ongoing studies investigating their potential for foundation use or anchoring. These studies primarily focus on the potential for permanent offshore foundations or anchoring of floating structures, while there is limited research on the potential for temporary uses, such as for the foundation of templates. For example, using helical piles for anchoring aquaculture is currently considered a cutting-edge practice [9]. The application of helical piles in nearshore aquaculture is considered advanced in terms of technology, however, the scale required for offshore wind use is greater in comparison. More information about helical piles, such as the working principle, capacity or challenges can be found in the literature review report [40].

Helical piles are installed through the application of torque and compression at the top, and have several advantages over the standardised piles in addition to their high uplift capacity, including reduced environmental impact, the ability to be easily decommissioned, and the ability to be designed for various soil conditions [40]. For most onshore applications, the installation and structural requirements can be met, these requirements however limit the available capacity for offshore applications [8]. This is mainly due to the fact that the required sizing of the helical piles offshore is significantly larger than the currently used helical piles onshore. In order to apply such torque and force, specialised equipment is required. In Appendix D, an estimation of the tool weight is presented. Due to the limited information at hand, data from onshore tools is utilised, which may result in an overestimation of the tool weight. For example, certain components of the tools, such as the engine or power pack, could potentially be situated on the vessel's deck. As a result, the weight of the installation tools would likely decrease significantly. Therefore, an estimation is performed on the tool weight in collaboration with engineers at HMC, using their experience with similar offshore tools such as drilling equipment.

The investments required for the addition of helical piles to the foundation system is rather difficult. The costs for producing the helical piles can not be governing. However, as the tools are not yet available for offshore applications, the costs of the installation tools might be significant. Especially if the tools used onshore are not able to be converted for offshore use. This would mean that a new tool needs to be designed, which has major impact on the required investments [25, 27, 52].

3.2. Geometry

The considered helical piles are composed of a one-diameter shaft and a single helix, as shown in Figure 3.1. Only circular-shaped shafts are investigated, as they offer higher resistance in loading as compared to square-shaped screw pile shafts [42]. The helical pile is defined by its shaft diameter D_c, wall thickness t_c, helix diameter D_h, plate thickness t_h, helix pitch p_h, and length H, which is assumed to be equal to the embedment depth of the helix plate. In this research, all dimensions are taken into account as variables, except for the pitch. The pitch remains constant and is set at $D_h/3$, a ratio commonly observed in documented field studies [12]. This pitch is taken to ensure clogging of the helix plate is avoided. A range is utilised for determination of the shaft wall thickness. The minimum shaft thickness is obtained following API guidelines, using a WSD method [5]. The derivation is shown in Equation 3.1. The maximum wall thickness maximum is limited to 10% of the shaft diameter, in order to ensure the pile is able to be manufactured [10]. The helical pile geometry is determined for maximum uplift capacity, as described in Section 6.2.7 and the results are shown in Table 9.1.

$$t_c = 0.00635 + \frac{D_c}{100} \tag{3.1}$$

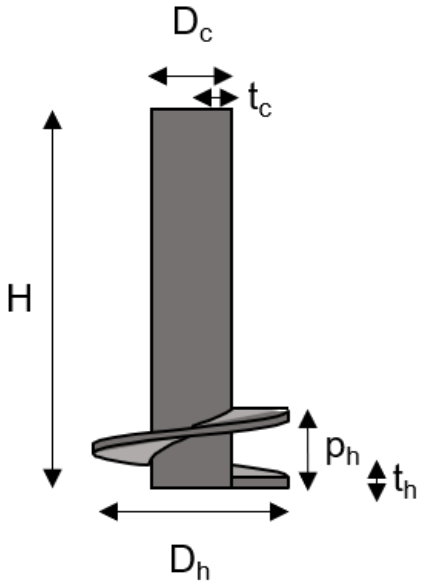

Figure 3.1: Schematic geometry of single helix, single diameter helical pile

The advancement ratio (AR) describes the relative vertical movement per pile rotation. The AR can be controlled to influence the installation force and torque. Over-flighting occurs when the AR is smaller than one, resulting in a penetration smaller than the pitch per pile revolution. Contrarily, under-flighting occurs when the penetration of the pile is greater than the pitch per revolution. If the penetration of the pile equals the pitch, the AR is equal to one and referred to as pitch-matched. If the installation of the helical pile is pitch-matched (AR=1), the soil disturbance is minimised. An illustration of these different ratios is depicted in Figure 3.2.

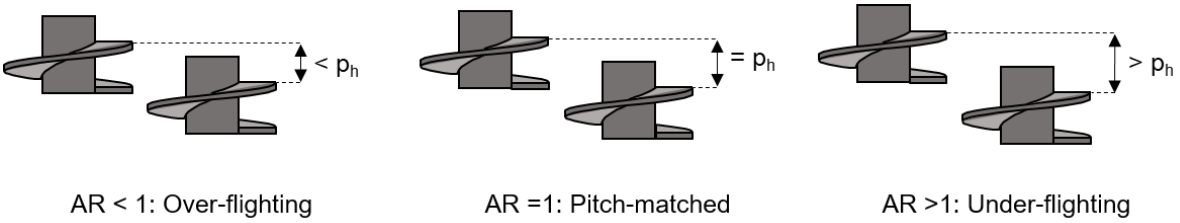

Figure 3.2: Illustration of different advancement ratios of helical piles

The helical piles are assumed to have an open-ended design. Closing the tip-end of the pile could lead to an increased chance of buckling, a reduction in compressive capacity, and increased installation requirements. Research has indicated that installing closed-ended piles to the same installation depth requires more effort compared to open-ended piles [45, 48]. Additionally, open-ended piles show greater pile resistance due to the continuous increase in plug resistance [29]. While these studies focus on standard piles, it is reasonable to assume that the same effects can be expected for helical piles. Furthermore, for an open-ended helical pile, soil is likely to remain within the shaft after decommissioning. Consequently, during the next installation process, the soil needs to be cleared or pushed out of the pile.

3.3. Grouping effects

Limited research has been conducted on the effect of helical pile grouping in scientific studies thus far. However, a numerical Finite Element Method (FEM) investigation was carried out to study the effect of grouping in soft clays subjected to uplift and lateral loading [56]. This study shows that the uplift and lateral capacity of grouped helical piles (GHP) increases as the group size and spacing increases. A conclusion supported by researchers studying the pile group effect of standardised piles in sand and clay [38]. Specifically, when the spacing between helical piles exceeds three times the diameter, the group efficiency factor surpasses 95%. The group efficiency describes the group effect on the ultimate capacity. Consequently, it can be concluded that for GHP with spacing greater than three times the diameter, the helical piles fail independently and thus have minimal influence on the overall behaviour.

4

Soil Behaviour of Sand

This chapter provides information about the soil fundamentals, describing the soil classifications and determination of soil parameters. Subsequently, these parameters are described and typical ranges found in offshore sand soils are presented. Furthermore, the failure mechanisms for helical piles and mud-mats are described. Finally, the soil-structure interaction is briefly explained.

4.1. Fundamentals

Most common soils offshore consist of a matrix of grains with inter-granular pores, mostly filled with water. A basic parameter for classifying soil types is the grain size, according to ISO-14688 [32]. Grain sizes offshore variate from gravel, soils coarser than 2 mm, to clay, soil finer than 0.002 mm [57]. Sand is ranged from 0.5 mm to 0.1 mm. The soil permeability typically decreases when the grain size decreases. When the soil permeability is high, all load changes are taken by the soil skeleton which is called drained loading. Conversely, for undrained loading there is no movement of water and therefore excess pore pressures are able to develop. In this study only drained conditions are considered, as the benchmark project is situated in sandy soil.

Soils resist shear through friction, and therefore the shear capacity can be quantified via a frictional mechanism (Coulomb). The friction angle quantifies the shear strength. When soil is under shear, volume changes can be observed in the soil. Generally, loose sands compact and dense sands dilate (volume expansion). Site surveys and laboratory testing are generally performed to identify the soil properties. Geotechnical surveys perform in-situ test, such as the cone penetration test (CPT), and collect soil samples for laboratory testing. Soil types influence the use of foundation systems and are therefore of high importance. The soil data used for this research is obtained from the benchmark project. The stiffness of the soil is determined with the use of DVNGL-RP-C212 [17]. The relevant soil parameters required in this research are explained below.

4.1.1. Soil parameters

Relative soil density, D_r, is used to describe how dense soil is. The higher the percentage of density, the more dense the soil. Generally, very loose sands have a relative density of 0% - 20%, and very dense sands in the range of 80% - 100% [41]. The effective unit weight of sand, γ', is found by subtracting the unit density of water from the unit density of the soil. Offshore, the values of effective unit weight of sand typically fall within the range of 8-15 kN/m^3 [24, 52]. Looser sands generally correspond to lower unit weights of soil, while denser sands correspond to higher values. Similarly, the denser soils tend to have higher angles for internal friction than the looser soils. The friction angle, φ, is used to describe the friction shear resistance of the soil. Offshore, friction angles are typically found in the range of 20°-45°, for very loose to very dense sand respectively [28, 33, 52]. The interface angle, δ, is a function of the shear stress and vertical effective stress, and depends, among others, on the surface roughness of the steel. The interface angle for offshore applications lies within the range of 24-30°[47]. The dilatancy angle, ψ, can be derived from the peak and critical friction angles, and can be visualised as the angle to the vertical axis in shallow failure mechanisms. For relatively dense sands, the dilatancy angle can be estimated as the internal friction angle minus 30°[8, 51].

4.2. Foundation failure mechanisms

4.2.1. Helical piles

In offshore engineering, it is crucial to distinguish between shallow and deep failure mechanisms. When the helical pile is embedded at shallow depths, uplift of the helical pile results in a failure surface that extends towards the ground surface. It is important to note that this particular failure mechanism specifically develops when subjected to uplift forces. However, as the depth increases, the failure becomes more localised, and bearing failure is experienced, as shown in Figure 4.1a [8, 26, 42]. The bearing failure mechanism can be employed for both compressive and tensile loads.

For the uplift capacity it is preferable, however, to maintain a shallow failure mechanism. The transitioning to the deeper failure mechanism only leads to a significantly higher required installation torque, while the capacity of the helical pile remains nearly constant. The specific depth at which this transition occurs is not precisely defined and varies based on depth to diameter ratios, ranging from 4 to 10 depending on the friction angle of the soil. In order to maintain this shallow failure mechanism, it is assumed that the maximum relative embedment ratio (H/D_h) should not exceed 8. It is assumed that the shallow failure mechanism, which occurs due to the application of vertical load, can be visualised as a truncated cone with its base in contact with the helix, as illustrated in Figure 4.1b [26]. This approach has consistently been proven effective in centrifuge tests conducted in different studies, regardless of whether installation effects were present or not [12, 31].

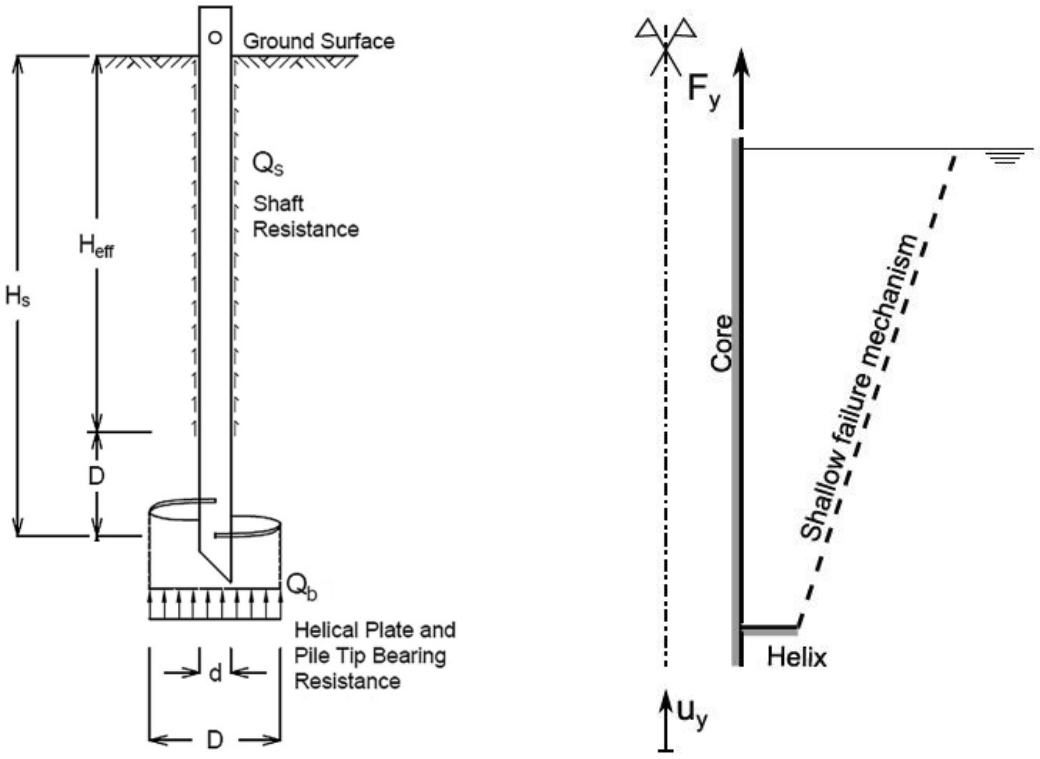

(a) Illustration of bearing failure mechanism (modified) [35] **(b)** Illustration of shallow failure mechanism (modified) [8]

Figure 4.1: Failure mechanisms due to axial loading on helical pile

The lateral design load should be considered in order to prevent excessive lateral deflection and avoid failure with the pile moving sideways or rotating through the soil. Lateral capacity of piles in sand is a difficult analytical analysis and is therefore often evaluated using empirical methods [46, 48]. The failure mechanisms for standard (straight shafted) piles are utilised in this study for the determination of helical piles. For *short pile mechanisms*, failure will only take place within the soil only. So, the pile does not fail in bending, and wedging of the soil will develop as failure mechanism [4, 48]. In the current study, the piles are treated as short and rigid as their diameter-to-length ratio is relatively low [46]. The risk of structural failure in these short piles is not considered to be the primary concern. If any potential failure arises due to this assumption, it can be effectively addressed by recalculating and adjusting the

steel width or grade, ensuring the stability and safety of the pile design. As the helical pile is connected to a mud-mat, it is assumed that the head is fixed. So, rotation of the pile is restrained, leading to a rigid body translation failure. The failure load is therefore the integrated lateral resistance along the (embedded) length of the pile, as shown in Figure 4.2.

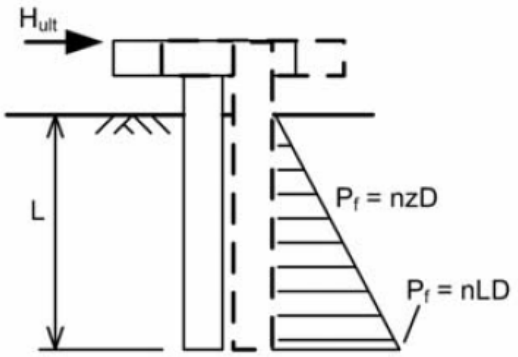

Figure 4.2: Simplified lateral capacity of short pile failure (fixed head, no hinge) [48]

Tubular piles, including the shaft of helical piles, can encounter plugging during their installation process. These failure mechanisms are illustrated in Figure 4.3. Plugging may occur through three failure mechanisms: unplugged penetration, plugged penetration, and partial plugging. In the case of unplugged penetration, the soil column inside the pile remains stationary, resulting in no downward movement of the soil. On the other hand, plugged penetration involves the soil column moving downwards in sync with the pile, causing a significant displacement of the soil. In partial plugging, the soil column also moves downwards with the pile, but slower. It is evident that during installation, the resistance experienced by the pile wall is usually higher than the resistance exerted on the soil plug [48].

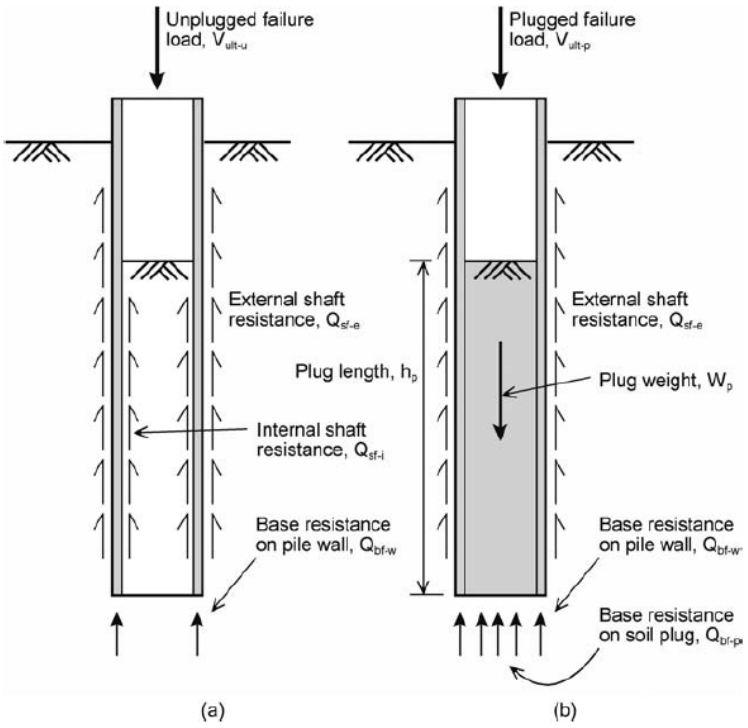

Figure 4.3: Open-ended pile failure mechanisms: unplugged (a) and plugged (b) [48]

4.2.2. Mud-mats

As the template is a temporary structure, only the bearing capacity and sliding capacity are discussed as failure mechanism for mud-mats. It is assumed that, for example, settlement of the mud-mats is not significant, and can be counteracted by the levelling system of the template.

The bearing capacity of a mud-mat relies on the underlying seabed to provide sufficient bearing capacity to support the structure, the interaction with the soil is shown in Figure 4.4. If the soil's bearing capacity is exceeded due to excessive loading or weak soil conditions, it can result in settlement or even collapse of the mud-mat. Lateral loading could provoke sliding failure. The lateral loading on the template is transferred to lateral loading on the mud-mats. The sliding capacity of the mud-mats depend on the vertical loading and the friction angle of the soil. Both the bearing and sliding capacity are determined using ISO 19901 [33].

The interaction of the soil and the mud-mats is modelled as a combination of lateral and rotational springs, which represent the axial and lateral behaviour. Each mud-mat contains one axial and one lateral spring to model the soil behaviour.

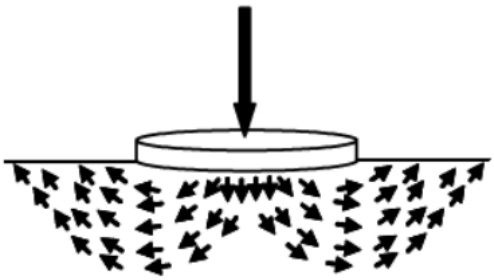

Figure 4.4: Representation of interaction mud-mat with soil under vertical loading [46]

5

Benchmark Project Specifics

This chapter offers an overview of the inputs utilised in this research. It covers essential aspects of the benchmark project, specifically on the equipment employed. Detailed insights are provided into the properties of the monopiles, vessel, template and its associated boundary conditions. Additionally, environmental conditions, such as wind speed, water currents, and wave characteristics, are thoroughly discussed. The chapter also describes the soil and seabed characteristics. Finally, the chapter presents various loading scenarios that the structure might encounter, with a focus on the governing load cases used for further analyses.

5.1. General information

The project that is used as benchmark is located at the east coast of the United States of America. The wind farm comprises 84 wind turbines, all using a monopile foundation. A template has been designed for this project and this structure is used as basis for the investigation into adding helical piles as foundation method. This template has been designed for maximum stiffness. So, the template is designed such that the natural period of the system with the monopile present in the template has an initial natural period lower than the predominant wave period. Structural design has been initially based on wave loads (among others) assuming the template is fully rigid. Additionally, the focus in this research is primarily placed on the global analysis of offshore monopile installation templates.

For template design generally the DNVGL-ST-N001 guidelines are used to obtain LRFD strength checks for structures subject to ULS loading [14]. Table 5.1 gives the load factors for ULS, note that the load factor is different for each type of loading (permanent (G), variable (Q), deformation (D), environmental (E) and accidental (A)). Throughout the complete study the LRFD approach is used unless stated otherwise.

Table 5.1: Load factors for ULS according to DNVGL-ST-N001 [14]

Load condition	**Load categories**				
	G	Q	D	E	A
ULS	1.0	1.0	1.0	1.3	N.A.

5.2. Utilised equipment

5.2.1. Monopiles

The template is designed for the monopile properties as shown in Table 5.2. The monopile dimensions vary due to the varying water depth and therefore varying penetration of the monopile. There is a significant difference in length between the smallest and largest monopile (22 meters). However, the difference in diameter of the monopile's bottom does not vary significantly, there is only 0.5 meter difference between the smallest and largest monopile.

To install the monopile for offshore wind turbines, specific equipment is required. This includes the flanged pile upending tool (FPUT), hammer, and sleeve with anvil. These components have significant

Table 5.2: Monopile and equipment properties benchmark project

Item	Value
Monopile weight	1000 - 1635 mT
Length monopile	68 - 90 m
Monopile diameter top	6.5 m
Monopile diameter bottom	8.4 - 8.9 m
FPUT weight	110 mT
Hammer weight	425 mT
Sleeve with anvil weight	318 mT

mass and are therefore important for load calculations. The FPUT is used to lift and position the monopile in an upright position. The hammer is used to drive the monopile into the seabed. The sleeve is a steel cylinder placed on top of the monopile to guide the pile during the initial phase of driving. The anvil, a heavy steel block, sits on top of the sleeve and provides a solid surface for the hammer to strike. When the hammer hits the anvil, the impact forces pass through the sleeve and drive the monopile into the seabed. The template should ensure monopile installation within specified tolerances, the maximum inclination angle is 0.5°.

5.2.2. Template

A design has been realised by HMC and is illustrated in Figure 5.1. The template comprises six legs with six mud-mats as foundation system. By utilising this hexagon shape, a significant increase in restoring arm can be realised due to the larger footprint of the template compared to the more standard 4-legged template. Therefore, the template is capable of resisting larger overturning moments. The frame is designed with a U-shape to allow for bringing in the monopiles and to be able to retrieve the template after piling operations have completed. The open sides of the frame provide tapered bumpers to constrain the monopile as it is brought into the frame. The dimensions and orientation of the template are shown in Table 5.3.

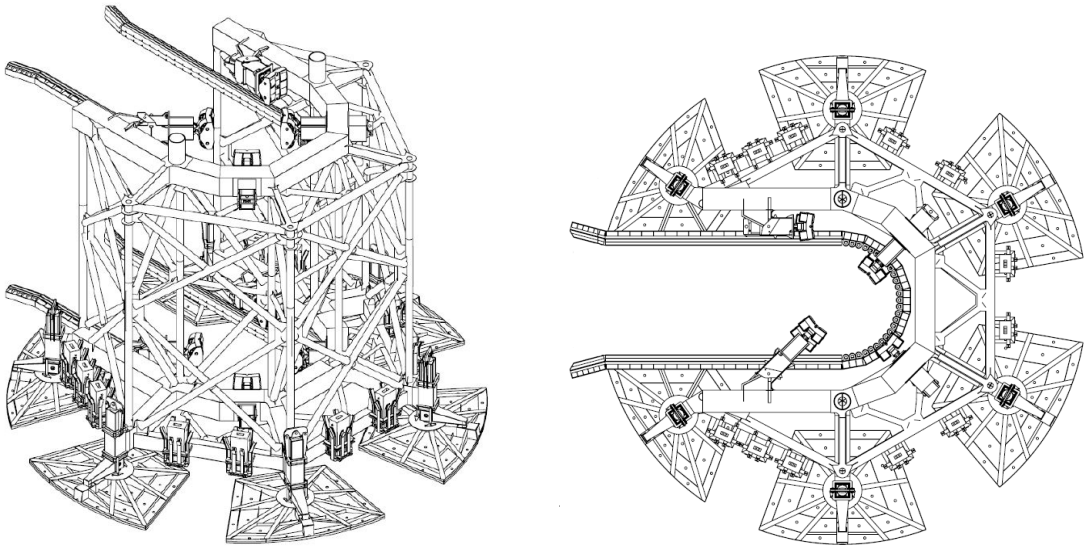

(a) Side view **(b)** Top view

Figure 5.1: Illustrations of monopile installation template designed for benchmark project

Two varying mud-mat dimensions are implemented, as depicted in Table 5.4. To prevent any interaction between the mud-mats and the monopiles, the two mud-mats positioned adjacent to the opening are smaller, as illustrated in Figure 5.1b.

Table 5.3: Template dimensions and mass

Item	Value
Height	30 m
Footprint diameter	42 m
Height upper centralizer	29 m
Height lower centralizer	5 m
Mass	1850 mT
Submerged mass	1550 mT

Table 5.4: Mud-mat size per type, type A corresponds to the mud-mats located next to the opening

Mud-mat	Area [m^2]
Type A	85.61
Type B	108.25

Boundary conditions

Underneath, a list of the three most important boundary conditions for the template is shown. Note that boundary conditions for the scour protection, clearances, and hydraulics are also determined but will not be considered in the current study. Only boundary conditions that relate to template design are considered and utilised. The boundary conditions are partly governed by the vessel choice, and are therefore subject to change when a different vessel is used. The boundary conditions for the benchmark project, shown below, are limited by the HMC vessel *Balder* its capabilities.

1. The monopile template footprint (diameter = 42 m) is limited by the scour protection dimensions (diameter = 44 m) and the installation tolerance ($\pm$ 1 m).
2. The vessel's crane capacity at certain set-down radii (2300 mT, 48 m) limits the template its weight to 1850 mT (including safety margins), also called the Not-To-Exceed Weight (NTEW).
3. The monopile template must fit on the vessel's deck, restricting the footprint and height of the structure. The design is restricted to a diameter of 44 m up to a height of 10 m, after which the structures is limited to a diameter of 38 m.

5.2.3. Vessels

An overview of HMCs fleet is located at Appendix A, this section contains general information about the vessels, their main dimensions and crane capacities. The load and clearance curves of the cranes and the deck arrangement of each vessel are also displayed at Appendix A. These are generally used to determine what vessel is able to perform the lifting operation and is able to provide deck space for the template during transport. The hook load capacity decreases significantly with an increasing radius for each vessel, as displayed in the load and clearance curves (see Figures A.6-A.12).

5.3. Environmental conditions

An overview of all the environmental conditions is shown in Table 5.5, and each condition is further explained in Sections 5.3.1 - 5.3.3.

Table 5.5: Environmental conditions benchmark project

Item	Value
Wind speed	12.9 m/s
Current speed (surface)	0.25 m/s
Current profile	Power law
Significant wave height	2 m
Design wave height	4.76 m
Minimum water depth	35 m
Maximum water depth	50 m
Seabed inclination angle	2°

5.3.1. Wind

Wind is a three-dimensional and highly variable flow of air, generally described as a combination of a mean wind and wind gusts. The mean wind flow is typically determined at a height of 10 meters, and the vertical wind profile can be described as in Equation 5.1. After derivation of the average wind flow, a constant wind profile is assumed with a wind speed of 12.9 meters per second.

$$\overline{U}_w(z) = \overline{U}_w(z_r)\frac{ln(z/z_0)}{ln(z_r/z_0)} \tag{5.1}$$

Where

z is the height above mean sea level (MSL)
z_0 is the surface roughness length
z_r is the reference height (typically 10 meter above MSL)

5.3.2. Current

Various types of currents can be determined including tides, wind drift, and current caused by temperature gradient. Currents are important for the structural design, marine operations, scouring, and dynamics such as vortex-induced vibrations. However, only the effect on the loading by currents is investigated in this research. The surface current speed is 0.25 meter per second and the current profile is determined using the power law, see Equation 5.2. A marine assessment on the benchmark project executed by HMC showed that the power law provides the most accurate approximation of the real current velocity profile. The current velocity profile over depth is shown in Figure 5.2.

$$U_{c,i} = U_{surface}\left(\frac{h_i}{d}\right)^{\frac{1}{7}} \tag{5.2}$$

Where

$U_{surface}$ is the current speed at the water surface
h_i is the vertical coordinate with respect to the seabed
d is the total water depth

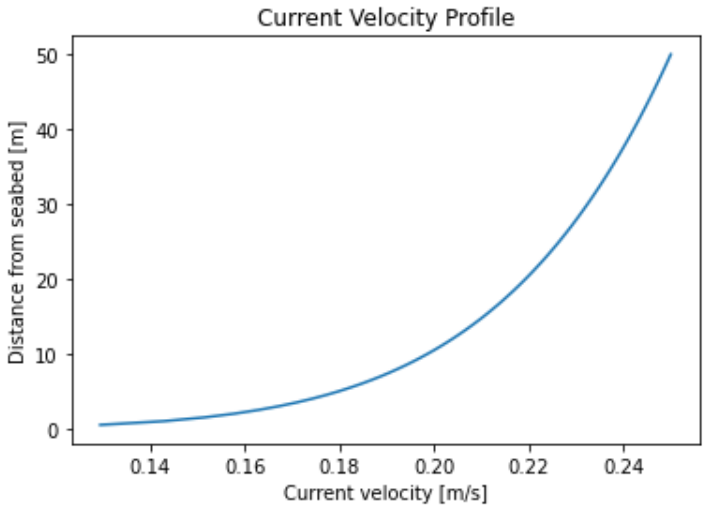

Figure 5.2: Current velocity profile using the power law

5.3.3. Waves

Sea waves are irregular, meaning that its a random process of wave heights, periods, and direction. The wave load on a structure depends on the shape of the waves, which in turn depends on the water depth. The installation phases shall at least be able to withstand a significant wave height of two meters.

An alpha factor of 0.84 is assumed, following the DNVGL-ST-N001 for short operational periods ($\leq$ 12 hours, with environmental monitoring) [14]. This alpha factor is used to account for weather forecasting inaccuracies. Additionally, a storm factor (STF) is applied to calculate the maximum wave height for which the template should be designed, which is derived in Equation 5.3.

$$H_{max} = STF \cdot \frac{H_s}{\alpha} = 2 \cdot \frac{2}{0.84} = 4.76m \tag{5.3}$$

Wave theories

Different wave theories can be applied for determining the wave loads, dependent on the dimensionless values of wave steepness and relative water depth. A graph is shown in Figure 5.3, which can be used to determine which theory is applicable for the investigated sea state. Airy wave theory is valid for linear waves in deep or intermediate water depths. On the other hand, Cnoidal and Stokes' theory are valid for non-linear periodic waves. Stokes' theory is suitable for waves that are not very long relative to the water depth. A first-order Stokes wave is identical to a linear wave, or Airy wave. Higher-order Stokes waves have crest which are steeper and troughs which are wider than for Airy waves [16]. Cnoidal theory is on the other hand more suitable for waves that are much longer than the water depth [43]. Generally, these theories (Cnoidal and Stokes) are more accurate, but more complex. The most accurate Stokes' fifth order wave theory is developed by Fenton and used in this research, with the use of the Fenton tool [21].

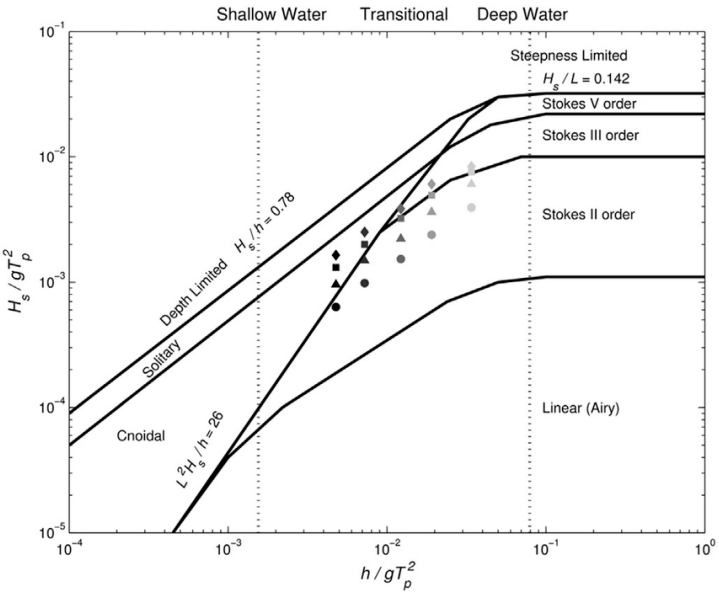

Figure 5.3: Wave steepness plotted as a function of relative water depth

Fenton tool

The Fenton tool [22] is utilised to compute water particle velocities and accelerations at various distances from the seabed, considering the wave profile, without requiring wave stretching. The wave train is typically described by three length scales, namely the water depth, wave height, and wave length (or in terms of dimensionless quantities derived from these parameters). However, the wavelength is unknown for the benchmark project. Therefore, it is essential to specify the current in this case as well. The current will influence the horizontal velocity of the water particles, and the tool uses this current speed to model particle velocities and accelerations. To ensure the largest wave loads are obtained, a range of wave periods should be considered.

The input required for the Fenton tool consist of the wave height, wavelength or period, current, number of Fourier components, and the number of steps. The zero-crossing period T_z can be obtained by dividing the peak period T_p by 1.2859, which depends on the sea state. The relative wave height H/d is specified, the same is required for the wavelength λ/d and the period $T\sqrt{g/d}$. Where g is the gravitational acceleration, which is a function of latitude but can be assumed to be $9.81m/s^2$ in

most cases [21]. Consequently, the current is specified, the mean current velocity is often utilised which can be determined using the theory from Section 5.3.2. Thereafter, the number of terms in the series has to be specified. Results of experiments by Fenton show that accurate solutions can be obtained with Fourier series of 10-20 terms [22]. Finally, the number of steps is specified in order to simulate smaller waves and stepping upwards in height. This is done to ensure the obtained results are accurate. A summary of the inputs used to generate the wave velocity and acceleration profiles over depth is reported in Table 5.6.

Table 5.6: Fenton tool input

T_p	T_z	H/d	$T_z \times \sqrt{g/d}$
6	4.7	0.0952	2.067
7	5.4	0.0952	2.411
8	6.2	0.0952	2.756
9	7.0	0.0952	3.100
10	7.8	0.0952	3.445

5.4. Soil and seabed

The first site visit was followed by a series of offshore geotechnical surveys. Geotechnical and chemical laboratory testing was completed as part of the site campaigns to assist in the assessment and evaluation of the soil properties. The majority of the seabed comprises fine to medium sand. It is assumed that the mud-mats do not penetrate the seabed and therefore the friction angle of the seabed is used. The friction angle of the soil beneath the seabed is assumed to be constant, and is used as input for the helical pile calculations. The stiffness in vertical and horizontal direction has been estimated by HMC based on empirical formulas, using the soil shear modulus from the soil characteristics present at the benchmark project.

The development area covers around 650 squared kilometer, in which the bathymetry has water depths ranging between 35.3 and 50 meters relative to mean sea level (MSL). The seafloor is relatively favourable with no changes in seabed topography with only one dominant seabed feature, scour depressions ranging from 0.2 to 1.0 meter. No slope angles greater than 2° are observed after slope analysis. If the seabed is inclined it is assumed that the template's weight and the total horizontal load needs to be projected onto the inclined seabed direction. The monopile installation template could be installed on a 44 meter diameter, 0.5 meter thick filter layer, if required. This layer is assumed to be flat and matching the seafloor slope. The filter layer consists of crushed angular rock, with a friction angle of 36°. The soil properties are shown in Table 5.7.

It is assumed, however, that the filter layer is not present when the template with helical piles is utilised and thus different soil properties are utilised. The filter layer can significantly jeopardise the installation of helical piles, so it is advisable to avoid using a filter layer. If a filter layer is necessary for protecting the monopile against scour, it should be installed after the monopile installation process.

Table 5.7: Soil properties of benchmark project which are used as input parameters

Item	Value
Friction angle seabed (φ)	31.6°
Friction angle filter layer (φ_f)	36°
Peak friction angle (φ_p)	45°
Interface friction angle (δ)	24°
Effective unit weight (γ')	10.47 kN/m^3
Soil density (D_r)	82%
Peak dilatancy angle (ψ_p)	16.5°
Axial stiffness	300 kN/mm
Lateral stiffness	212 kN/mm
Max. seabed inclination	2°

5.5. Basic design load cases

Multiple load cases are determined in order to examine which load cases are governing for the structural design of the template. Generally, detailed design phases consider more load cases than basic design phases. In this section, the governing load cases are described, all other load cases are not further analysed in this research. Additionally, all load cases are considered statically and thus no time domain calculations are performed.

5.5.1. General load cases template installation procedure

An example of a complete overview of all load cases considered in a general template operation can be located in the Table 5.8. These load cases are described for a project utilising a mud-mat founded monopile installation template.

Table 5.8: Example of all considered load cases for template without helical piles

Load case	Installation step	Name
1.1	Template installation	Lowering of the template through splash zone
2.1	Monopile installation	Engage monopile with upper guide
2.2	Monopile installation	Lower monopile just above lower centralizers
2.3	Monopile installation	Vertical alignment of monopile, while suspended from crane and no sea bed penetration
3.1	Monopile driving	Correcting monopile inclination
3.2	Monopile driving	Horizontal impact load hammer
3.3	Monopile driving	Correcting monopile inclination with hammer stabbed
4.1	Template recovery	Template recovery from seabed
4.2	Template recovery	Lift of template, upper centralizers at monopile top
4.3	Template recovery	Lift of template, upper centralizers retracted
4.4	Template recovery	Lift of template, lower centralizers at monopile top
4.5	Template recovery	Lift of template through splash zone
5.1	Contingency case	Template only
5.2	Contingency case	Template with monopile at SWP
5.3	Contingency case	Template with monopile at final penetration depth

Generally, the following two load cases are governing. First, the load case in which the monopile is suspended from the crane and (partly) engaged in the template. The vertical alignment of the monopile with a rigging off-lead angle leads to a critical load case. The environmental loading on the monopile exerts significant loading to the template, in which the template should transfer these loads to the soil. Second, the load case that concerns the situation of the monopile with the hammer, sleeve and anvil attached. The monopile is inclined, and the upper guides experience maximum load. The lower guides make no contact with the monopile and thus experience no load.

5.5.2. Investigated load cases helical pile template

The load cases considered in this research are limited to the situation that the template has landed onto the seabed. Thus, load cases due to lowering and lifting of the template are not considered, for example when taking the template through the waterline. In Table 5.9 the considered load cases for the template with helical piles as foundation system are presented. It is assumed that the two generally governing load cases will be governing for the template with helical piles as well. Therefore, only those two load cases will be investigated in more detail. It is assumed that in the period when the monopile has been stabbed, but not driven, all the environmental loads are reacted by the template and any affect from self-weight penetration of the monopile is ignored (in both load cases).

5.5.3. Governing load cases

Two load cases will be investigated in detail and calculations will be performed. The in general governing load cases, determined by experience of HMC, for monopile installation templates are considered, being load case 2.3 and 3.3 described in Table 5.9.

Table 5.9: All considered load cases in this research

Load case	Installation step	Name
1.1	Helical pile installation	Environmental loading on template, helical piles not installed
1.2	Helical pile installation	Environmental loading on template, helical piles installed
2.1	Monopile installation	Engage monopile with upper guide
2.2	Monopile installation	Lower monopile just above lower centralisers
2.3	Monopile installation	Vertical alignment of monopile, while suspended from crane and no sea bed penetration
3.1	Monopile driving	Correcting monopile inclination
3.2	Monopile driving	Horizontal impact load hammer
3.3	Monopile driving	Correcting monopile inclination with hammer stabbed
4.1	Helical pile recovery	Retrieving helical piles, monopile at final penetration depth
5.1	Contingency case	Template with helical piles installed, no monopile
5.2	Contingency case	Template with monopile at self-weight penetration
5.3	Contingency case	Template with monopile at final penetration depth

Load case 2.3: Vertical alignment of monopile, while suspended from crane
Load case 2.3 might be governing due to the off-lead angle of the rigging due to crane tip motions, as illustrated in Figure 5.4. The off-lead angle is considered to be 1°, which is the maximum allowed off-lead angle. This is determined by HMC, considering the environmental conditions and the vessels capabilities at the project's location. Note that the load case also considers maximum seabed inclination of 3°. Furthermore, it is assumed that the monopile tip is just above seabed, thus no contact with the seabed exists. This load case will most probably result in the maximum overturning moment.

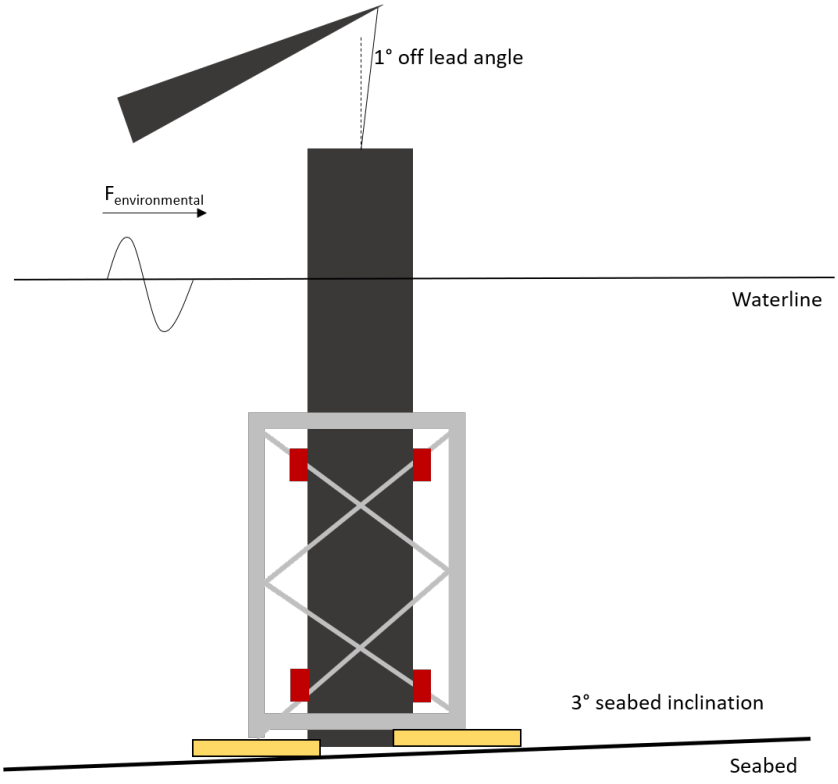

Figure 5.4: Load case 2.3: Vertical alignment of monopile with crane off-lead angle

Load case 3.3: Correcting monopile inclination with hammer stabbed

Load case 3.3 considers the monopile with hammer, sleeve and anvil connected, pressing on the upper guides with maximum force on the pile, as illustrated in Figure 5.5. The lower guides are not in contact with the monopile. Similarly to load case 2.3, a seabed inclination of 3°is considered. The monopile is partly embedded, to small self-weight penetration depth of 5 meter, with a 0.5° monopile inclination.

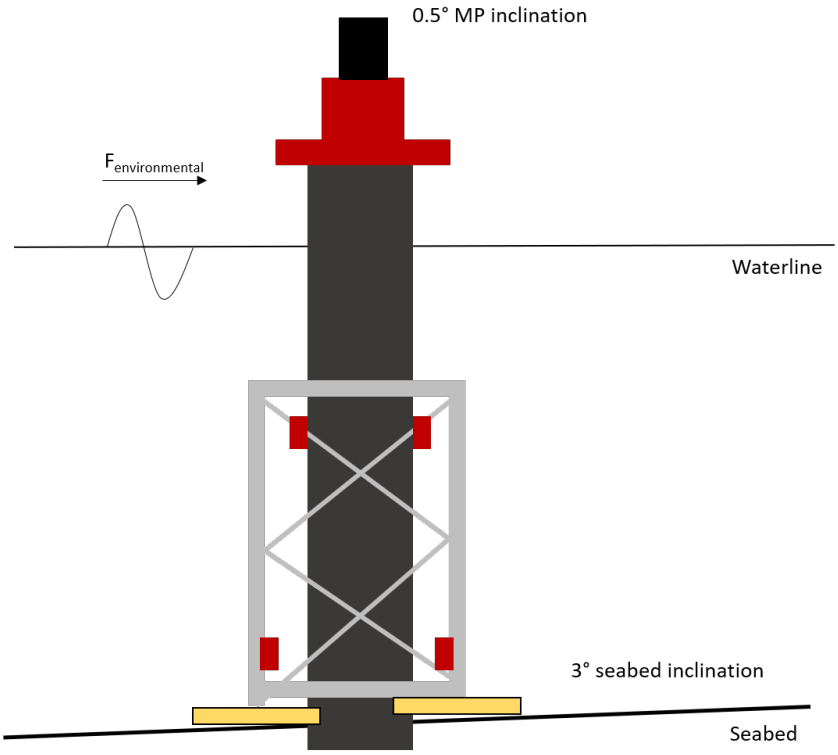

Figure 5.5: Load case 3.3: Correcting monopile inclination with hammer stabbed

6

Foundation Mechanism Requirements

This chapter provides detailed information about the derivation of the capacities of the different foundation mechanisms, being mud-mats and helical piles. First, the mud-mat mechanisms are described: the bearing capacity and the sliding capacity. Also, the effect of a potential filter layer on the seabed is explained. The capacity of mud-mats is generally visualised by capacity envelopes, and the determination of such envelopes is defined. Subsequently, the derivations of the helical pile capacities are described, for uplift, compressive, and lateral capacity. Additionally, the derivations of the installation requirements are presented, showing the amount of required installation force and torque. The environmental loading and crowd force exert loading on the helical pile, which causes stresses in the pile and helix. Therefore, structural checks are performed to ensure the helical pile does not fail due to these stresses. To conclude this section, the determination of the optimal geometry is described, which is optimised for maximum uplift capacity.

6.1. Mud-mats

Loads on the mud-mats, such as suction forces and increased dynamics during lifting and lowering, should be reduced as much as possible. Mud-mats have small holes to allow for a smooth set-down and lift-off of the template. These holes are omitted in bearing and sliding capacity calculations, and the mud-mat is modelled as a flat metal plate. It is assumed that the effect of the openings on the bearing capacity is negligible and will only enhance the out- and inflow of water during placement and lift-off. Furthermore, the mud-mats should be designed for wave slamming loads during lift through the splash zone. It is assumed in this research that the mud-mats are designed to withstand these loads and no further analysis is performed.

The forces due to environmental loading acting on the monopile are generally distributed to the mud-mats through a ball joint, which transfers the horizontal and vertical load. However, the moment can, by definition, not be transferred by the ball joint. The horizontal and vertical stiffness of the mud-mats are typically represented by springs and modelled with software. The stiffness values are determined using a preliminary assessments considering the mud-mat size and soil characteristics.

The bearing capacity and sliding capacity of the mud-mats are assessed according to ISO 19901-4 [33], and the material factor is defined by DNVGL-OS-C101 [15]. Figure 6.1 showcases the assumed rectangular shape and orientation of the mud-mats used for calculations. This is assumed to simplify the analysis as this is a rather complicated problem. Note that the two mud-mats in the top part of this illustration are of type A, the smaller sized mud-mats. The mud-mat area is kept constant in this assumption, despite the change in shape. Additionally, it is assumed that the mud-mats are at sea bed level and therefore not skirted. The full derivations are shown in Appendix C.

6.1.1. Bearing capacity

The bearing capacity is assessed for each mud-mat individually, using Equations 6.1 - 6.6. If each mud-mat has enough capacity, the template can be considered having in total enough bearing ca-

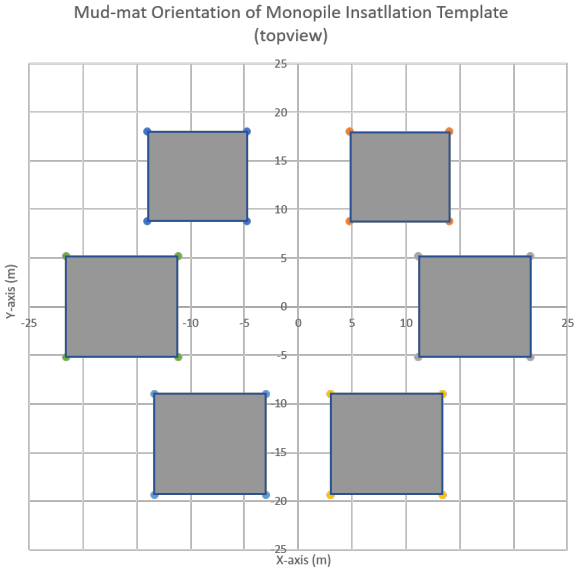

Figure 6.1: Simplified geometry and orientation mud-mats for calculations

pacity. Performing the bearing capacity verification therefore requires making assumptions on the load distribution from total frame loads onto individual mud-mat loads. The overturning moment on the frame is converted into vertical downward and uplift loads on the individual mud-mats for which the centre does not fall on the rotation axis. The template's weight is assumed to be equally shared between the mud-mats in contact with the soil. Uplift of mud-mats occurs if the uplift component of the overturning moment exceeds the weight on the individual mud-mat. If uplift occurs on one of the mud-mats, then the moment redistribution is re-evaluated excluding the mud-mat(s) that experience uplift. A mud-mat that experiences uplift can not transfer any loads or moments as it has no contact with the soil.

$$Q_v = q_v A' \tag{6.1}$$

Where

q_v is the unit bearing capacity
A' is effective area of the mud-mat

The surface area of the foundation element is reduced due to the eccentricity. The eccentricity, e, is the distance from the center of the mud-mat to the point of action of the loading. For rectangular foundations, eccentricity can occur with respect to either axis of the foundation, which is addressed by e_1 and e_2. The mud-mats are schematised as squared foundation elements, with a surface equal to the actual mud-mats. The length and width of the equivalent foundation element is therefore determined as follows.

$$L = B = \sqrt{A} \tag{6.2}$$

The effective area of the foundation element is reduced due to the eccentricity, and can be obtained by the following equations.

$$L' = L - 2e_1 \tag{6.3}$$

$$B' = B - 2e_2 \tag{6.4}$$

$$A' = L' \cdot B' \tag{6.5}$$

The unit bearing capacity is shown in Equation 6.6.

$$q_{\mathsf{v}} = 0.5\gamma' B' N_{\gamma} K_{\gamma} + \sigma'_{v0} \left(N_{\mathsf{q}} - 1\right) K_{\mathsf{q}} \tag{6.6}$$

Where

q_v is the design vertical bearing resistance
N_Y, N_{q} are drained bearing capacity factors, as a function of φ'
$K_{\mathsf{q}}, K_{\mathsf{q}}$ are correction factors that account for inclined actions, foundation shape, depth of embedment, inclination of base, and inclination of the seafloor
φ' is the effective friction angle
γ' is the characteristic value of submerged unit weight of soil
σ'_{v0} is the in situ effective overburden stress at foundation base level
B' is the minimum effective lateral foundation dimension, also referred to as effective foundation width

6.1.2. Sliding capacity

The sliding resistance in drained conditions is shown in Equation 6.7 and can be assumed as a linear connection between vertical and horizontal load depending on the friction coefficient. Sliding resistance verification is performed for individual mud-mats. However, it is assumed that the template horizontal load is equally shared among the (working) mud-mats. This is based on the fact that if a mud-mat does not have enough sliding capacity, another mud-mat can take over. Sliding failure only exists if the template moves as a whole, as the template is assumed to be rigid. Obviously, the sum of all mud-mat's sliding capacity should be larger than the total horizontal load applied on the template.

$$H_d = Q \left(\frac{\tan \varphi}{\gamma_m} \right) \tag{6.7}$$

Where

Q is the factored vertical action
φ is the internal friction angle
γ_m is the material factor

6.1.3. Filter layer

If the filter layer is present, the bearing capacity may also be governed by the strength of the next layer. Therefore, the procedure is repeated for the foundation load acting on the second layer. This second layer is in this case the seabed. A stress spreading angle (λ) is determined, which is limited to 8 degrees. This angle is used to determine the dimension of the equivalent load transfer surface at the interface layer between layer 1 and layer 2, as shown in Equations 6.8 and 6.9.

$$B'_2 = B' + 2 \cdot D_1 \cdot \tan(\lambda) \tag{6.8}$$

$$L'_2 = L' + 2 \cdot D_1 \cdot \tan(\lambda) \tag{6.9}$$

Where

B'_2 is the effective width of the load transfer area between layer 1 and 2
L'_2 is the effective width of the load transfer area between layer 1 and 2
D_1 is the thickness of layer 1
λ is the stress spreading angle.

The effective area of the load transfer zone between the layers 1 and 2 follows as shown in Equation 6.10.

$$A'_{12} = B'_2 \cdot \ L'_2 \tag{6.10}$$

The effective weight of the material in layer 1, between the effective area of the mud-mat and the second soil layer is added to the original vertical load that was transferred to the mud-mats. However,

the horizontal load remains unchanged, conservatively assuming that no lateral load transfer occurs within the first layer. With this new loads the previous equations are used to verify the bearing capacity of the load transfer area. The sliding failure, as might occur at the interface between layer 1 and layer 2 is verified against the internal friction angle of the second layer.

6.1.4. Capacity envelope plots

Due to the interaction between the vertical and horizontal loading, failure envelopes can be determined that show the reduction in actual bearing or sliding capacity from the ultimate values. For sand, the figures show a cut-off by the sliding capacity-line: if the combination of vertical and horizontal load is below this line, then the sliding resistance is insufficient.

The capacity envelopes are produced as follows: first the maximum bearing capacity of the foundation element is determined. This is done by using the maximum vertical load on a mud-mat, assuming no horizontal loading is present. This gives a maximum bearing capacity, which is shown by the bearing capacity line that intersects with the y-axis in the envelope-plot. Subsequently, for all values of the vertical load that are between zero and the maximum bearing capacity, the smallest horizontal load is sought for which the vertical load is equal to the bearing capacity.

6.2. Helical piles

The helical pile is idealised as a shaft with a horizontal plate attached to it, which is a good approximation as experimental and numerical research has shown [1, 31]. The helical pile design in this study is optimised to have maximum uplift capacity. It should be noted, however, that the calculation of helical pile capacity was based on a number of assumptions. Therefore, it is reasonable to infer that there is potential for further optimisation of the helical piles, taking into consideration factors such as design parameters, installation techniques, and materials. The full derivations on the helical pile can be found in Appendix D.

6.2.1. Uplift capacity

The uplift capacity can be determined by using Equation 6.11, which assumes a shallow failure mechanism [26]. Section 4.2 provides an explanation of various failure mechanisms. The outcome of this study on the uplift of helical piles was found to be consistent with centrifuge test of different helical pile geometries and soil properties [8].

$$Q_u = \left[1 + F_{s1}\frac{H}{D_h} + F_{s2}(\frac{H}{D_h})^2\right] \cdot \gamma' \frac{\pi}{4} D_h^2 H \tag{6.11}$$

Where

H is the depth to the helix
D_h is the diameter of the helix
$\gamma\prime$ is the effective unit soil weight
F_{s1}, F_{s2} and F_{ps} are the uplift factors

6.2.2. Compressive capacity

The compressive capacity based on the helical bearing failure mechanism (see Section 4.2) is given in Equation 6.12. Note that these equations are only applicable for sand, and not for clay [19].

$$Q_c = \gamma' H A N_q + \frac{P_s}{2} H_{eff}^2 \gamma' K_0 \tan(\delta) \tag{6.12}$$

Where

γ' is the effective unit weight of the soil
H is the depth to the helix
A is the surface area of the helix
N_q is the bearing capacity factor ($= e^{\pi \tan(\varphi)} \tan^2(45° + \frac{\varphi}{2})$)
K_0 is the initial coefficient of lateral earth pressure ($= 1 - \sin\varphi$)

φ is the internal friction angle
P_s is the perimeter of the pile shaft ($= \pi D_c$)
H_{eff} is the effective shaft length ($= H - (D_h/3)$)
δ is the steel-sand interface friction angle

6.2.3. Lateral capacity

The lateral performance of both normal shafted and helical piles is enhanced when subjected to compressive vertical loading, with helical piles experiencing a greater improvement. Conversely, the lateral performance deteriorates when the piles are subjected to uplift loading. The main drawback of the enhanced lateral capacity with the increasing vertical compressive load is the greater bending moment exerted on the pile's shaft. This implies that extra investigation is required to determine whether the shaft is going to yield [2].

According to API-RP-GEO-2 and ISO 19901-4, the unit lateral bearing capacity for sand can be found using Equation 6.13, assuming shallow depths [4, 33]. It is assumed that the piles are *short*, and therefore Equation 6.13 is applied.

$$p_{us} = (C_1 z + C_2 D)\, \gamma' z \tag{6.13}$$

Utilising the API method, see Equation 6.13, leads to an overestimation of the lateral capacity for depths larger than five pile diameters [48]. The ultimate lateral capacity can also be determined using Equation 6.14, assuming a fixed-head short pile with no hinge [46, 48]. The failure load is therefore the integrated lateral resistance along the (embedded) length of the pile, as shown in Figure 4.2.

$$H_{ult} = \frac{1}{2} n D^3 \left(\frac{L}{D}\right)^2 \tag{6.14}$$

Where,

L is the length of the pile
D_o is the outer diameter of the pile
$n = \gamma' K_p^2$
γ' is the effective unit soil weight
K_p is the passive earth pressure coefficient ($K_p = \frac{1+\sin\varphi}{1-\sin\varphi}$)
φ is the friction angle

6.2.4. Installation requirements

The existing maximum torque, approximately 10.6 MNm, represents the maximum amount of rotational force that a large casing-rotator can apply onshore. It is reasonable to assume that this torque can also be applied offshore. Nevertheless, the weight of the torque equipment is substantial, ranging from 30 metric tonnes for the smaller 2.7 MNm tool to 120 metric tonnes for the largest 10.6 MNm tool [7]. In other words, as the available torque increases, so does the weight of the torque tool.

The required torque and force for installation (also called crowd force) depends on, among others, the advancement ratio (AR), which is the vertical displacement per rotation divided by the helix pitch. If the AR is equal to one, also referred to as pitch-matched installation, helical movement is ensured and soil disturbance is minimised [8]. Consequently, due to this minimised soil disturbance the maximum uplift capacity can be acquired. However, the correct amount of crowd force must be applied on the helical pile to ensure this vertical displacement. The to be applied torque and force depend on the installation depth of the helical pile.

A method has been developed and validated against centrifuge tests to estimate the force and torque requirements with depth [13]. The depth-dependent torque can be approximated with Equation 6.15, each component in this equation is calculated independently as a function of geometrical variables, cone penetration test (CPT) results and interface properties. The crowd force can be estimated following a similar methodology, as shown in Equation 6.16. The full derivation of the installation torque and crowd force are shown in Appendix D.

$$T(H) = T_c(D_c^2, \overline{q}_c(H), a, H) + T_b(D_c^3, \overline{q}_c(H), \delta) + T_h(D_h^3, D_c^3, \overline{q}_c(H), a, t_h, K_0) \tag{6.15}$$

$$F_{y,c}(H) = F_c(D_c, \overline{q}_c(H), \delta, H) + F_b(D_c^2, \overline{q}_c(H)) + F_h(D_h^2, D_c^2, \overline{q}_c(H), a, t_h, K_0) \tag{6.16}$$

Where,

T_c, T_b and T_h are the torque related to the shaft, base and helix respectively
F_c, F_b and F_h are the forces related to the shaft, base and helix respectively
$\overline{q}_c(H)$ is the averaged cone resistance (CPT)
δ is the sand-steel interface friction angle
K_0 is the coefficient of lateral earth pressure ($= 1 - sin\ \varphi$)
a is the stress drop index [36]
t_h is the plate thickness
D_c and D_h are the shaft diameter and helix diameter respectively
H is the depth to the helix

The installation requirements might become significant as depth increases, limiting the practical achievable embedment of the helix pile. The currently available installation tools might not be able to apply such forces and torques, limiting the application of helical piles. However, one of the hypotheses of the force prediction method is that the helical pile is fully plugged during installation. Consequently, the contribution of the base component to the total force is significant. This means that if the fully plugged effect can be reduced, the total required force will also decrease. Therefore, Equation 6.16 is conservative and thus the upper bound for practical applications [8, 20].

6.2.5. Structural requirements of shaft

The shaft must be able to resist shear and normal stresses resulting from the installation torque and force. The structural requirements of the shaft is based on the stresses due to the installation loads as these loads are more severe than the loads that occur during operation. The maximum shear stress can be obtained by using Equation 6.17. The minimum shaft thickness is utilised (see Equation 3.1), if structural requirements allow for it. This approach is preferred due to the goal of minimising both the cost and mass of the helical pile. However, if required, the shaft thickness is enlarged to increase strength. The crowd force generates a vertical normal stress inside the shaft, which can be derived using Equation 6.18.

$$\tau = 16\,\frac{T}{\pi}\,\frac{D_c}{D_c^4 - (D_c - 2t_c)^4} \tag{6.17}$$

$$\sigma_y = \frac{4}{\pi}\,\frac{F_{y,c}}{D_c^2 - (D_c - 2t_c)^2} \tag{6.18}$$

Where,

T is the installation torque
$F_{y,c}$ is the crowd force
D_c is the shaft diameter
t_c is the shaft thickness

Subsequently, the equivalent Von Mises stress is calculated to verify that the yield strength limit of steel is not exceeded, using Equation 6.19. This value represents the equivalent stress that would cause the same deformation as the actual combination of the normal and shear stress. If the yield strength is exceeded by the Von Mises stress, the material may undergo plastic deformation or failure.

$$\sigma_{eq,c} = \sqrt{\sigma_y^2 + 3\tau^2} \leq f_y \tag{6.19}$$

Additionally, as the crowd force increases with pile length and embedment, there is a risk of buckling of the shaft. This is a rather difficult derivation and therefore a simplification is used. It is assumed that the base of the helical pile is clamped, but the top of the shaft is able to rotate and move freely. Therefore, Equation 6.20 is utilised which uses Euler's first mode of elastic buckling of a column. This force should be larger than the crowd force to be able to install the helical pile. Note that this approximation

is rather conservative, as the soil around the shaft will provide additional resistance against buckling [8, 27, 52].

$$F_{y,cr} = \pi^2 \frac{EI}{(KH)^2} \geq F_{y,c} \tag{6.20}$$

Where,

E is the Young's modulus
I is the second moment of area
K depends on the support conditions of the column ($K = 2$ in this case)
H is the shaft length

Similarly, the structural strength of the helical pile under lateral loading is considered. To check whether the assumption of a rigid body is correct in this case, some structural checks are performed. First, a simple estimation of the deflection is executed, using Equation 6.21. The ultimate resistance, leading from Figure 4.2 is translated to a force, to calculate the deformation of the pile. This is done using Figure 6.2. Second, the maximum bending stress in the pile for the ultimate lateral resistance is derived in order to check whether the assumptions are valid in terms of structural strength, using Equation D.27. In Appendix D the full derivation of this derivation is shown.

$$w = \frac{FL^3}{3EI} \tag{6.21}$$

$$\sigma_{max} = \frac{My}{I} \tag{6.22}$$

Where,

F is the force translated to the end of the pile
L is the length of the pile
E is the Young's modulus
I is the second moment of area
M is the moment exerted by the force F
y is the length to the centre of the shaft

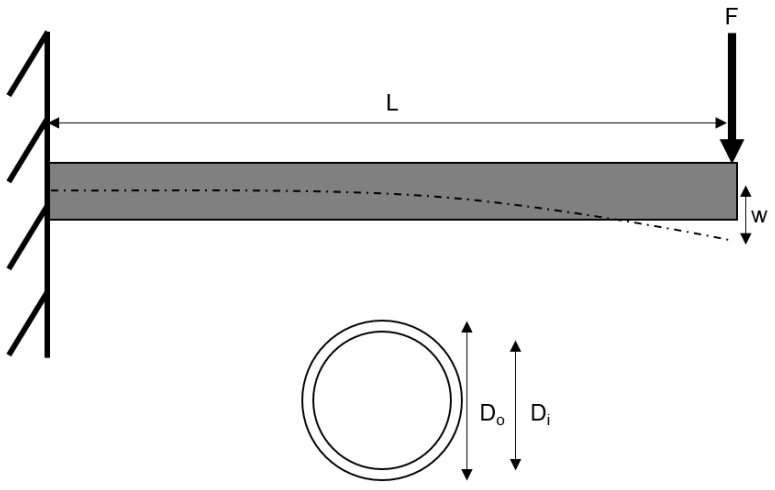

Figure 6.2: Lateral deformation of inclined beam, and diameters of pile

6.2.6. Structural requirements of helix

During installation and uplift, significant loads act on the helical plate generating a bending moment at the helix-shaft connection. Failure of the helix plate can occur through bending as a result of plastic deformation before the shaft's ultimate resistance is reached [42]. The maximum of the two loads calculated in Equations 6.11 and 6.16, $F_{y,max}$, is used to calculate the maximum bending moment. The load is assumed to be a distributed constant load q, as shown in Equation 6.23. The maximum horizontal stress is calculated using Equation 6.24, which the results from this bending moment in the helix [54]. If this stress exceeds the yield strength limit of steel, the helix will fail.

$$q = \frac{4F_{y,max}}{\pi(D_h^2 - D_c^2)} \tag{6.23}$$

$$\sigma_x = k\frac{qD_h^2}{4t_h^2} \leq f_y \tag{6.24}$$

Additionally, it is assumed that the connection between the shaft and the plate consists of two weld joints and that the shear load is evenly divided over these two joints (but opposite in direction). The strength of the weld is calculated through the Von Mises criterion as shown in Equation 6.25, more details are shown in Appendix D.5.

$$\sigma_{eq,w} = \sqrt{\sigma_w^2 + 3\tau_w^2} \leq f_y \tag{6.25}$$

The constant k depends on the ratio of the helix diameter and shaft ratio. As shown in Table 6.1 the larger the ratio, the higher the value of k. A study into this relation, using a Finite Element Method model and comparing it to an analytical model, shows that the analytical approach over-predicts the bending moment in the plate, and thus makes this analytical approach conservative [8]. Similarly to the structural requirements of the shaft, the soil around the helix will provide additional resistance, but this contribution is not taken into account.

Table 6.1: Coefficient k as function of the helix diameter and shaft diameter ratio [54]

D_h/D_c	1.25	1.5	2.0	3.0	4.0
k	0.135	0.410	1.04	2.15	2.99

6.2.7. Optimisation helical pile design

Optimisation of the helical pile geometry is carried out for maximising the uplift capacity rather than its compressive or lateral capacity. The optimisation is chosen for maximising the uplift capacity, as it is assumed that the mud-mats can bear the compressive loading. Furthermore, the lateral capacity of the helical piles would already provide enough to bear with the horizontal loading. Some design parameters were assumed to be constant, such as the pitch and helix thickness. However, the shaft and helix diameter, and the shaft thickness are varied to optimise the helical pile. The length of the pile depends on the maximum achievable embedment depth.

Methodology

The derivation of the uplift capacity is a rather complicated process. Given a maximum torque that can be provided during installation, in a set of soil conditions from the benchmark project, the uplift capacity of a helical pile is determined. The maximum uplift capacity depends on the design of the helical pile and the maximum embedment depth of the pile. The embedment depth can be limited by four constraints: the maximum available installation torque, shallow depth criterion (H/D =8), structural shaft requirements or structural helix requirements.

Thereafter, the helix diameter and helix-to-shaft diameter ratio is varied to find the maximum embedment depth that can be achieved, taking the four constraints into consideration. An increase in embedment depth automatically leads to an increase in uplift. A visualisation of the methodology is presented in Figure 6.3.

The soil conditions of the reference project are used for determination of the helical pile uplift, compressive and lateral capacity, and these are shown in Table 6.2. Additionally, it is assumed that the soil conditions, except for the CPT data, are constant over depth and constant for the complete wind

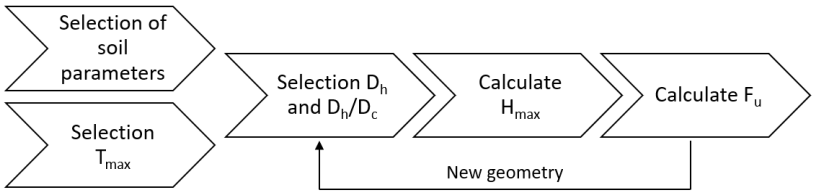

Figure 6.3: Visualisation of methodology for determination of uplift capacity helical pile

farm area. In Figure 6.4 the visualisation of the CPT data is shown, which is similarly assumed to be equal for every location within the wind farm. The graph shows the tip resistance as a function of depth (meters below the seabed).

Table 6.2: Soil conditions used for helical pile capacity determination

Item	Value
Density D_r	82%
Peak friction angle φ_p	45°
Soil-steel interface friction angle δ	24°
Dilatancy angle ψ_p	16.5°
Soil density $\gamma\prime$	10.47 kN/m^3

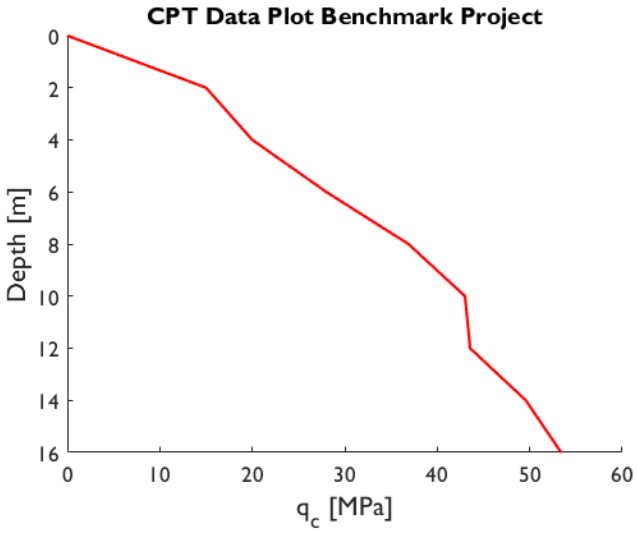

Figure 6.4: CPT data from benchmark project used as input for uplift capacity derivation

7

Loading on Template and Monopile

In this chapter the determination of different loading mechanisms on the monopile and template are described. First, the determination of the environmental loading is discussed, explaining wind, current, and wave loading. Furthermore, the hydrodynamic loading exerted on the template, estimated using the stick model method, is explained. Subsequently, derivations for loading exerted by the template, monopile, and equipment due to inclination is described. To conclude this chapter, the moment distribution is discussed, which uses an uncoupled and coupled analysis. The uncoupled analysis does not account for soil interaction, whereas the coupled analysis does.

7.1. Environmental loading

Environmental loads include loads from wind, currents, and waves, but also from other external forces such as ice floes or forces induced by earthquakes. The wave height and current speed are determined in accordance with the definitions in DNVGL-ST-N001 [14]. It is assumed that the sea bed is impermeable and flat, and that disturbances are of infinite length so that the flow is two-dimensional. Additionally, the fluid is assumed to be homogeneous and incompressible.

Environmental loads have been assessed for the benchmark project. The environmental loading is dominated by wave loading. Wave loading has been assessed using Morison's method, and thereafter compared to software models evaluated by HMC. Two models are conducted by HMC, a diffraction method (WAMIT) and a computational fluid dynamics (CFD) model. Results for the diffraction method are obtained using the frequency domain software LiftDyn. CFD analyses have been performed using the software OpenFOAM v1812. The values of the forces and moments reported are obtained from the average of the maxima of 5 load cycles. The models are performed for the largest diameter monopile (8.9 meters) and the largest water depth (50 meters), as this would result in the highest loading. It is seen that the results of the diffraction analysis and the CFD model are aligned and the Morison is within 10-15 % of the other models (see Appendix B). With the Morison method providing the largest loads and moment. Thus, using the Morison method gives an overestimation of the loading and can be assumed to be a conservative method when calculating the wave loading.

The loading on the installation template is generally considered negligible in the design as it is relatively low compared to the loading experienced by the monopile. The primary reason for this is that the template is fully submerged and has a significant distance from the surface, where the loading is generally the largest. Conversely, the monopile possesses a substantial diameter and length extending from the seabed, through the splash zone and even partially above the water surface. As a result, the monopile is subject to various loads, including wave, current, and wind loading, and therefore experiences significant loading. However, to check whether the assumption of neglecting the loads on the template is valid, an assessment is carried out using a so called stick model (see Section 7.1.5).

Maximum load on the monopile and template take place when the wave particle acceleration is at the maximum, therefore the wave loads are inertia dominated. The Keulegan-Carpenter (KC) number is often utilised to determine if the force is drag or inertia dominated, and therefore used to determine if a component may be neglected. For KC numbers smaller than 3, the force is inertia dominated, and for KC numbers larger than 45, the force is drag dominated. When the KC value is in between, both

drag and inertia terms should be accounted for. However, both terms are evaluated and the inertia coefficient is corrected using the MacCamy-Fuchs method. Subsequently, the force and moment can be calculated, where local hydrodynamic loads are computed using the sectional flow velocity and acceleration, as shown in Figure 7.1.

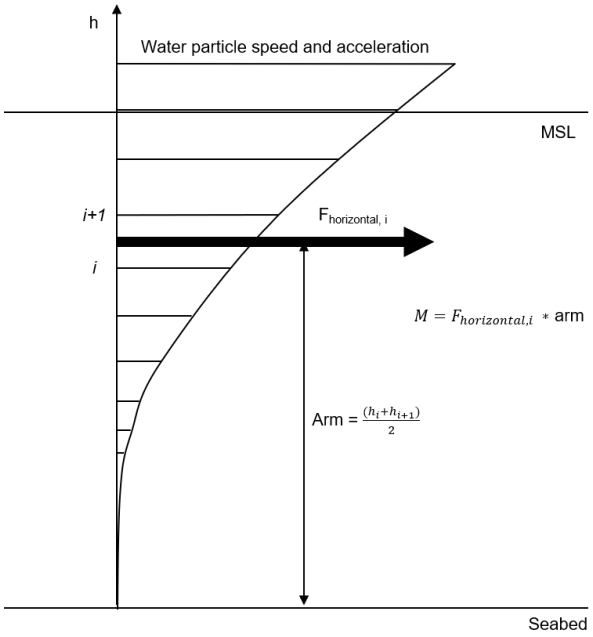

Figure 7.1: Sketch of sectional forces and moments profile

7.1.1. Wind

Wind force is determined by the drag equation as shown in Equation 7.1. The wind profile is assumed to be constant, and set to the mean speed at 10 meter height to determine the load. Wind loads will be acting on the emerged part of the structures. However, in this research, the analysis focuses solely when the template is placed on the seabed, thereby excluding any wind loading on the template itself. Consequently, wind calculations are carried out only for the exposed section of the monopile. The largest monopile size is utilised, with a length of 90 meters and a diameter of 8.9 meters, assuming a constant diameter. Considering a maximum water depth of approximately 50 meters, the emerged portion of the monopile reaches a maximum length of about 40 meters. The reference area used in Equation 7.1 then simply becomes the diameter multiplied with the emerged monopile length.

$$F_{wind} = \frac{1}{2}\rho_{air}U_{wind}^2 C_d A \tag{7.1}$$

Where

ρ_{air} is the air density
U_{wind} is the wind speed
C_d is the drag coefficient
A is the reference area

This wind load on the monopile leads to a moment with respect to the pile bottom, which is shown in Equation 7.2. It is assumed, due to the constant wind velocity, that the load attachment is at the middle of the emerged part of the monopile.

$$M_{wind} = F_{wind}\left(d + \frac{L}{2}\right) \tag{7.2}$$

Where

d is the water depth
L is the length of the emerged part of the monopile

7.1.2. Current

Current velocity is a function of space and time, and its depth profile is usually modelled using the power law, see Equation 5.2. So, current speed strongly depends on depth and is therefore calculated per section, as illustrated in Figure 7.1. The force induced by currents also follows the drag equation, similar to the wind force, as shown in Equation 7.3. The current will exert loads on the template and the submerged part of the monopile, and have been computed for the larger diameter monopile (8.9 meter) and for a water depth of 50 m. The current loading on the template is analysed using the equivalent diameter per section derived with the stick model (see Section 7.1.5).

$$F_c = \sum F_{c,i}\delta h = \sum \frac{1}{2}\rho_{water} U_{c,i}^2 C_d B \delta h \tag{7.3}$$

Where

ρ_{water} is the water density
$U_{c,i}$ is the current speed at section i
C_d is the drag coefficient
B is the reference width of the structure
δh is the height of each section

Using the horizontal load exerted by the current, the moment can be determined with respect to the monopile bottom, which is shown in Equation 7.4.

$$M_c = \sum F_{c,i} h_i \tag{7.4}$$

7.1.3. Waves

To determine the force exerted by waves, the Morison equation is utilised. This equation shows an approximation of the wave force per unit length on a slender tubular, as shown in Equation 7.5. The equation is space and time dependent, as well as it depends on the water depth.

The wave loads in the analysis do not include wave spreading, which refers to the phenomenon where ocean waves disperse and spread out as they travel across the surface of the water, resulting in a decrease in their height and energy density. If wave spreading was taken into account a load reduction could be expected, making the current load evaluation conservative. Similarly, the analysis does not incorporate the effect of wave shielding, where a physical obstacle such as a monopile installation template obstructs and reduces the energy and height of incoming waves. Disregarding the shielding effect also leads to a conservative outcome by not accounting for the potential reduction in loading.

$$F_{waves}(z) = f_d(z) + f_i(z) = \frac{1}{2}\rho_{water} C_d D u(z)|u(z)| + \frac{\pi}{4}\rho_{water} C_M D^2 \dot{u}(z) \tag{7.5}$$

Where

$f_d(z)$ is the drag force
$f_i(z)$ is the inertia force
ρ_{water} is the water density
C_d is the drag coefficient
D is the member diameter
$u(z)$ is the water particle velocity
C_M is the inertia coefficient
$\dot{u}(z)$ is the water particle acceleration

However, if the waves are diffracted by a structure, it is necessary to solve the more complex problem of the incident wave train. MacCamy & Fuchs have solved this problem for a vertical circular cylinder [39]. Using a correction factor on the Morison equation, the diffraction effects on the monopile are taken into account, using Figure 7.2.

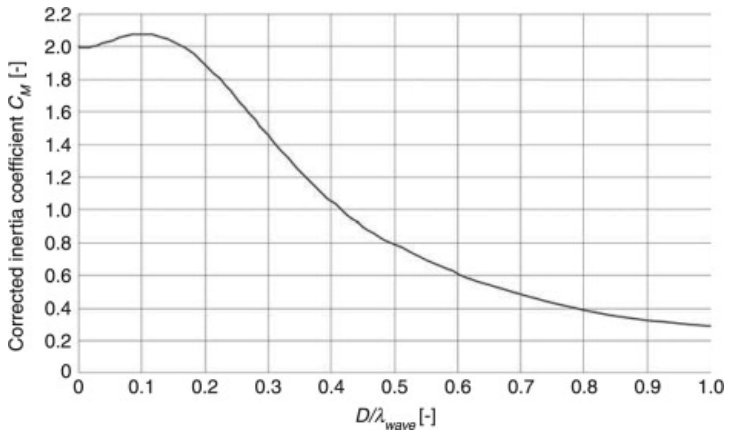

Figure 7.2: MacCamy-Fuchs correction [55]

7.1.4. Other environmental loads

Occasionally, and dependent on the location of the wind farm, other external forces may load the structure. Such forces can be exerted by, for example, ice floes, mudslides, and earthquakes. It is important to acknowledge the potential impact of these external forces on the structural integrity of monopile installation templates and wind farms. While these external forces are not within the scope of this research, their impact can be crucial. Therefore, consideration is important for the assessment and design of wind farms in areas prone to these hazards.

7.1.5. Estimation of hydrodynamic loading on template

Determination of the loads on offshore structures exerted by currents and waves is rather complicated. These structures generally have many members, of different sizes and orientation, and water particle kinematics are nonlinear and depend on time and space. A simplified model, called the *equivalent stick model*, is utilised as an approximation. The equivalent stick model is a summation of all the loads on all tubulars, per range of water depth. This method is utilised to verify the assumption of disregarding the load exerted on the template. Its primary focus is to assess the order of magnitude of the hydrodynamic loading experienced by the template.

The monopile installation template is initially simplified to the structures shown in Figure 7.3. As shown, the hexagon template is represented as a U-shaped, rectangular structure (see top-view in Figure 7.3 a), containing two broadsides (Figure 7.3 b) and one end-on side (Figure 7.3 c). Opposite of the end-on side is the opening of the template, which allows for bringing the monopile into the template. Two load directions are being analysed: one in which the wave attack angle is perpendicular to the broadside, and another in which it is perpendicular to the end-on side.

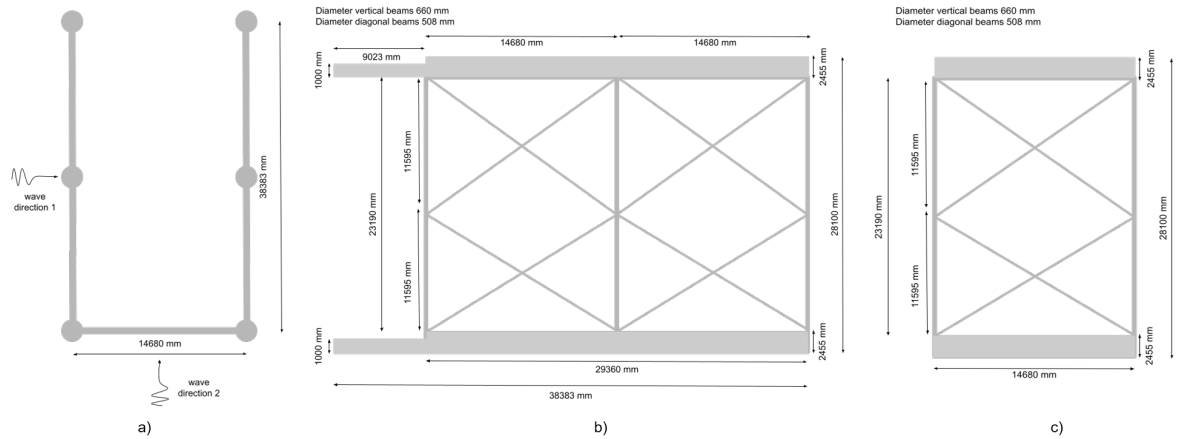

Figure 7.3: Representation of the stick model top-view (a), broadside (b), and end-on side (c)

To determine the equivalent diameter, the diameter of the vertical members can be added up. However, for the diagonal and horizontal members, trigonometrical calculations are required. When the flow is perpendicular to these diagonal and horizontal members, the equivalent diameter of the diagonal members can be calculated using Equation 7.6. Similarly, for perpendicular flow, the equivalent diameter of the horizontal members can be determined using Equation 7.7.

$$D_{eq,i} = \frac{D_i}{\sqrt{\sin\theta_i}} \tag{7.6}$$

$$D_{eq,i} = \sqrt{D_i L_i} \tag{7.7}$$

Where,

D_i is the diagonal of member i
θ_i is the angle of member i
L_i is the length of member i

When the water particles align with the orientation of the members, the horizontal members do not contribute to the loading and are therefore not included in the derivation of the equivalent diameter. However, the diagonal members, with particles flowing along with their orientation, do impact the loading and their contribution is determined using Equation 7.8.

$$D_{eq,i} = D_i\sqrt{\sin\theta_i} \tag{7.8}$$

Thereafter, the equivalent diameter per section in depth is determined and consequently the stick model for the broadside and end-on side are created, as depicted in Figure 7.4. The elevation is zero at the seabed and increases towards the highest point of the template. The equivalent diameter is shown on the x-axis.

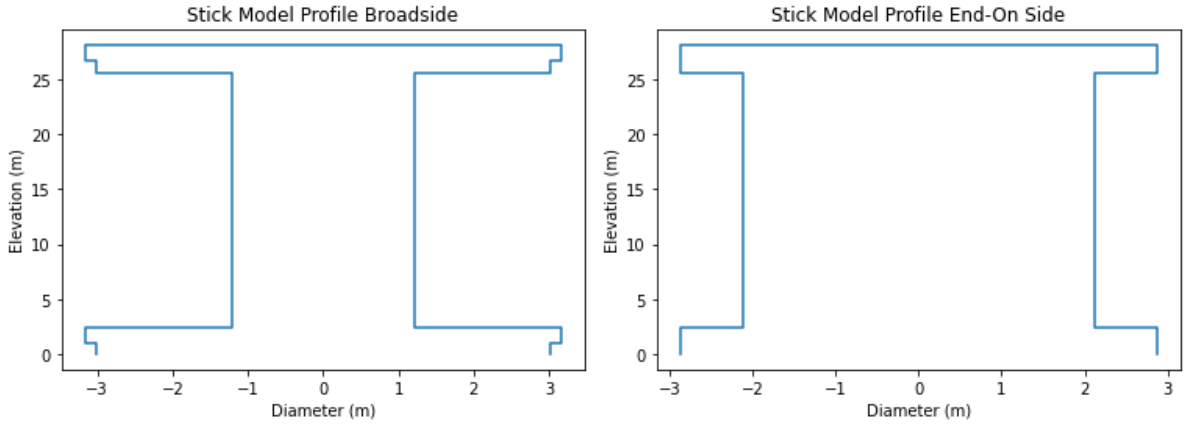

(a) Stick model of the template broadside

(b) Stick model of the template end-on side

Figure 7.4: Equivalent diameter of the template determined with the stick model approach

The equivalent diameter obtained using the stick model approach is used in the Morison equation to determine the loading on the template. The equivalent stick model does not account for different phases on the structure. It assumes maximum loading on every part of the structure at the same time. Therefore, the stick model is a conservative approach. However, the Morison equation is utilised and thus accounts for the phase shift between the drag and inertia load. As the maximum wave particle acceleration is always out of phase with the maximum wave particle velocity, simple addition of these two factors is impossible. The maximum force due to these load components may be approximated by vector addition, as shown in Equation 7.9.

$$f_{max}(z) \approx \sqrt{f_{d,max}^2(z) + f_{i,max}^2(z)} \tag{7.9}$$

7.2. Permanent loading

The Not-To-Exceed Weight (NTEW, 1550 mT submerged) of the template is determined and exerts a vertical loading on the mud-mats, as described in Equation 7.10. It is important to consider the submerged mass, obtained by subtracting the density of water from the density of steel, divided by the density of steel. Generally, the submerged mass of a steel structure is reduced by approximately 15%.

$$F_v = NTEW_{submerged} \cdot g \tag{7.10}$$

7.3. Loading by monopile inclination or crane off-lead angle

In the two load cases that are considered, the monopile inclination and crane off-lead angle cause additional horizontal load and thus additional overturning moment. The mass of the monopile and required tooling is used to determine the horizontal loading, see Equations 7.11 and 7.12. These horizontal forces result in a moment with respect to the lowest point of the monopile, as shown in Equations 7.13 and 7.14. All input parameters are shown in Table 7.1.

$$F_{h,MP} = gW_{MP} \cdot \tan(\beta) \tag{7.11}$$

$$F_{h,T} = gW_T \cdot \tan(\beta) \tag{7.12}$$

$$M_{MP} = F_{h,MP} \cdot L_{MP} \tag{7.13}$$

$$M_T = F_{h,T} \cdot L_T \tag{7.14}$$

Where

W_{MP}, W_T is the mass of the monopile and tools respectively
g is the acceleration of gravity
β is the monopile inclination angle or the crane off-lead angle
L_{MP} and L_T are the length of the arms with respect to the lowest point of the monopile

Table 7.1: Input parameters for off-lead angle and inclined monopile loading derivations

Item	Value
Off-lead angle crane	1°
Inclination angle	0.5°
Self-weight penetration depth	5 m
Weight monopile	1635 mT
Weight lifting tool (FPUT)	110 mT
Weight hammer, sleeve and anvil	743 mT
Acceleration of gravity	9.81 m/s^2
Pile length	90 m
Upper guide (from seabed)	29 m
Lower guide (from seabed)	5 m

7.4. Moment redistribution mud-mats

The maximum load on a mud-mat should not be exceeded, in order to ensure stability. If this maximum capacity is exceeded, the template may not be able to ensure precise installation of the monopile foundations. The overturning moment on the frame, mainly caused by the loads on the monopile, exerts a vertical force on the mud-mats. The horizontal load on the template similarly exerts force on the mud-mats. A sketch of the mud-mat orientation is depicted in Figure 7.5. Two analyses are considered: an uncoupled analysis and a coupled analysis.

7.4.1. Uncoupled analysis

An uncoupled analysis is performed, meaning that the soil-structure interaction is not accounted for. As the stiffness of the template is maximised, it is assumed that the template horizontal load is equally shared among the working mud-mats. Additionally, it is assumed that all mud-mats experience a constant vertical load based on the template's submerged mass. The schematic depicted in Figure 7.5 is used to determine the loads on the mud-mats. The overturning moment caused by environmental loading leads to a decrease in load on two mud-mats, an increase in the two opposite mud-mats, and the load on the two mud-mats in the symmetry axis remain constant. This effect on the mud-mats is visualised in Figure 7.5.

The loads, due to the environmental loading, on the upper and lower guides are used to determine the loading transferred to the mud-mats. Simple force and moment equilibrium equations are used to determine these loads. It is assumed that at the pivot point, the sum of the forces and moments should be equal to zero (see Equations 7.15 and 7.16). Additionally, it is assumed in this derivation that the aligned mud-mats are equally loaded. So, for example, the load on two mud-mats under compression due to the overturning moment are equal.

$$\sum F_y = -F_g + F_{MM,c} + F_{MM,sym} + F_{MM,u} = 0 \tag{7.15}$$

$$\sum M = F_g \cdot L_g + F_l \cdot L_l - F_u \cdot L_u - F_{MM,s} \cdot L_{MM,s} - F_{MM,u} \cdot L_{MM,u} = 0 \tag{7.16}$$

Where,

F_g is the gravitational force exerted by the template's mass
F_{MM} is the vertical force exerted by the mud-mats (compressive, symmetry axis or uplift)
F_u is the force of the upper guide
F_l is the force of the lower guide
L is the arm from the pivot point to the corresponding load attachment

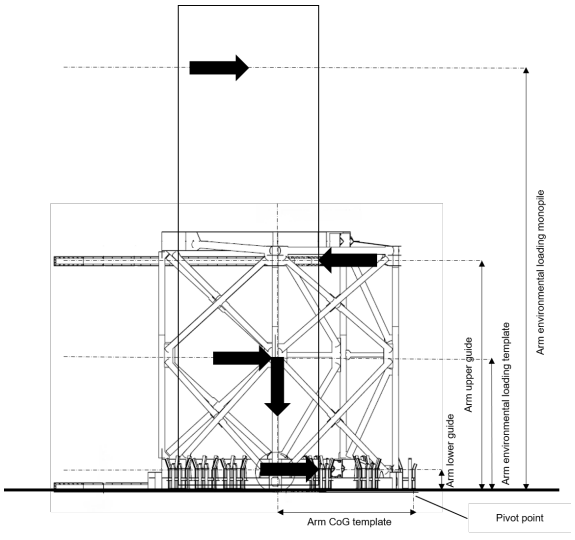

(a) Load application on the template

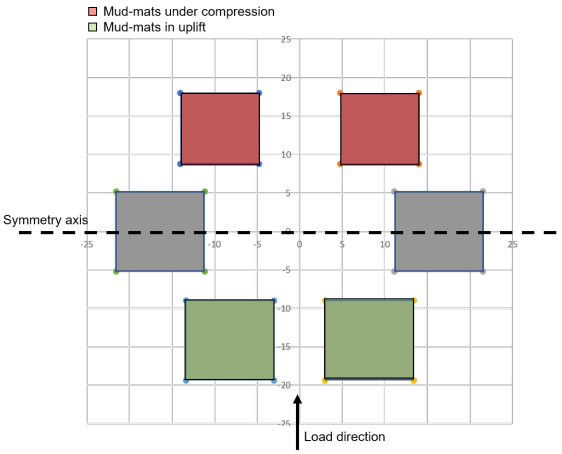

(b) Simplified schematic of overturning moment on template with mud-mat configuration

Figure 7.5: Uncoupled analysis on mud-mat load due to overturning moment

7.4.2. Coupled analysis

With the use of an internally developed software application at HMC, the pressure on the mud-mats due to the environmental loading can be evaluated. This programme calculates the pressure on the foundation mechanism under static loading conditions and takes the soil-structure interaction into account. The mud-mats are represented using a combination of rectangles and triangles, and increasing the mesh density improves accuracy but also increases the computational time required to solve the

analysis. The soil is represented as a spring-system with one axial and one lateral spring per mud-mat. The programme uses stiffness in kN/m^3 as input, so the spring stiffness (kN/m) has to be divided by the mud-mat area. It is assumed that the stiffness is similar for each mud-mat, and thus for each mud-mat type. The two main load cases (load case 2.3 and 3.3) are investigated using different approaches, including variations in the angle of attack (per 45°). The results are validated against the manual calculations explained in Section 7.4.1. An example of the output is presented in Appendix E.

8

Results Benchmark Project

The findings resulting from the input of the benchmark project are presented in this chapter. These sections provide results for the environmental loading, seabed inclination, and loading exerted by the (inclination of) equipment. These results are used to determine the loading on the template for each governing load case, and consequently to determine the load distribution on the mud-mats. Finally, the mud-mat capacity envelopes are shown for both load cases, which include the maximum factored load for both the uncoupled and coupled approach.

8.1. Environmental loading

The total loading can be located in Table 8.1, where each interface load is displayed. The loads are described in detail in the Sections 8.1.1 - 8.1.3.

Table 8.1: Environmental loading on monopile and template

	Force [kN]	**Moment [kNm]**
Monopile		
Wind load	23.5	1644
Current	7.25	205
Waves (T_p of 8 s)	3028	122058
Template (end-on side)		
Wind load	0	0
Current	1.73	27.9
Waves (T_p of 8 s)	88	1730

8.1.1. Wind

The wind load is determined using the drag equation, leading to a wind force acting on the monopile of 23.5 kN. This in turn leads to a moment, with respect to the monopile bottom, of 1644 kNm. For this determination, it is assumed that the monopile has a constant diameter, and the wind speed is also assumed constant over height.

8.1.2. Current

The loading exerted by current is derived for the monopile and leads to a load of 7 kN, and a moment with respect to the seabed of 204 kNm. This is illustrated in Figure 8.1.

The total force exerted by the current on the template broadside is 1.16 kN and the moment therefore is 19.5 kNm, which is 16.0% and 9.52% of the monopile loading, respectively. For the end-on side, the loading is 1.73 kN and the moment therefore becomes 27.9 kNm, which leads to 23.8% and 13.6% of the monopile loading, respectively. The load and moment over depth on the template are illustrated in Figures 8.2 and 8.3.

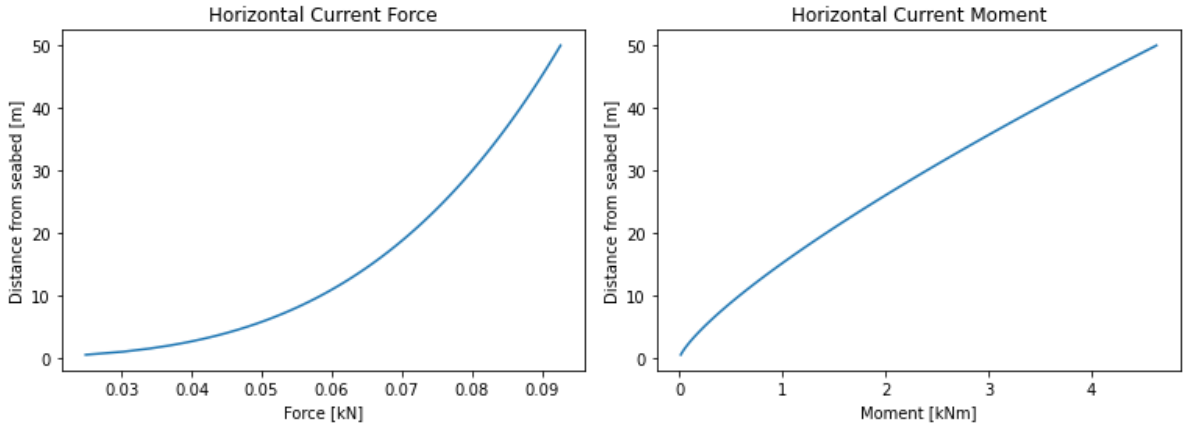

(a) Current horizontal loading

(b) Current horizontal moment

Figure 8.1: Current effects on the monopile

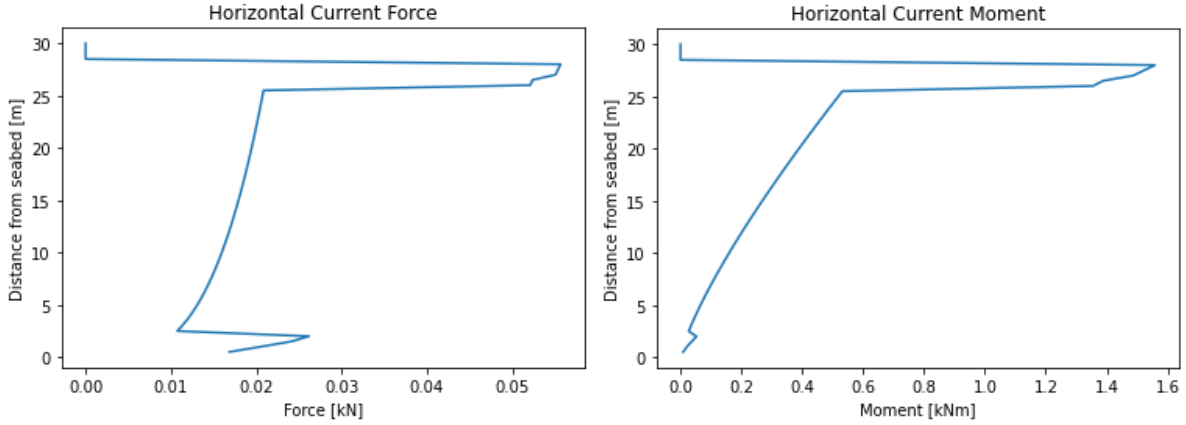

(a) Current horizontal loading

(b) Current horizontal moment

Figure 8.2: Current effects on the template (broadside)

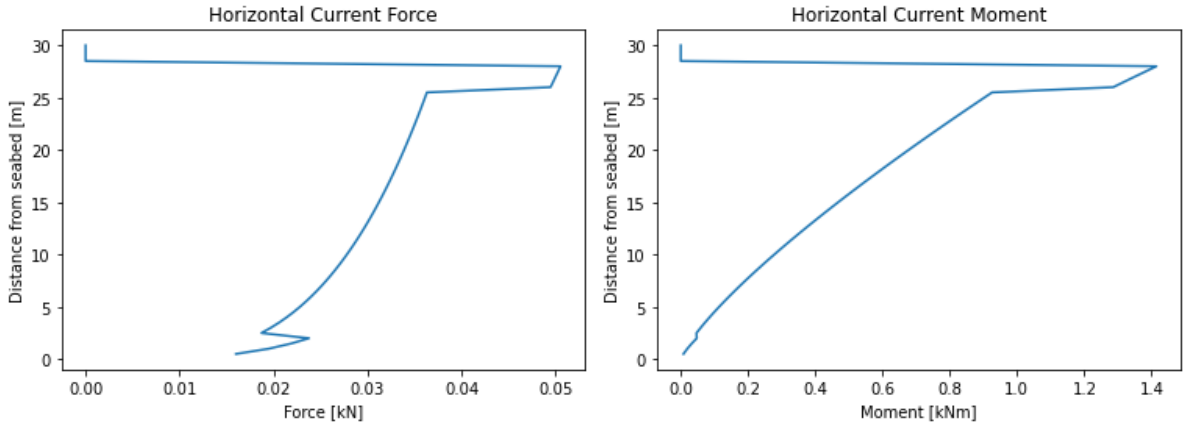

(a) Current horizontal loading

(b) Current horizontal moment

Figure 8.3: Current effects on the template (end-on side)

The total current loading, where the current loading and moment on the template and monopile are added up is shown in Figure 8.4. Note that the loads are added up for the end-on side, as this leads to the highest total loading.

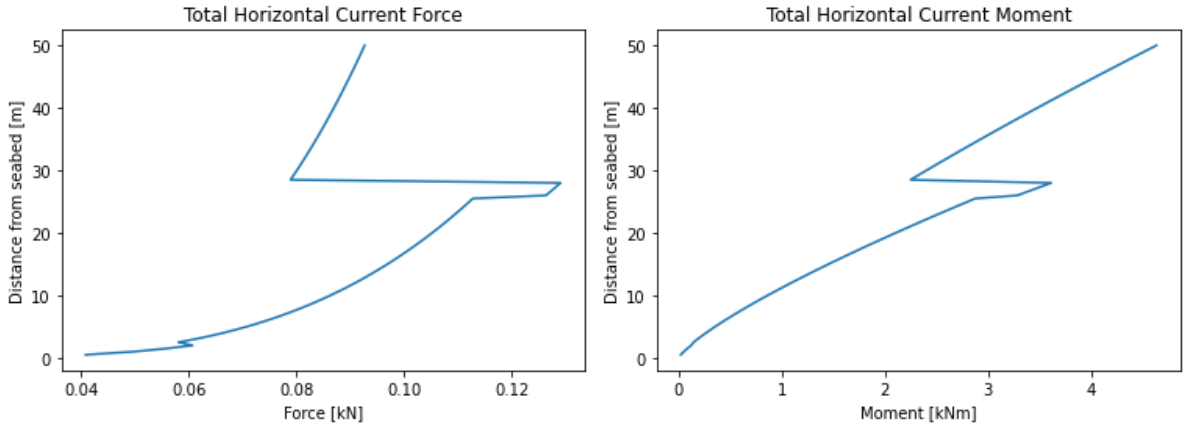

(a) Current horizontal loading

(b) Current horizontal moment

Figure 8.4: Total current effects (on the monopile and template combined)

8.1.3. Waves

The wave loading is determined for the loading on the monopile and template. The results are shown below, see Table 8.2. The derived wave loads are checked with the software models, WAMIT and CFD, and the results are shown in Appendix B. Note that this result represents for flow perpendicular to the end-on side, in which the loading on the template is largest. Moreover, the wave loading, displayed in Table 8.2, is calculated with the MacCamy correction for the monopile, but this correction is not applied to derive the loading on the template.

Table 8.2: Wave loading on monopile and template for varying peak period

	Force [kN]	**Moment [kNm]**
Monopile		
T_p of 6 s	2440	109754
T_p of 7 s	2839	120579
T_p of 8 s	3028	122058
T_p of 9 s	3083	117199
T_p of10 s	3087	111103
Template (end-on side)		
T_p of 6 s	22	481
T_p of 7 s	50	1038
T_p of 8 s	88	1730
T_p of 9 s	133	2481
T_p of 10 s	178	3152

8.2. Governing load cases

The loading on the two governing load cases is determined. This leads to the following total loading, shown in Table 8.3. This result is shown for a peak period of 8 seconds, as this results in the highest environmental loading. The LRFD factor is determined using DNVGL-ST-N001 for steel structures subject to ULS loading. Note that the load due to inclination and off-lead angle also is determined as *environmental loading* and thus has the same LRFD factor as the environmental loading [14]. This is assumed because the inclination is caused by environmental conditions. The loading on the upper and lower guides are determined using a moment equilibrium around the bottom of the monopile, which has to equal zero. The negative sign in front of the horizontal load on the lower guide, for load case 2.3, means that the load direction is in opposite direction.

Table 8.3: Results environmental and non-environmental loading (T_p 8 seconds)

	Load case 2.3		Load case 3.3	
Item	**Fh [kN]**	**M [kNm]**	**Fh [kN]**	**M [kNm]**
Waves and current MP	3028	122058	3028	122058
Wind	23.49	1644	23.49	1644
Waves and current template	89	1730	89	1730
Off-lead angle crane	299	26892	0	0
Inclination MP	0	0	204	11006
Total (unfactored)	**3439**	**152324**	**3344**	**136321**
LRFD factor	1.3	1.3	1.3	1.3
Total (factored)	**4471**	**198022**	**4347**	**177217**
Horizontal load lower guide	-2848	-	0	-
Horizontal load upper guide	7319	-	6111	-

8.2.1. Seabed inclination

The effect of the maximum inclination of the seabed on the vertical and horizontal loading is shown in Table 8.4. The vertical loading and horizontal loading decreases and increases, respectively, for an increasing seabed inclination angle.

Table 8.4: Vertical and horizontal loading for inclined seabed

Load case	Inclination [°]	Vertical load [kN]	Horizontal load [kN]
LC 2.3	0	15205.50	4471.08
	1	15203.18	4471.76
	2	15196.24	4473.81
	3	15184.66	4477.22
LC 3.3	0	15205.50	4347.29
	1	15203.18	4347.95
	2	15196.24	4349.94
	3	15184.66	4353.26

8.2.2. Loading on mud-mats

The loading experienced by the template is transferred via the mud-mats into the soil. Two approaches were utilised to determine the loading on the mud-mats, an uncoupled and a coupled method, for which the results are shown in Table 8.5. The uncoupled method shows that the two mud-mats facing uplift axial loading due to the environmental loading, have negative vertical loading. This indicates that the mud-mats experience uplift and are thus disconnected from the soil. When there is no contact with the seabed, no load transfer is possible. As a result, the vertical and horizontal loads are distributed among the remaining mud-mats.

Table 8.5: Vertical and horizontal load on mud-mats using two approaches: an uncoupled and coupled method

	Uncoupled		Coupled	
	Fv [kN]	**Fh [kN]**	**Fv [kN]**	**Fh [kN]**
Load case 2.3				
Mud-mat A	6056	1118	3640	642
Mud-mat B	6056	1118	4043	808
Load case 3.3				
Mud-mat A	5420	1087	3608	624
Mud-mat B	5420	1087	4008	785

8.3. Mud-mat capacity

The results of the uncoupled and coupled analyses are used to determine the load on the mud-mats. The largest vertical force on mud-mat type A is searched for, for each load case and wave direction. The corresponding maximum factored load is thereafter used to plot a red and purple dot, for the coupled and uncoupled approach respectively. The capacity envelopes are shown in Figure 8.5 for load case 2.3 and 3.3 for mud-mat type A, the smallest mud-mat. Note that in these calculations, the filter layer is still present and therefore the friction angle of this layer is utilised.

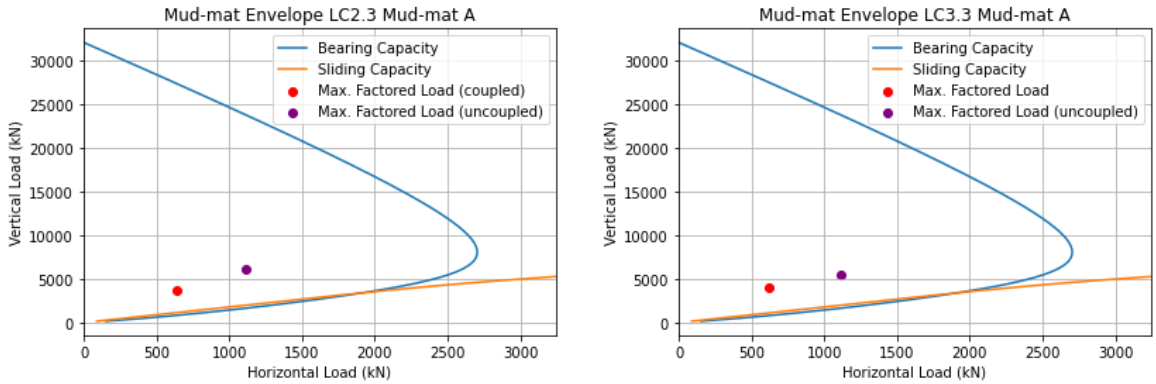

(a) Bearing and sliding capacity of load case 2.3, mud-mat A

(b) Bearing and sliding capacity of load case 3.3, mud-mat A

Figure 8.5: Bearing and sliding capacity envelopes for different load cases

9

Results Helical Piles

This chapter presents the optimisation of the helical pile geometry, and the resulting helical pile capacities. Furthermore, it describes the modification to the loading on the mud-mats, when helical piles are incorporated into the foundation system. From this point on, only load case 2.3 is considered as it turned out to be governing load case, as the findings showed in Chapter 8. Moreover, the seabed inclination is neglected, as its influence is not significant.

9.1. Optimised geometry

The optimisation for maximum uplift led to a diameter of the helical plate of 1.2 meter. The helical pile properties, following from this optimisation process, are shown in Table 9.1. The ratio of D_h/D_c is optimised and equal to 1.5, which corresponds to a shaft diameter of 0.8 meters. Therefore, grouping effects are not considered, as the distance between the helical piles will be larger than three times the diameter. The soil parameters derived from the benchmark project are employed. The maximum installation torque onshore is currently slightly over 10 MNm. However, the required equipment's mass and dimensions is significant and therefore it is assumed that 8 MNm can be achieved offshore. Furthermore, to maintain the shallow foundation failure mechanism, the H/D ratio is established at a maximum of 8.

Table 9.1: Helical pile properties (note that the numbers are rounded)

Item	**Value**
D_c	0.8 m
D_h	1.2 m
t_c	0.014 m
t_h	0.1 m
Length shaft	9.6 m
Steel (grade 350)	7850 kg/m^3
Mass shaft	2669 kg
Mass plate	493 kg
Mass helical pile	3162 kg
Installation tool (see Appendix D.6)	50000 kg
Total mass (6 piles and 6 tools)	318974 kg (319 mT)

9.1.1. Optimal design for constant installation torque

The uplift capacity and installation depth are depicted in Figure 9.12, as a function of both the helix diameter and Dh/Dc ratio. Results are shown for a constant maximum installation torque of 8 MNm. These results are used to determine the optimal helix diameter and the optimal Dh/Dc ratio. The maximum uplift capacity can be obtained by the using a helix diameter of 1.2 meters and a ratio of 1.5, as shown in Figure 9.1.

The lower Dh/Dc ratios are limited by the maximum installation depth to ensure a shallow failure mechanism is maintained. In the case of higher Dh/Dc ratios, the core diameter is relatively small and thus restricted by the structural requirements, presumably buckling. When large helix diameters are used in combination with high ratios, the uplift capacity is likely limited by the bending of the helix plate. Conversely, for low ratios, the core diameter is larger, and the maximum achieved installation depth is limited by the available maximum installation torque. Consequently, this limited installation depth leads to a lower maximum uplift capacity.

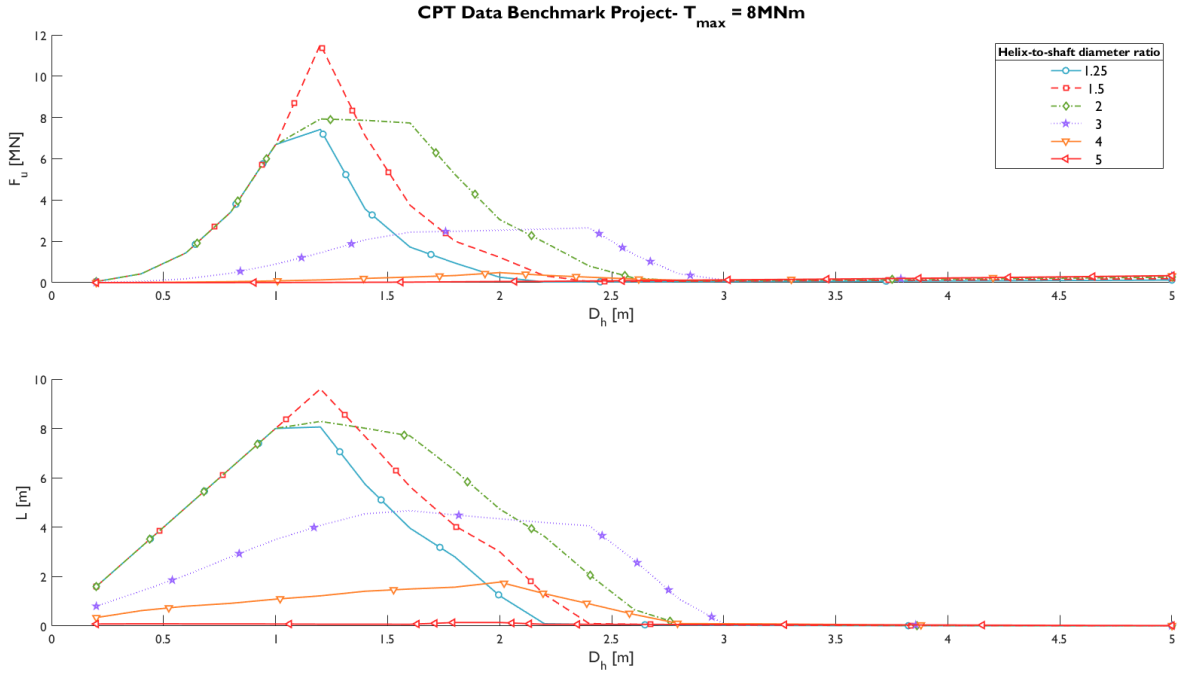

Figure 9.1: Uplift capacity and installation depth for a maximum installation torque of 8 MNm

9.1.2. Optimal design for varying installation torque

Figure 9.2 demonstrates the relationship between a varying installation torque and the uplift capacity, and geometry parameters of a helical pile. The graph shows that an increase in maximum installation torque directly results in a higher uplift capacity. Similarly, an increasing torque results in a larger optimal helix diameter. Conversely, the optimal D_h/D_c ratio decreases for an increasing installation torque, as the structural requirements of the shaft and helix plate become more limiting. It can be observed that for a maximum installation torque above 6 MNm, the optimal helix diameter and ratio no longer change. Consequently, it is assumed that no further optimisation of the geometry can enhance the maximum uplift capacity under these specific soil conditions.

9.2. Helical pile capacity

9.2.1. Uplift capacity

The analysis of the helical pile's uplift capacity revealed that the maximum capacity is limited by the depth-to-diameter ratio. In this study, the maximum installation depth is reached at 9.6 meters, which is 8 times the helix diameter. This shallow failure constraint directly affects the maximum uplift capacity of the helical pile, as illustrated in Figure 9.3. In Figure 9.3 (a), the maximum applicable torque is shown as a possible constraint. The required torque for installation over depth is shown in the figure. It can be observed that the maximum torque is not yet reached. Figure 9.3 (b) displays the crowd force ($F_{y,c}$), the uplift capacity (F_u), and the critical buckling force (F_{cr}). This critical buckling force shows for which compressive load buckling occurs, which is visualised by the dotted horizontal line. It can be observed that buckling does not occur. Finally, Figure 9.3 (c) shows the stresses in the helix and shaft. The equivalent stress of the shaft during installation ($\sigma_{eq,c}$), bending stress in the plate (σ_x), and

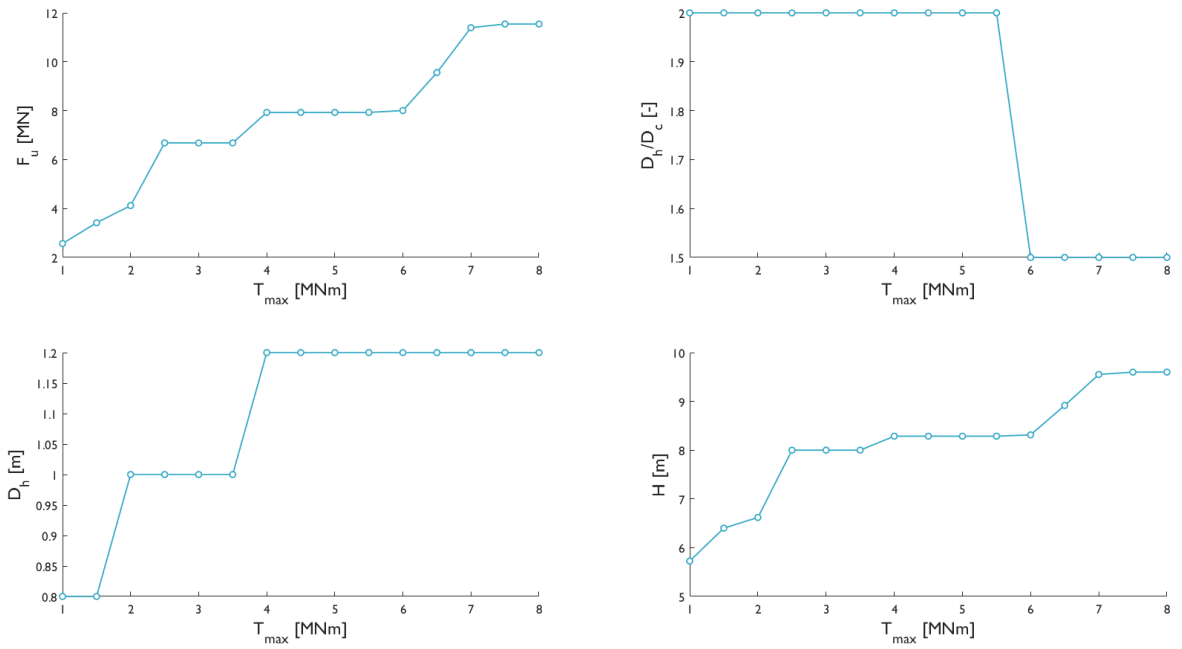

Figure 9.2: Optimal configuration for uplift capacity, D_h/D_c ratio, helix diameter, and installation depth for varying torque

the equivalent stress inside the weld joint ($\sigma_{eq,w}$) are depicted. All the stresses must be lower than the yield strength, or failure might occur. It can be observed that the equivalent stress in the shaft during installation is close to the yield strength, and thus is close to potential failure. Based on these considerations, the maximum uplift capacity determined for this helical pile is found to be 11.7 MN (Figure 9.3 (b)).

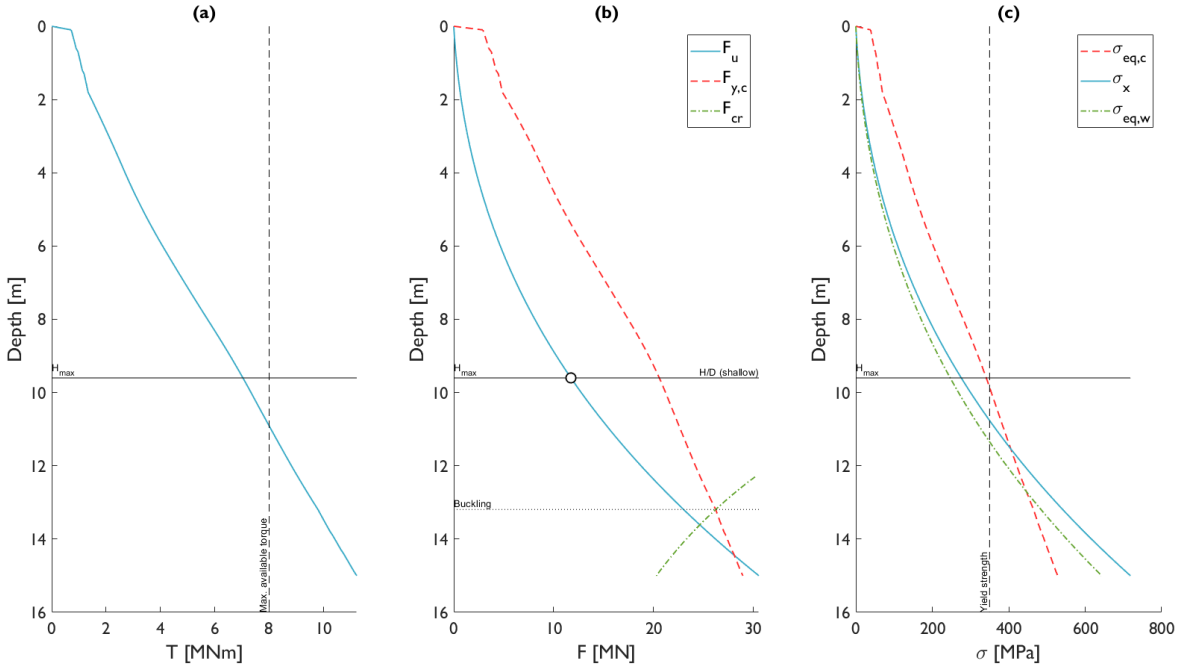

Figure 9.3: Determination of maximum embedment and uplift capacity of helical pile

9.2.2. Compressive capacity

Subsequently, the compressive capacity of the helical pile could be derived. All the parameters used to determine the uplift capacity are also applied in assessing the compressive capacity. The compressive capacity depends on the helix diameter and the D_h/D_c ratio. Additionally, the embedment depth of the pile affects the capacity and this depth depends on the helix diameter. The compressive capacity, as a function of varying helix diameter is shown in Figure 9.4. The optimised helix geometry (for uplift) corresponds to a maximum compressive capacity of 2.00 MN. Note that around 85% of the total capacity is acquired by the helix, and the remainder by the shaft of the helical pile.

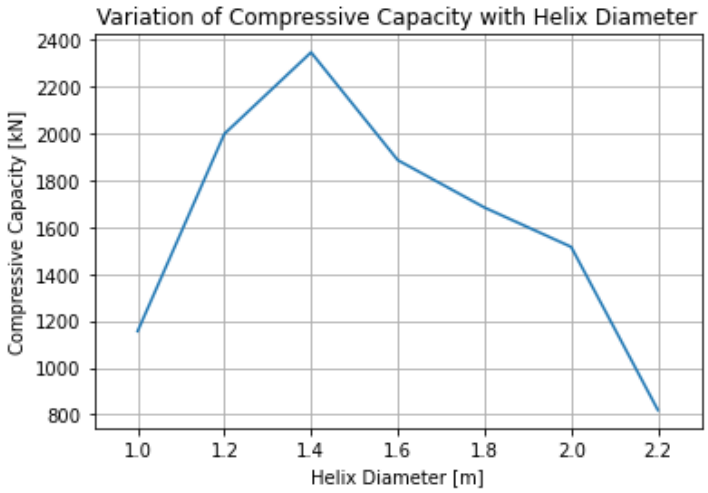

Figure 9.4: Compressive capacity with varying helix diameter

9.2.3. Lateral capacity

The determination of the lateral capacity of a helical pile in sand is a rather difficult process. Therefore, the lateral capacity of a standard pile is determined and the diameter is taken as variable, using API standards [4]. This shows the possible influence of the helix plate to the shaft, leading to a higher lateral capacity with an increasing diameter. Additionally, the installation depth of the pile influences the lateral capacity. Similarly, an increasing installation depth leads to an increasing capacity. Figure 9.5 shows the result of the lateral capacity with an varying diameter and for a varying installation depth. To determine the total lateral capacity, the integral of Figure 9.5b is taken. This results in a lateral capacity of 4.34 MN.

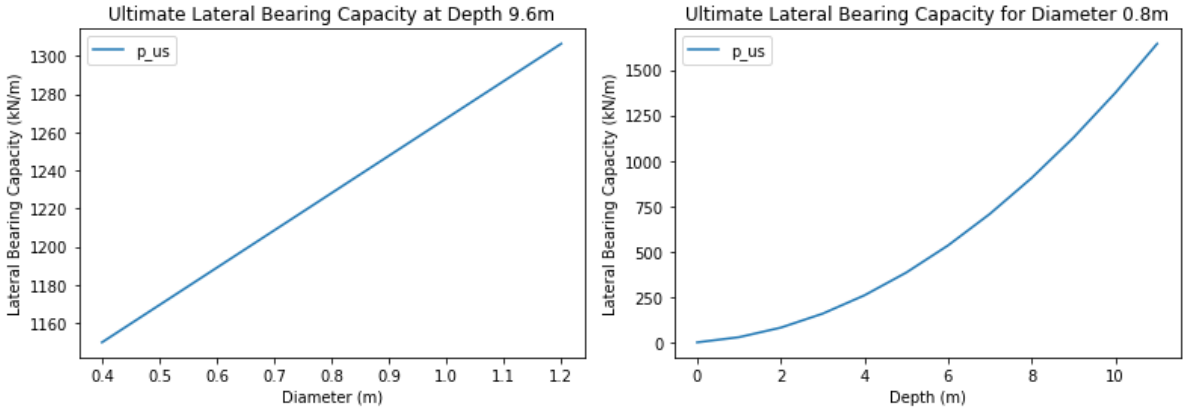

(a) Lateral capacity of a standard pile with a varying diameter

(b) Lateral capacity of a standard pile with a varying installation depth

Figure 9.5: Ultimate lateral capacity of a pile

However, as stated, this API method appears to be optimistic at greater depths (usually depths larger

than five pile diameters). Therefore, the lateral capacity is determined using the analytical approach (Equation 6.14). The ultimate lateral capacity is 2.17 MN, for a standard pile of 0.8 meters in diameter and embedded to 9.6 meters.

The structural strength checks showed that the deformation of the pile is maximum 2.5% of the total length (embedment) of the pile. Additionally, it appeared that for the ultimate resistance the maximum bending stress exceeds the maximum allowable stress by a factor 2 [3], and therefore it can be expected that the pile could fail (see Appendix D). Nevertheless, it is assumed that the rigid body assumption is acceptable because the chance of having such a significant lateral loading is very small. Additionally, the deformation is not significant for this maximum loading. The bending stress can be optimised if required, for example by enlarging the shaft thickness. The bending stress should be checked if the significant lateral loading on the pile might occur.

9.3. Influence on loading and capacity of mud-mats

The introduction of helical piles into the monopile installation template design alters the loading behaviour on the mud-mats, as illustrated in Figure 9.6. It is assumed that the helical pile stabs through the centre of the mud-mat, and the area of the mud-mat is not affected. The load distribution can be explained as follows: the vertical compressive load is supported by both the mud-mat and the helical pile. However, in the case of uplift loading on the leg, and thus on the mud-mat and helical pile, only the helical pile can bear this load. Additionally, the helical pile uplift capacity ensures the mud-mats remain in contact with the seabed, and therefore the load is distributed among all six mud-mats for the uncoupled approach instead of four. This leads to a decrease in maximum factored loading, which shifts the factored load to a more preferable location in the capacity envelope plots. The vertical load, on mud-mat A for load case 2.3, reduces to 5562 kN. Similarly, the horizontal load to decreases, to 745 kN.

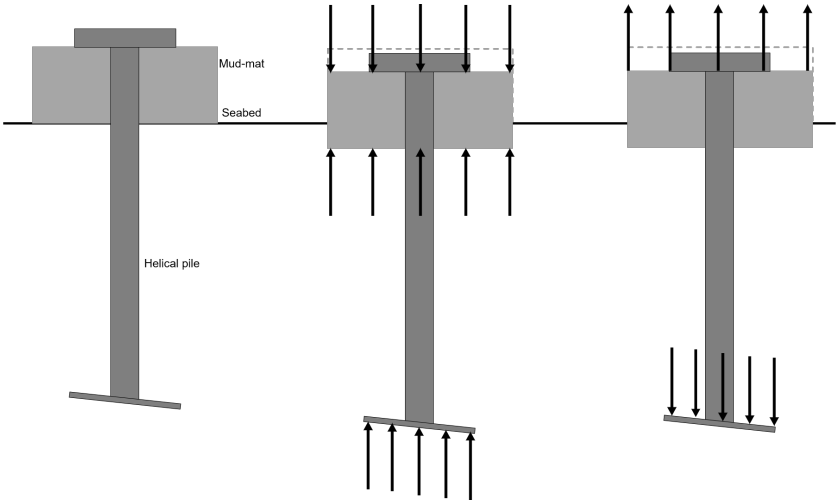

Figure 9.6: Schematic of helical pile connection to mud-mat, and its assumed load distribution

The compressive capacity is added to the bearing capacity plot of the mud-mats, see Figure 9.7, to illustrate the potential impact of introducing helical piles to the foundation system. It is assumed that the capacities can be simply added. The extra capacity provided by the helical piles does affect the envelope concerning its horizontal load dependency. It is assumed that the ratio is maintained, and thus the shape of the envelope remains the same.

The additional lateral capacity of the helical pile can also be included into the mud-mat capacity envelope plot, as shown in Figure 9.8. The helical pile provides additional lateral capacity, which is simply added to the mud-mat lateral capacity. However, as the interaction between these two mechanisms is unclear, and a lot of assumptions were made, the chance of overestimation is significant. Therefore, the lateral capacity obtained by the mud-mat is neglected, as the helical pile is assumed to be rigid and has a fixed head due to the connection to this mud-mat. Subsequently, the capacity envelope obtains the following plot, as shown in Figure 9.9, with a lateral capacity solely from the helical pile capacity.

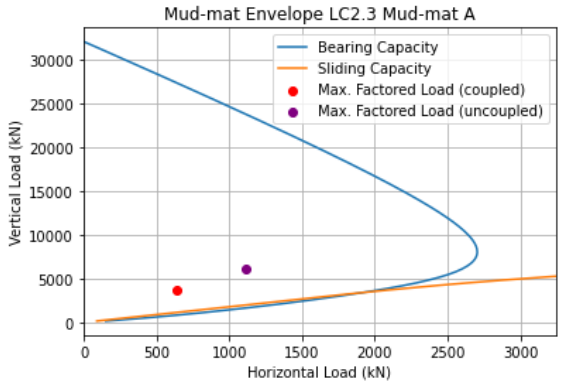

(a) Mud-mat A without helical piles (note, there is a filter layer present)

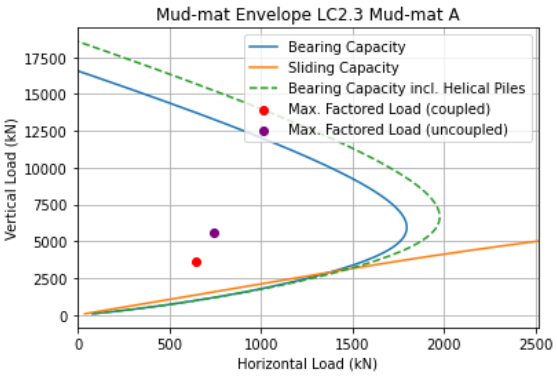

(b) Mud-mat A with helical piles

Figure 9.7: Mud-mat capacity envelope for load case 2.3 without and with compressive helical pile capacity

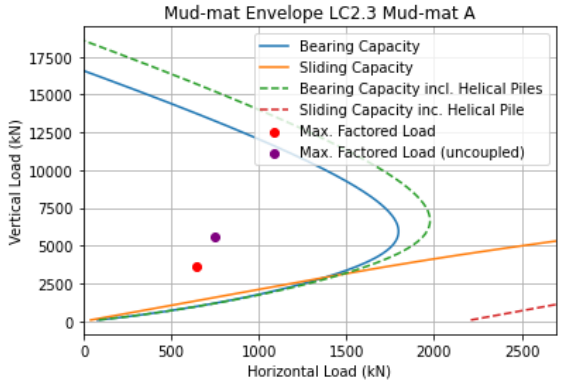

(a) Mud-mat A

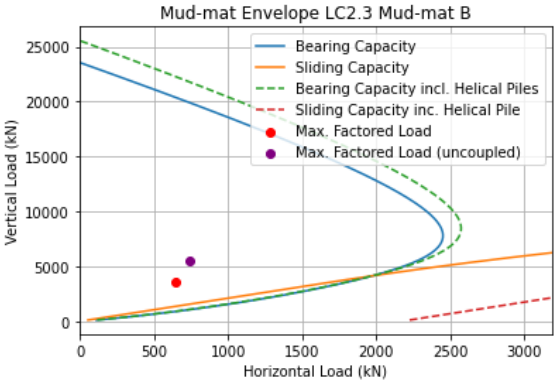

(b) Mud-mat B

Figure 9.8: Mud-mat capacity envelope for load case 2.3 with compressive and lateral capacity of helical pile

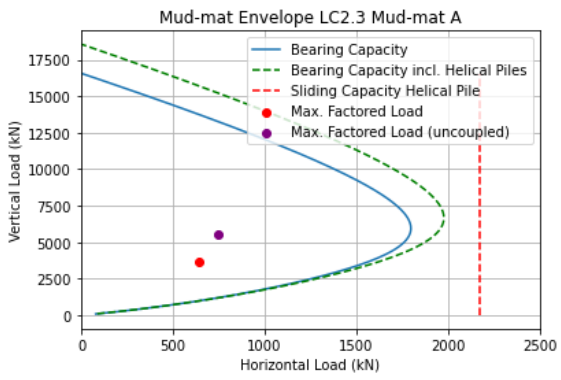

(a) Mud-mat A

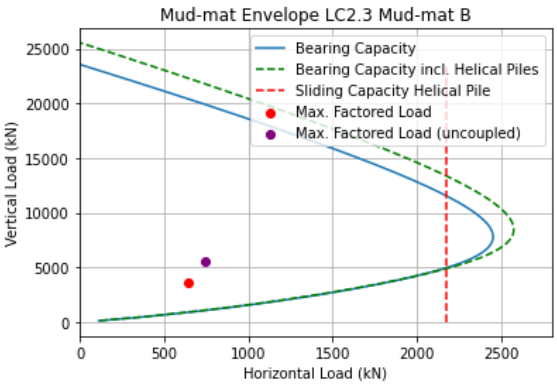

(b) Mud-mat B

Figure 9.9: Mud-mat capacity envelope for load case 2.3 with helical pile capacity, without sliding capacity of mud-mats

10

Parameter Variations to Assess Influence on Performance

This chapter introduces and discusses a series of experiments conducted to assess the impact of variations to the template, mud-mats, helical piles, and soil parameters on the overall system performance. This leads to new load combinations, which in their turn are used to update the capacity envelopes. Only mud-mat type A is shown, the smaller sized mud-mat. These plots give useful insights in the capacity of the mud-mat as well as the maximum factored load that the mud-mat can experience for that specific load case. Similarly, the behaviour of helical piles due to design and soil variations are presented. The findings are summarised in the last section of this chapter. The maximum factored loads, utilised for the derivation of the capacity envelope plots with a reduced template mass and size, are displayed in Table 10.1.

Table 10.1: Load on mud-mats using two approaches: an uncoupled and coupled method. Input for design variations

	Uncoupled		**Coupled**	
	Fv [kN]	**Fh [kN]**	**Fv [kN]**	**Fh [kN]**
Load case 2.3				
Mud-mat A	5562	745	3640	642
Load case 2.3 - 10% mass reduction				
Mud-mat A	5308	745	3394	642
Load case 2.3 - 20% mass reduction				
Mud-mat A	5055	745	3148	642
Load case 2.3 - 30% mass reduction				
Mud-mat A	4802	745	2906	642
Load case 2.3 - 40% mass reduction				
Mud-mat A	4548	745	2861	642
Load case 2.3 - 13.6% size reduction				
Mud-mat A	5939	745	3852	644
Load case 2.3 - 13.6% size and 30% mass reduction				
Mud-mat A	5179	745	3105	645

10.1. Soil characteristics

In Figure 10.1, the effective unit weight and friction angle are varied to show their influence on the bearing and sliding capacity of the mud-mats. It can be observed that higher effective unit weights of sand result in increased bearing capacity, but the influence on the sliding capacity is negligible. The soil of the benchmark project has a unit soil weight of 10.47 kN/m^3. Looser sands correspond to the lower unit weight of soil values, and dense sand to the higher values. Similarly, the denser soils have higher angles for internal friction. The friction angle of the benchmark project is 31.6°, and concerns the

friction angle of the seabed (so no filter layer is present). The bearing and sliding capacity increases with an increasing friction angle.

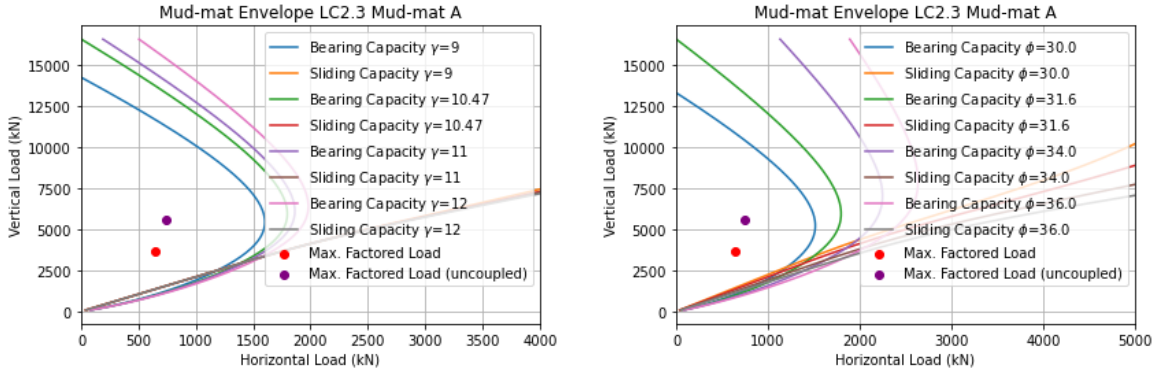

(a) Varying effective unit soil weight

(b) Varying friction angle

Figure 10.1: Mud-mat capacity envelope for load case 2.3 with varying soil conditions

The soil parameters are also varied to understand their influence on the helical pile behaviour. The investigated behaviour focuses on uplift, compressive and lateral capacity as well as on the installation requirements. Below, depicted in Figures 10.2 - 10.5, results of the uplift and embedment depth as a function of helix diameter and the helix-to-shaft diameter ratio are shown, for increased soil properties. The effective unit weight is increased to 12 kN/m^3, the peak friction angle to 50°, the interface friction angle to 30°, and the dilatancy angle is increased to 20°. The uplift capacity increases to 13.2 MN (+12.8%) for an increased unit weight, and raises to 13.1 MN (+12%) for an increased friction angle. An increase in interface angle negatively affects the embedment depth and thus uplift capacity. As a result, the uplift capacity for an interface angle of 30° corresponds to 7.82 MN (-33.2%). The increased dilatancy angle leads to an increase in uplift capacity to 13.5 MN (+15.4%).

The compressive and lateral capacity increase to 2.29 MN (+14.6%) and 2.49 MN (+14.6%), respectively, for an effective unit weight of 12 kN/m^3. Similarly, an increase can be observed for an increasing friction angle to 50° which leads to a compressive capacity of 4.32 MN (+116%). The lateral capacity increases for an increasing friction angle, to 2.53 MN (+16.8%). It is important to note that for the updated determination of the compressive and lateral capacity the achieved installation depth, depicted in Figures 10.2 - 10.4, is utilised.

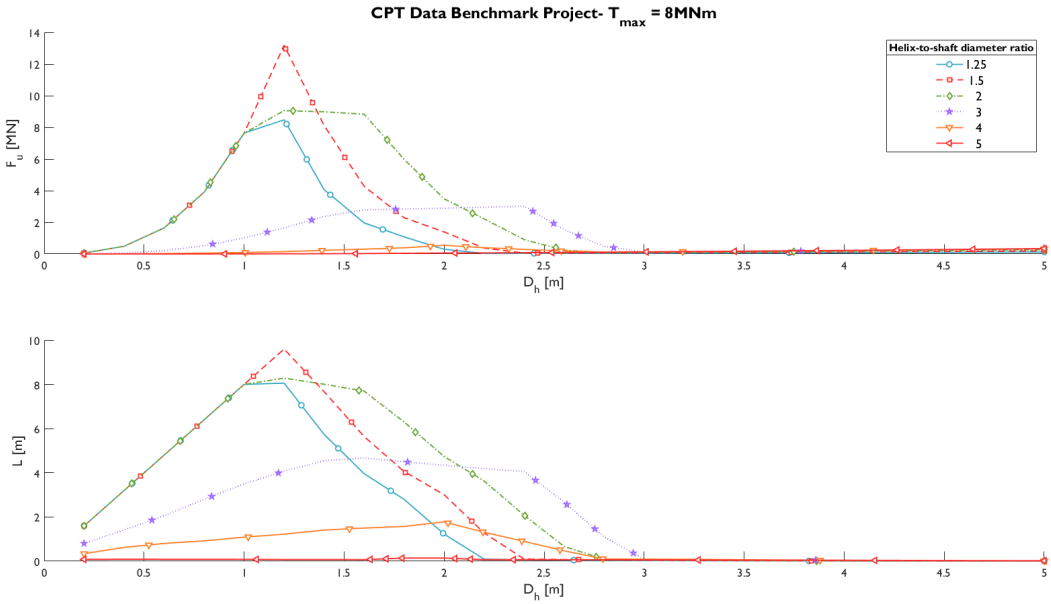

Figure 10.2: Uplift capacity and installation depth for a maximum installation torque of 8 MNm, with increased unit weight

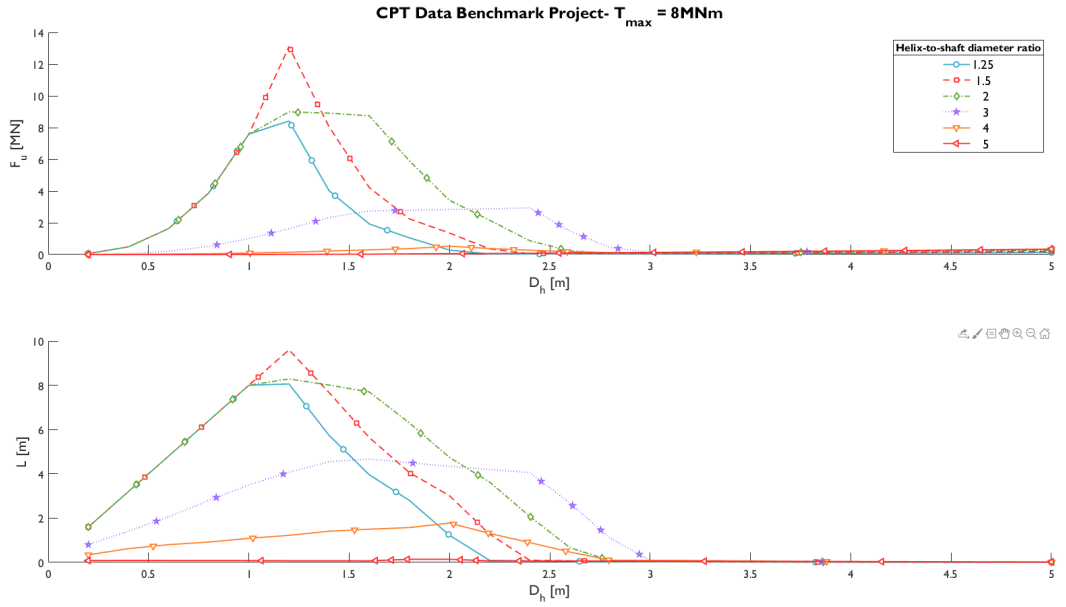

Figure 10.3: Uplift capacity and installation depth for a maximum installation torque of 8 MNm, with increased friction angle

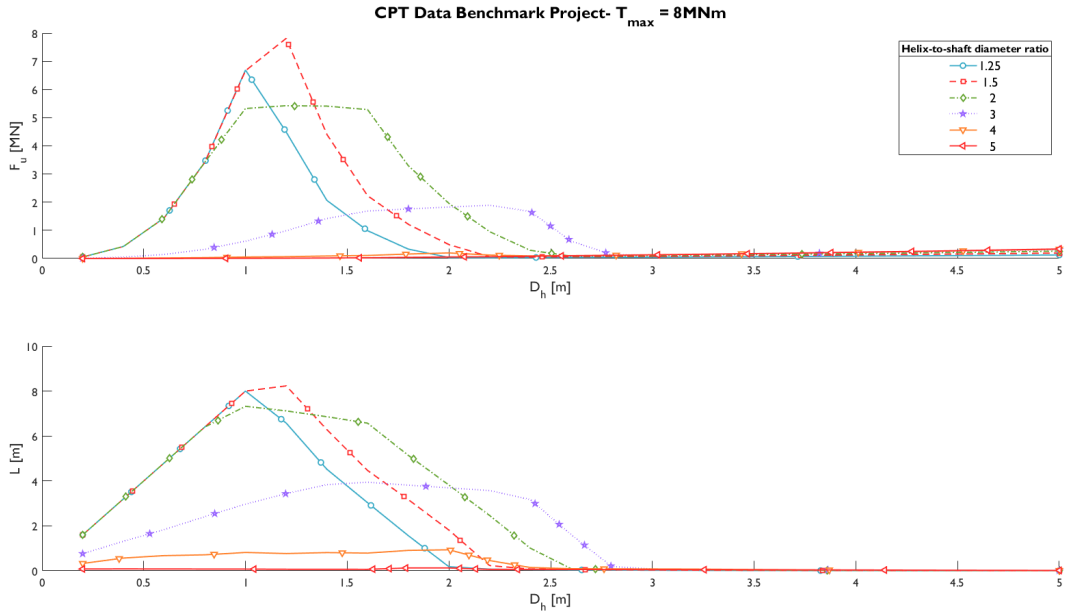

Figure 10.4: Uplift capacity and installation depth for a maximum installation torque of 8 MNm, with increased interface angle

10.2. Helical pile geometry

The geometry of the helical pile is varied to see the influence on the helical pile behaviour. The helix plate thickness and shaft thickness are increased, as illustrated in Figures 10.6 and 10.7. The helix plate thickness is increased to 0.2 meters. It can be observed that the uplift capacity deteriorates to 9.12 MN (-22.1%). This is caused by the fact that the embedment depth is now limited by the equivalent stress in the shaft exceeding the yield stress. The obtained embedment is reduced to 8.75 meters. The increase in helix thickness also has a negative influence on the installation requirements, as both the torque and crowd force increase for an increasing helix thickness. The shaft thickness is increased to the practical maximum, 10% of the shaft diameter. This shows no influence on the uplift capacity, and little influence on the installation and torque requirements. It is important to note that the

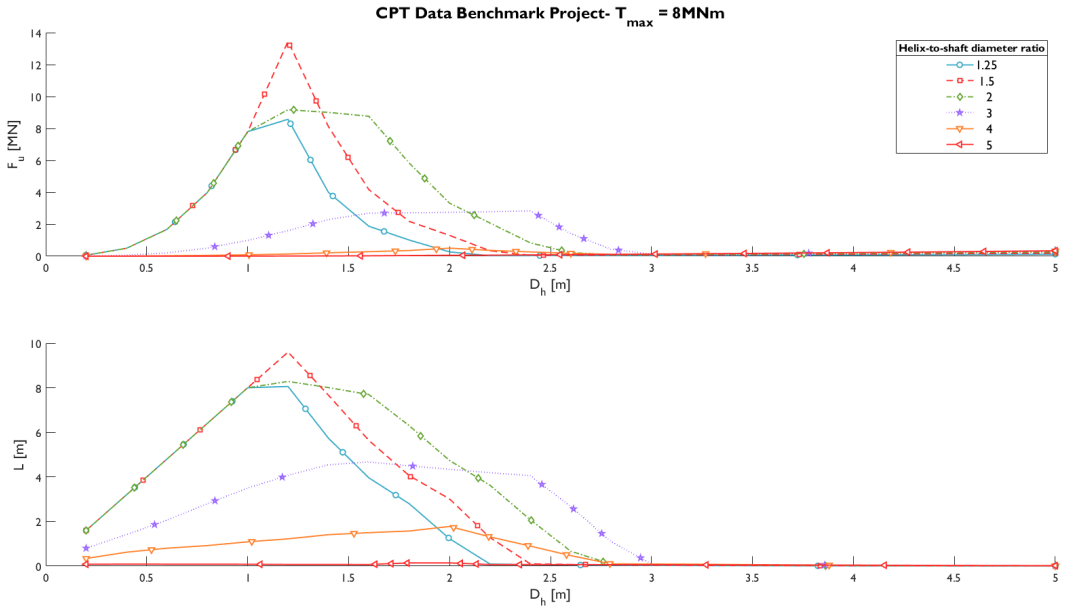

Figure 10.5: Uplift capacity and installation depth for a maximum installation torque of 8 MNm, with increased dilatancy angle

structural strength of the helical pile does increase. The shaft and helical thickness are not considered in the determination of the compressive and lateral capacity, and thus assumed to have no influence on their performance. The helical pile is optimised for maximum uplift capacity, and therefore varying the helix diameter, shaft diameter, and pile length have a negative influence on the performance. The helix diameter positively influences the compressive capacity. If the helical diameter is enlarged to 1.5 meters, the compressive capacity raises to 3.02 MN (+51.2%). The helix diameter is not considered in the derivation of the lateral capacity and therefore also not considered in this design variation. It is assumed that enlarging the helix diameter has little influence on its lateral performance. An increase in shaft diameter leads to a deterioration in compressive capacity. If the shaft diameter is enlarged to 1 meter, the compressive capacity decreases to 794 kN (-60.3%). The lateral capacity increases to 2.71 MN (+1%), and thus has little influence.

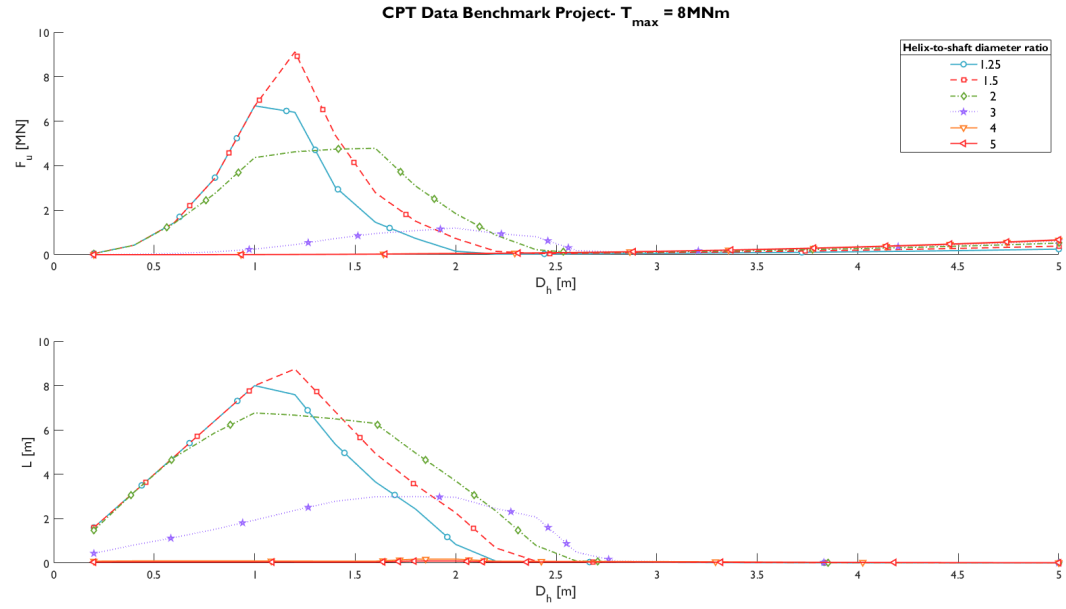

Figure 10.6: Uplift capacity and installation depth for a maximum installation torque of 8 MNm, with increased helix thickness

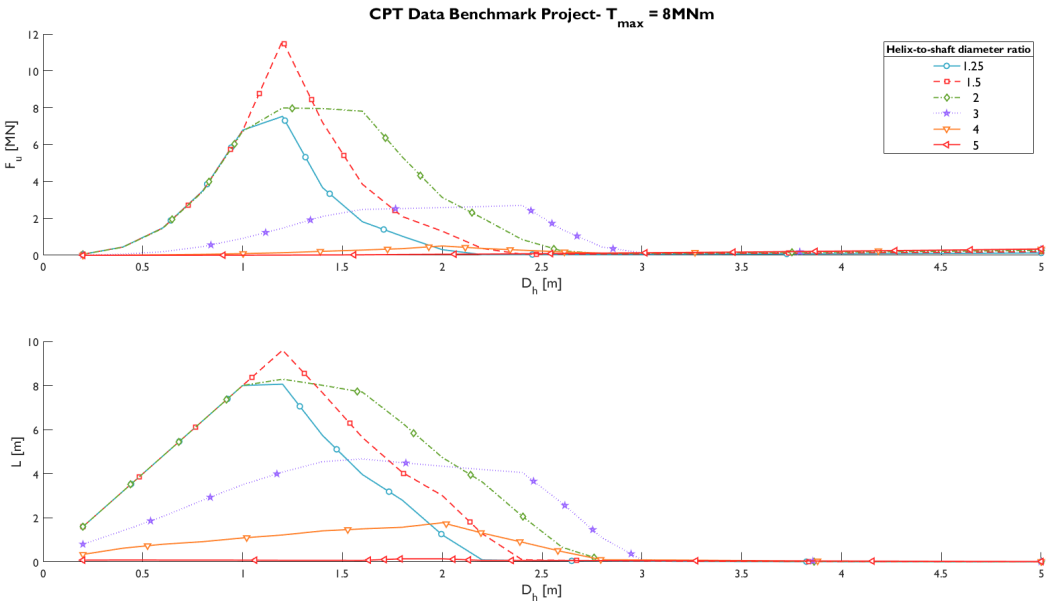

Figure 10.7: Uplift capacity and installation depth for a maximum installation torque of 8 MNm, with increased shaft thickness

10.3. Mud-mat dimensions

The mud-mat size is reduced by decreasing the area with 10%, 20%, 30%, and 40%. Reductions over 40% lead to possible failure. Note that the restoring arm is kept constant, so only the size of the mud-mats is adjusted. By doing so, its ensured that the monopile can be inserted safely into the template. The results are shown in Figures 10.8 - 10.10.

The findings from the analysis show that reducing the size of the mud-mat has a significant impact on both the bearing and sliding capacity. However, the sliding component of the mud-mats is neglected, and it is assumed that the helical pile's lateral capacity solely is able to bear the horizontal load. The maximum factored load by a reduction of 40% is now positioned outside the original bearing capacity envelope, as shown in Figure 10.10. This outcome indicates a higher probability of soil failure, as the soil is unable to sustain the applied load. However, it is important to note that this analysis does not account for load distribution among the mud-mats. The different mud-mats, particularly those of larger size, may have varying capacities. Additionally, considering the environmental loading, each mud-mat has a unique loading condition, which could result in differences in capacity among them. The addition of the helical pile however creates additional capacity, and therefore with a mud-mat area reduction of 40%, the maximum factored load is still within the envelope and thus can be considered a safe design.

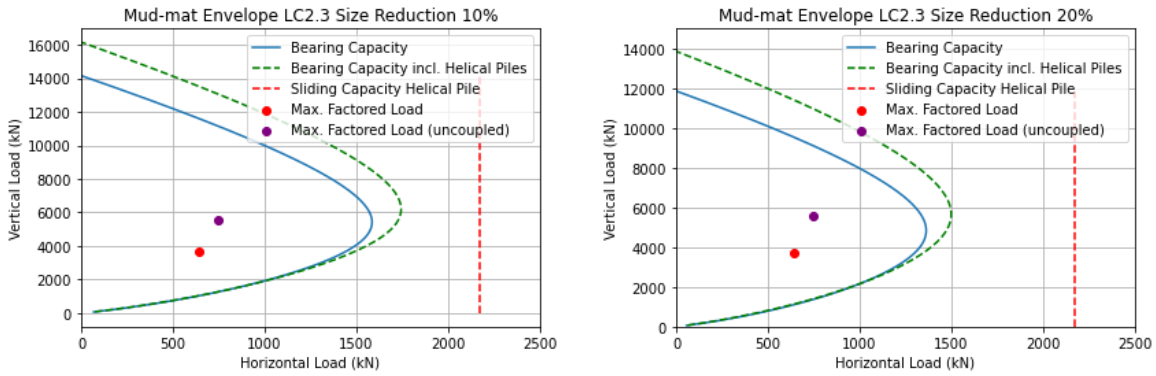

(a) 10% mud-mat size reduction

(b) 20% mud-mat size reduction

Figure 10.8: Mud-mat capacity envelope for load case 2.3 with mud-mat size reduction

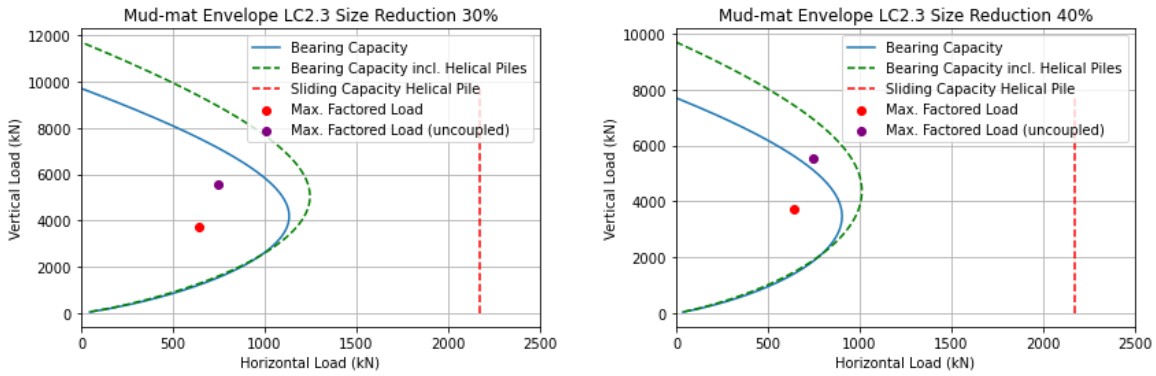

(a) 30% mud-mat size reduction

(b) 40% mud-mat size reduction

Figure 10.9: Mud-mat capacity envelope for load case 2.3 with mud-mat size reduction

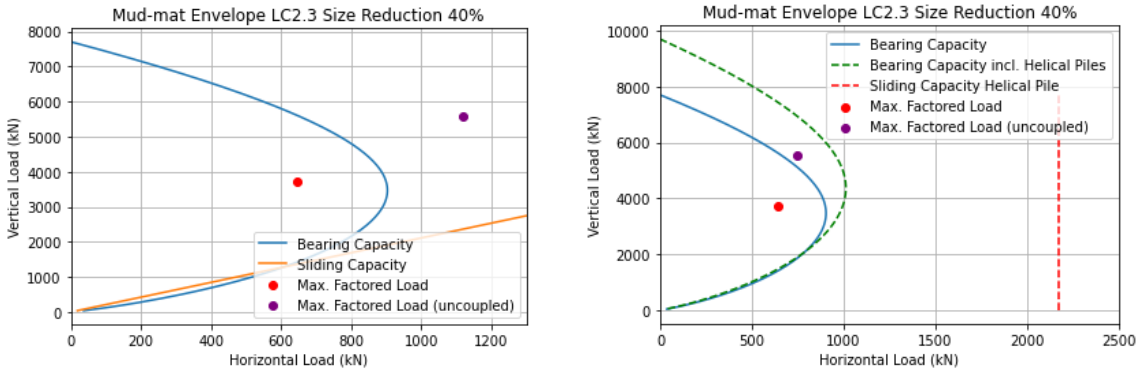

(a) 40% mud-mat size reduction without helical piles

(b) 40% mud-mat size reduction with helical piles

Figure 10.10: Mud-mat capacity envelope for load case 2.3 with mud-mat size reduction

10.4. Template mass

A reduction of the template mass is considered and used to determine the updated mud-mat loading. This is done for the coupled approach as well as for the uncoupled method. This new loading is used to create updated mud-mat capacity envelopes. The load cases are not modified and therefore the load on the template has not changed, except for the loading exerted by the mass of the template. Figure 10.11 shows the mud-mat capacity envelope for load case 2.3, with a mass reduction of 310 mT (20%) and 465 mT (30%). It is assumed that further reduction of the template's mass is not reasonable, as the structural performance of the template would deteriorate significantly. At least a reduction of 20% is required to compensate the added weight due to the integration of the helical pile mechanism (see Table 9.1).

The observed findings indicate that reducing the mass has minimal impact on the bearing capacity and sliding capacity. Nevertheless, there is an effect on the maximum factored load, which shifts to a more advantageous position. This shift is caused by a decrease in the vertical load exerted on the mud-mat. On the other hand, it is crucial to note that reducing the mass to a certain extent can cause the maximum factored load to fall below the sliding capacity line. This indicates a failure in sliding of the mud-mat. The additional lateral capacity due to the integration of the helical pile, however, shifts the sliding capacity away from the factored load in a more favourable position.

10.5. Template dimensions

Reduction in template size is only possible if the mud-mat area is reduced. This is caused by the distance between the two mud-mats that needs to be maintained. This distance is crucial for the safe insertion of the monopile, thereby minimising potential interactions among the mud-mats, template, and monopile. By reducing the mud-mat area by 40% and preserving a 9.5-meter distance between

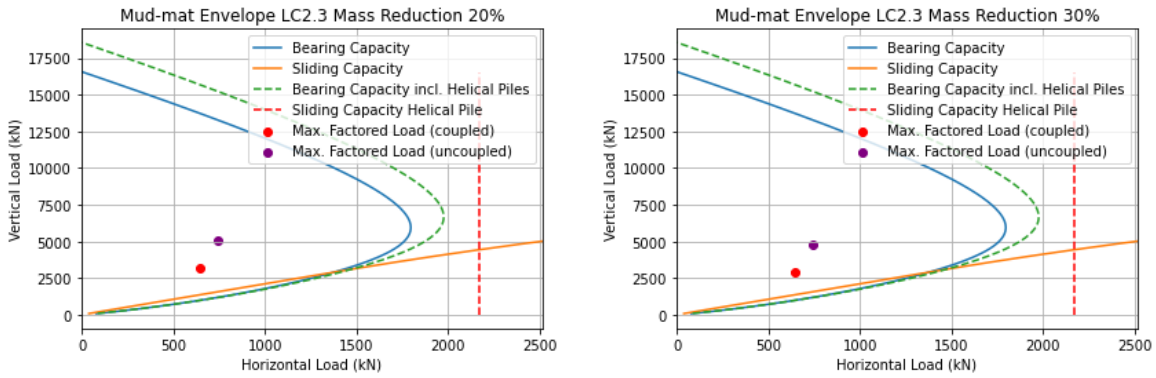

(a) 20% mass reduction

(b) 30% mass reduction

Figure 10.11: Mud-mat capacity envelope for load case 2.3 with mass reduction

small-sized mud-mats, the arm length of the template could potentially be reduced to 14.54 meters. It is important to note that the mud-mat orientation is kept the same. The arm length is reduced by 11%, from initially 16.35 meters to 14.54 meters. The reduced arm length affects the loading on the mud-mats, which is shown in Figure 10.12. The decrease in arm leads to an increase in maximum factored vertical loading. To conclude, the overall template size is reduced by 13.6%: the radius of the template is reduced to 18.13 meters, and previously measured 21 meters.

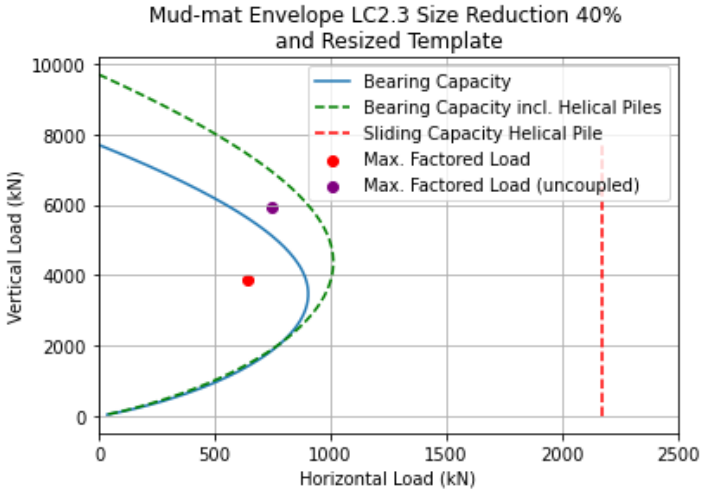

Figure 10.12: Mud-mat capacity envelope for load case 2.3 with mud-mat size reduction and reduction of template size

10.5.1. Reduction of both template mass and size

In this next assessment, the template mass and size are both reduced, by 30% and 13.6%, respectively. The results are depicted in Figure 10.13. Evidently, there is potential for further mass reduction. Nevertheless, the structural requirements of the template, such as stiffness, are not considered in this assessment. Consequently, an investigation into the behaviour of mass reduction on the template's structural performance is suggested.

10.6. Parameter influence summary

An overview of the investigated variables is depicted in Figure 10.14. This overview shows the influence on the performance of the helical pile capacity, installation requirements and mud-mat capacity, if the parameters are increased. A preferable influence on helical pile or mud-mat capacity implies an increase in their capacity. Conversely, concerning installation requirements, a preferable influence relates to a decrease in required installation force or torque.

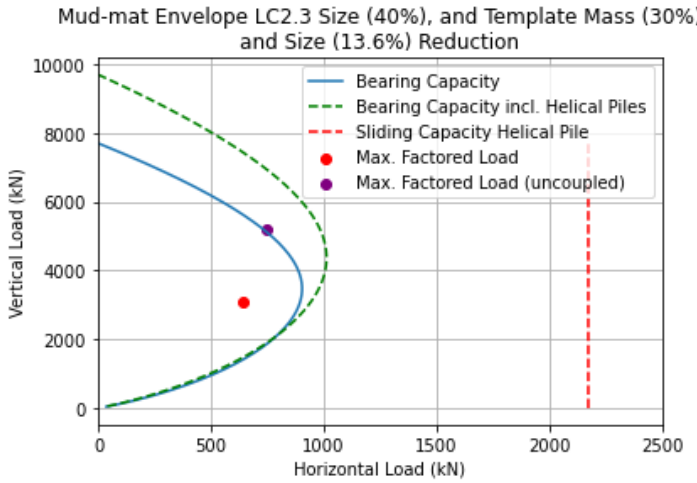

Figure 10.13: Mud-mat capacity envelope for load case 2.3 with reduced mud-mat size, and reduction in template mass and size

When the helix thickness and interface angle are increased, the equivalent stress of the shaft becomes limiting. This affects the achieved embedment depth, thereby negatively influencing the compressive and lateral capacity. Furthermore, an increase in embedment depth would, if possible, directly lead to an increase in capacity. Additionally, an increase in effective unit weight leads to a decreased embedment depth, as the limiting factor shifts to the equivalent stress experienced by the helix plate. However, the uplift, compressive, and lateral capacity of the helical pile still increase.

	Variables	Helical pile capacity			Installation requirements		Mud-mat capacity	
		Uplift	Compressive	Lateral	Crowd force	Torque	Bearing	Sliding
Geometry	Helix diameter (Dh)							
	Shaft diameter (Dc)							
	Helix thickness (th)	*reduced embedment (σ shaft limiting)*						
	Shaft thickness (tc)				*structural strength increases*			
	Pile length (H)	*if possible*	*if possible*	*if possible*				
Soil conditions	Effective unit weight (γ')	*σ helix limiting*						
	Friction angle (φ)							
	Interface angle (δ)	*reduced embedment (σ shaft limiting)*						
	Dilatancy angle (ψ)							

Legend
Preferable influence
Negligible influence
Unpreferable influence
No influence

Figure 10.14: Influence of parameters on helical pile and mud-mat performance

11 Discussion

This chapter summarises and discusses the results. Subsequently, further improvements and limitations are briefly discussed based on the findings of this study. The findings of this chapter is used to form conclusive remarks, and to give recommendations for further studies.

11.1. Results

11.1.1. Benchmark project

Results for the benchmark project indicate that the monopile experiences the most significant hydrodynamic loading. The hydrodynamic loading on the template itself, analysed utilising the equivalent stick model approach, is found to be negligible. Evaluating the two load cases showed that load case 2.3, wherein the crane has an off-lead angle of 1°, is governing. However, the difference between the two considered load cases is relatively small. Therefore, both load cases should still be considered in further analyses. The uncoupled method, utilised to determine the maximum factored load, demonstrates greater loading on the mud-mats than the coupled method. This uncoupled approach tends to be conservative as it does not consider soil interaction. Uplift occurs for 2 mud-mats, using the uncoupled approach. The maximum factored loads were plotted in the capacity envelopes, which showed these are within the capacity envelopes, but these are close to sliding failure. This is commonly observed in the design of monopile installation templates, leading to the use of so called skirts. Skirts are usually added to enhance the sliding capacity of mud-mats. These skirts are typically over-designed as they should be able to bring additional sliding capacity to the weakest type of soil in a wind farm. Additionally, the uncertainty of soil parameters leads to even more over-designing of the skirts. Moreover, there is a risk that the skirt is not fully penetrating the soil at every location, in that case the mud-mat foundation is failing [11, 25, 40, 52].

11.1.2. Helical piles

Results obtained from the helical pile analyses indicate that the uplift, compressive and lateral capacities are significant. The dimensions of the optimised helical pile are within reasonable offshore standards, suggesting that the helical pile geometry is manageable [27, 52]. The design is optimised for maximum uplift capacity, and it is worth noting that the maximum available installation torque has not yet been reached. Additionally, the critical buckling force has not been exceeded, as depicted in Figure 9.3, the left plot and middle plots, respectively. These findings suggest that there is still some margin for increasing the helical pile's performance in terms of installation torque and buckling resistance. However, the equivalent stress experienced by the shaft is close to the yield strength. If the yield strength becomes a limiting factor, the shaft thickness could be increased or materials with higher yield strengths could be considered. However, this may result in higher costs and mass. The utilisation of helical piles for templates may be limited due to the substantial dimensions and mass of the equipment necessary for applying the required installation force and torque. Onshore tools are available, but the tools still need to be developed for offshore use [7, 18, 37]. The compressive capacity of the helical piles is only 13% less than its available maximum, which is achieved for a helix diameter of 1.4 meters.

Most of the capacity is derived from the helix, rather than from its shaft. Determination of the lateral capacity in sand is a difficult process, and therefore the accuracy is not known. A lot of assumptions were made, but the acquired capacity is attempted to be conservative. This approach involves utilising the ultimate lateral capacity derivation rather than utilising the API derivation for shallow depths, and the assumption that no helix is present. Similarly, the sliding capacity of the mud-mats has been entirely ignored in the overall lateral capacity of the system. The helical pile would still significantly increase the sliding capacity of the system. Incorporating the additional (uplift, compressive, and lateral) capacities of the helical piles into the mud-mat design poses challenges due to the unknown behaviour of the mud-mat with the helical pile connection. However, assuming that the uplift capacity of the helical pile can be fully mobilised when integrated into the mud-mat design, it can prevent the mud-mats from uplifting, leading to a more evenly load distribution among the mud-mats. This leads to overall lower loading on the mud-mats, and the addition of the compressive and lateral capacity significantly reduces the likelihood of bearing and sliding failure. Numerical analyses or experiments would provide useful insights into the behaviour of the combined foundation mechanisms.

11.1.3. Design variations

Regarding design variations, reducing the mass of the template has minimal influence on the capacity, but has effect on the maximum factored load. On the other hand, reducing the mud-mat size significantly affects the capacity. Reducing the mud-mat dimensions would offer several advantages, such as improved dynamical behaviour of the template when taken through the waterline, leading to an increased operability window during installation [6, 11, 25, 27]. Other advantages of mud-mat size reduction are a decrease in cost, mass, and CO2 emissions. Moreover, the mud-mat size reduction enables the possibility of reducing the size of the template. The 9.5-meter separation of the mud-mats is crucial for safely inserting the monopile. By decreasing the mud-mat area by 40%, the template's arm length could potentially reduce to 14.54 meters. This reduction leads to an overall template size reduction of 13.6%, having a footprint diameter of 36.3 meters, instead of the previously measured 42 meters. Note that it is assumed in this case that the reduction in template size does not directly affect the mass of the template. The reduced footprint of the template might lead to increased crane capabilities. The crane capabilities increase for a decreasing set-down radius (see Figures in Appendix A). However, the reduced arm due to the template size reduction leads to an increase in vertical loading on the mud-mats, yet a decrease in the template's mass could counter-act this loading. Therefore, it is suggested to assess the structural implications of reducing the dimensions and mass of the template in further studies.

Furthermore, the soil properties play a crucial role in the capacity of both the helical piles and mud-mats. It is shown that increasing the effective unit weight and friction angle would positively influence the helical pile capacity, its installation requirements, and mud-mat capacity. It can be concluded from these findings that denser soils show increased performance. However, a study into helical piles used for offshore anchoring indicates that there is no significant difference in capacity between medium and dense sands. A greater installation depth can be achieved in medium dense sands, while dense sand compensate this depth with higher soil strength [8]. However, the embedment depth can not be increased in the current study, as this would lead to the transition into deep failure mechanism. Consequently, in the current situation, denser sand would enhance the performance of helical piles. Furthermore, a higher interface angle between the helical pile and the soil negatively influences the uplift capacity and its installation requirements. This would also influence the compressive and lateral capacity, as the helical pile can no longer be installed to its maximum installation depth, as the equivalent stress in the shaft limits the achievable embedment. Finally, the dilatancy angle only influences the uplift capacity and has a positive effect when increased.

Moreover, variations on helical pile geometry show that increasing the helix plate thickness negatively affects the uplift capacity. This is caused by the decrease in embedment depth, now limited by the equivalent stress in the shaft. This decreased achievable depth similarly leads to a negatively influenced compressive and lateral capacity. The increase in shaft thickness has negligible influence on the uplift capacity and installation requirements, and is not considered for determining the compressive and lateral capacity. Furthermore, the compressive and lateral capacity are influenced by changes in helical pile geometry, in which the uplift capacity is maximised. An increase in helix diameter positively affects the compressive capacity but an increase in shaft diameter negatively affects the compressive capacity. Note that, the compressive capacity, as depicted in Figure 9.4, decreases at a certain point, which

is caused by a decreasing maximum achievable installation depth for a helical pile with an increasing helix diameter. Conversely, an increase in shaft diameter positively affects the lateral capacity. The helix is not considered in lateral capacity determination, and is assumed to have negligible influence.

11.2. Further improvements and limitations

11.2.1. Installation requirements and tools

The required installation force and torque of the helical pile strongly depend on the achieved installation depth. Currently, when the embedment depth reaches 9.6 meters, it corresponds to an installation torque of 7 MNm and a crowd force surpassing 20 MN. So, the efficiency of the helical pile could be questioned, as the realised uplift capacity is 11.7 MN. Thus, if the helical piles can be installed at a depth below their maximum capacity while still meeting the desired capacity, there will be a substantial reduction in the required crowd force and installation torque. This ability of choosing the demanded installation depth would enhance the application of helical piles.

Furthermore, the upper bound for the required installation requirements is determined, as it is assumed that its a close-ended pile (or in other words, the pile is assumed to be fully plugged). If the effect of reduced plugging can be introduced to the derivations, the installation requirements would significantly decrease, and an increase in capacity could be observed.

Additionally, it is uncertain if the required installation force and torque can be applied and if the equipment is available for offshore application. The availability or the significant expenditure for designing a new tool could introduce challenges to the practicality of incorporating helical piles into the foundation mechanism of installation templates. For example, it is not considered how the tool can be mounted onto the template.

The application and practicalities of the tool are not considered. The tool should be able to exert crowd force and torque on the downward moving helical pile. Moreover, it is advisable to investigate the feasibility of utilising the surrounding helical piles their capacity for installation. The potential of gradually installing helical piles while leveraging piles to facilitate their embedding should be considered. The tool should also be able to remove soil, if plugging of the pile occurs. As the tooling does not yet exist for offshore application, an estimation of the cost is rather difficult. Consequently, making a comparison with the more expensive gripper tool is complex.

11.2.2. Helical pile design

This study exclusively considered a single-helix helical pile. However, multiple helices could potentially increase the uplift and compressive capacity, mostly dependent on the spacing of the helical plates [40]. The influence of multiple helices on the lateral capacity is unknown and could be investigated using numerical analyses or experiments.

Moreover, a revised optimisation process could lead to reduced installation requirements while ensuring sufficient uplift, compressive, and lateral capacity. For example, the pitch is assumed constant in the current study, and determined to minimise soil disturbance. Similarly, the AR is kept constant, and equal to 1, during installation. Maintaining an AR below 1 would decrease the required crowd force, but would increase soil disturbance. So, it is suggested to investigate the influence of the pitch and AR on helical pile performance.

11.2.3. Template design and helical pile configuration

The potential reduction in template dimensions is promising. However, the reduction in mass is not accounted for. It can safely be assumed that by reducing the size of the mud-mats and the template, the total mass decreases. This should be investigated, also considering the structural requirements of the template. Moreover, as the template's footprint might be reduced, the template can be operated closer to the vessel. This reduced set-down radius enhances the crane performance, and thus the operability.

Optimising the arrangement of helical piles within the template design could lead to improved performance. The helical piles are now assumed to stab through the middle of the mud-mats. The helical could, for example, be employed at the largest distance from the centre of gravity to obtain the maximum restoring arm. Furthermore, not every helical pile needs to be employed consistently. When an assessment on wave direction is performed for a monopile installation process, it could potentially be efficient to install helical piles solely on the template's legs where the structure requires additional

capacity. For example, the helical piles can be installed on the legs where the mud-mats experience uplift loading.

There are alternative configurations for integrating the helical piles into the template's design. For instance, the helical piles could be integrated into the mud-mats primarily for their uplift capacity, as depicted in Figure 11.1. In this configuration, the mud-mats should be able to handle the compressive load on the leg, while the helical piles resist the uplifting loads acting on the leg. During compressive loading the mud-mat may potentially settle and thus lower further into the soil, as indicated by distance d in Figure 11.2. If uplift loading is exerted on the settled mud-mat, it moves distance d until the helical pile bears the uplift load. A possible solution to prevent this movement is to apply pre-tension to the helical pile during installation. Additionally, this may also enhance the sliding capacity of the mud-mats by exerting (downward) vertical load on the mud-mats. It is important to note that this pre-tension must be considered as an additional load on the helical pile, as the soil exerts loading on the pile.

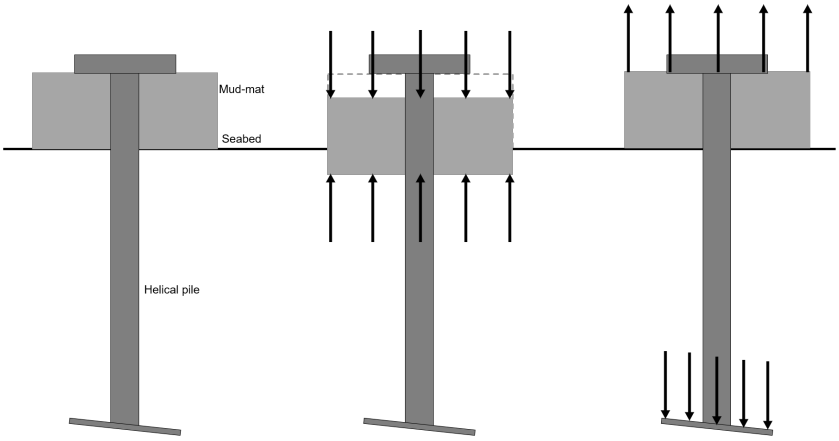

Figure 11.1: Schematic representation of alternative helical pile connection to mud-mat, and its load distribution

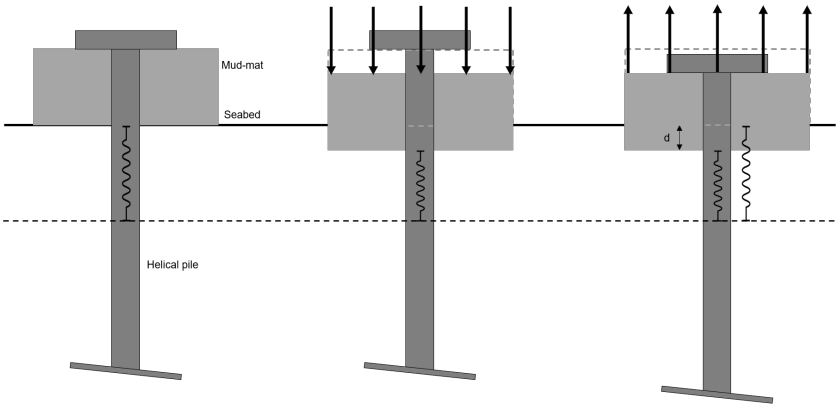

Figure 11.2: Settlement of mud-mat and applying pre-tension to the helical piles

11.2.4. Soil

The maximum uplift capacity of the helical pile is now constraint by the assumed depth-to-diameter ratio, to ensure the shallow failure mechanism is maintained. However, further study into the specific transition into this deep failure mechanism is required as the maximum installation torque and structural requirements were not yet limiting. This transition depends on the soil characteristics and, consequently, varies with location. Therefore, the ratio maintained in this study is not valid for every soil condition.

The loading on the template is validated to CFD and WAMIT models, and therefore can be assumed to be accurate. However, the load distribution among the legs, and thus mud-mats and helical piles, is uncertain. The load distribution is now determined using the uncoupled and coupled approach, which are simplified methods. The influence of the helical pile is, for example, not included in the coupled

method. The soil interaction plays a significant role. Therefore, it suggested that the load determination should be investigated, considering an accurate soil-structure interaction model (for example using FEM).

Furthermore, the resistance of soil against buckling and deflection is not considered. Similarly, investigation into the effects on the plugging of helical piles and the utilisation of materials with higher steel strengths could have significant effects on the structural requirements. These suggestions will reduce the likelihood of structural failure and therefore the helical pile could potentially reach a deeper installation depth, or the helix diameter could be increased. These design variations would lead to higher capacities.

Finally, this study exclusively investigated sand properties, and it is found that denser soils would enhance performance. However, the influence of multiple soil layers has not been considered (except for cone resistance values for the determination of the uplift capacity). Therefore, the potential influence of different soil characteristics within different locations remain uncertain. It is important to note that these soil characteristics may also vary within a template and wind farm.

12

Conclusion

The current study aimed to study the effects on a monopile installation template, when integrating helical piles to its foundation system. The central question in this study was as follows:

How, and to what extent, does adding helical piles affect the footprint of the monopile installation template designed for the benchmark project?

The analyses of the environmental loading on the monopile and template were validated against software models, and were found to be slightly overestimating the hydrodynamic loading. The benchmark project demonstrated that the monopile experiences significant wave loading, while the hydrodynamic loading on the template is negligible. Load case 2.3 with a 1° off-lead angle was found to be governing, but the difference between load cases was relatively small, so consideration of both cases in further analyses is suggested. Uncoupled analysis of the loading showed that uplift occurs for two mud-mats, but that the mud-mats do not fail.

The geometry of the helical pile was optimised taking geotechnical and structural constraints into consideration, while estimating the corresponding maximum uplift capacity. The results show that the installation depth was limited by the H/D ratio, to maintain a shallow failure mechanism. The results show that helical piles can provide significant uplift capacity in these soil conditions. However, the required crowd force and torque for installation are significant and development into these installation tools is necessary. Adding helical piles to the foundation leads to the redistribution of loading on the mud-mats. The mud-mats do no longer experience uplift, and therefore all six are able to transfer loads. However, challenges exist in understanding the behaviour of the combined foundation mechanisms, necessitating numerical analyses or experiments for deeper insights. Moreover, further studies should investigate the possibility applying pre-tension to the helical piles, possibly enhancing the sliding capacity of the mud-mats. The performance of helical piles can be further improved by optimising its design, lowering the need of significant installation requirements, and by using a higher steel grade to improve structural strength.

The investigation into various design variations of the template and variations in soil properties and helical pile geometry has provided valuable insights into the performance and behaviour of the monopile installation template. The findings have demonstrated that reducing the mud-mat dimensions offers significant advantages in terms of improved dynamical behaviour during installation, decreased costs, reduced environmental impact, and increased operability. The reduction in mud-mat size also allows for a potential reduction in the template's overall size, offering potential benefits in terms of operational efficiency and crane capabilities. Resulting in a 13.6% overall template size reduction, with its radius decreasing from 21 meters to 18.13 meters.

However, it is important to note that while reducing the template's mass has a limited impact on capacity, modifications to the mud-mat dimensions and helical pile geometry can lead to significant changes in performance. The study highlights the role of soil properties in influencing both the helical pile and

mud-mat capacities. Denser soils generally lead to improved performance, but careful consideration of installation depth and failure mechanisms is necessary. It is recommended that further studies look into the structural implications of reducing template dimensions and mass. These studies could explore the potential trade-offs between reduced footprint and increased vertical loading on mud-mats, aiming to optimise both structural integrity and operational feasibility.

The findings of this thesis contribute to the application of helical piles offshore and the advancement of monopile installation template design. The results, as well as the methodology of this study, can be utilised by the academic world or (offshore) companies as starting point for further research. The findings and methodology can also be utilised for further study into permanent helical pile applications. Additional recommendations for future work are presented in Chapter 13.

13

Recommendations

In this chapter recommendations for further studies are presented. The recommendations are focused on the helical piles, installation requirements and tools, the monopile installation template, and the soil.

13.1. Helical piles

- The findings in this study revealed that significant efforts are required for installation in terms of crowd force and torque. On this basis, future research should examine the design of a helical piles. For example, studies could investigate the use of multiple helices, a varying shaft diameter, or different pitches. Moreover, the helical pile design should be analysed for reducing installation requirements, while meeting the capacity requirements.
- In the current study the helix thickness is assumed to be constant, and is modelled as a flat plate. Further studies could look into the modelling of a real helix, or optimise the helix thickness.
- The estimation of the lateral capacity of piles in sand is a difficult process, and is even more complicated for helical piles. Therefore, study into the lateral capacity of helical piles could enhance the understanding of the behaviour of helical piles offshore.
- The current study assumed that the capacity of the helical piles could be added to the mud-mat capacity. However, the behaviour of the foundation mechanisms when incorporated into one design is unknown. Further studies should investigate the influence of the integrated foundation mechanisms on their capacity. This could be examined using numerical analyses or experiments.
- The helical piles are installed vertically in the current study. Nonetheless, little research has been done into the effect of inclined helical piles. The inclined helical pile might influence the capacities and installation requirements, and should therefore be investigated.
- The findings of this study could be used as input for the application of helical piles for pre-piling templates. This template is used for the installation of pin-piles, generally used for tripods or jacket structures. Similarly to monopile installation templates, the size of these structures is growing [40]. Consequently, the pre-piling template faces similar challenges as monopile installation templates.
- The current study presented findings for temporary utilisation of helical piles. Research is currently investigating the possibilities of permanent utilisation. The results of this study can be used to explore, for example, the utilisation of helical piles for the foundation of aquaculture or floating wind turbines.
- Finally, the number of offshore wind turbines within a wind farm is significant. Consequently, the number of helical pile installations is significant. Therefore, it is suggested to assess a fatigue study on the helical piles.

13.2. Installation requirements and tools

- The study showed that tools required for installation are not available for offshore applications yet. Therefore, studies into the installation equipment for offshore helical piles is suggested. A study into these installation equipment could give useful insights into their application, weight, and cost.

- The derivations for the installation requirements show the upper bound, as it is assumed that the piles are fully plugged. The effect on the derivations of partially plugged or unplugged piles should be investigated and validated against numerical analyses or experiments.
- The duration of the installation process of helical piles should be examined. The duration of the installation and decommissioning will have impact on the feasibility of the application, as time offshore is costly. Especially the duration of decommissioning, as the installation of helical piles can be performed simultaneously with monopile upending and insertion.

13.3. Monopile installation template

- The findings of this study revealed that the mass and dimensions of the template could be reduced. However, further studies into the effects on structural performance by these reductions are suggested. The template's stiffness, for example, should be examined in order to minimise the likelihood of resonance.
- The helical pile configuration within the template should be investigated. Improvements could potentially be obtained by, for example, optimising the helical pile placement, solely uplift-configuration, or a study into partially installed helical piles.
- It is beyond the scope of this study to investigate the possibility of reducing the number of legs of the template. This reduction in number of legs would directly result in a larger distance between the mud-mats (and thus for bringing the monopile in), which potentially could lead to further reduction of the template dimensions. Similarly to a reduction in size or mass, the structural performance should be studied in order to ensure adequate stiffness, stability, and structural strength.
- Further studies could look into loading transferred to the legs, in order to understand the load transfer within the template. The current study uses simplified methods to obtain the loading, which could be improved to ensure a more accurate estimation.
- Moreover, the current study investigated the static performance of the template. Further studies should examine the dynamical performance of the template when helical piles are incorporated. For example, when taking the template through the waterline. This study could look into load cases wherein the template is not located on the seabed.

13.4. Soil

- Structural checks in the current study do not consider soil effects. The resistance of the soil should be checked, as it can be expected to enlarge the resistance against, for example, buckling and deformations.
- A study into the transition zone of shallow into deep failure mechanisms of helical piles, for a range of soil conditions.
- This study focused solely on sand soils, and findings revealed that denser sands show greater potential. The behaviour of helical piles in different soil types should be investigated. The approach used in the current study can be modified to examine the performance in different types of seabed. For example, seabeds containing multiple layers, but also for different soil classifications, such as clay.

References

1 Al-Baghdadi, T. A. (2018). *Screw piles as offshore foundations: Numerical and physical modelling* (Doctoral dissertation). University of Dundee Dundee, UK.

2 Al-Baghdadi, T. A., Brown, M. J., Knappett, J. A., & Al-Defae, A. H. (2017). Effects of vertical loading on lateral screw pile performance. *Proceedings of the Institution of Civil Engineers - Geotechnical Engineering*, *170*(3), 259–272. https://doi.org/10.1680/jgeen.16.00114

3 American Institute of Steel Construction. (2016). *Specification for Structural Steel Buildings* (tech. rep. ANSI/AISC 360-16).

4 American Petroleum Institute. (2011). *Geotechnical and Foundation Design Considerations* (tech. rep. API-RP-2 GEO).

5 American Petroleum Institute. (2014). *Planning, Designing, and Constructing Fixed Offshore Platforms - Working Stress Design* (tech. rep. API-RP-2A-WSD).

6 Bouman, T. (2022). *Expert interview: Helical piles for templates*.

7 BUMA CE CO., L. (n.d.). *BUMA Construction Equipment Casing Rotator*. http://www.bumace.com/product/product02.html

8 Cerfontaine, B., Knappett, J., Brown, M. E., Davidson, C., & Sharif, Y. (2020). Optimised design of screw anchors in tension in sand for renewable energy applications. *Ocean Engineering*, *217*, 108010. https://doi.org/10.1016/j.oceaneng.2020.108010

9 Chance. (2020). Aquaculture anchoring. https://hubbellcdn.com/literature/SF04307E_0720%20Aqua%20Farming%20Applications.pdf

10 Corporation, J. S. (2018). *TSUBASA- Pile Rotary Penetration Steel Pipe Pile with Toe Wing*. https://www.jfe-steel.co.jp/en/products/list

11 Dam, J. (2022). *Expert interview: Template design and foundation*.

12 Davidson, C., Brown, M., Knappett, J., Brennan, A., Augarde, C., Coombs, W., Wang, L., Richards, D., White, D., & Blake, A. (Eds.). (2019). *Isspea 2019: 1st international symposium on screw piles for energy applications* [1st International Symposium on Screw Piles for Energy Applications, ISSPEA ; Conference date: 27-05-2019 Through 28-05-2019]. University of Dundee. https://doi.org/10.20933/100001123

13 Davidson, C., Brown, M. J., Cerfontaine, B., Al-Baghdadi, T., Knappett, J., Brennan, A., Augarde, C., Coombs, W., Wang, L., Blake, A., Richards, D., & Ball, J. D. (2022). Physical modelling to demonstrate the feasibility of screw piles for offshore jacket-supported wind energy structures. *Géotechnique*, *72*(2), 108–126. https://doi.org/10.1680/jgeot.18.P.311

14 Det Norske Veritas. (2016). *DNVGL-ST-N001 - Marine Operations and Marine Warranty* (tech. rep. DNVGL-ST-N001).

15 Det Norske Veritas. (2019). *DNVGL-OS-C101 - Design of Offshore Steel Structures - General* (tech. rep. DNVGL-OS-C101).

16 Det Norske Veritas. (2021a). *DNVGL-RP-C205 - Environmental Conditions and Environmental Loads* (tech. rep. DNVGL-RP-C205).

17 Det Norske Veritas. (2021b). *DNVGL-RP-C212 - Offshore Soil Mechanics and Geotechnical Engineering* (tech. rep. DNVGL-RP-C212).

18 Egyptian Foundation Engineering. (n.d.). *EFE Casing Oscillators*. https://www.efebauer.com/products/accessories-for-rotary-drilling-rigs/casing-oscillators/

19 Elsherbiny, Z., & El Naggar, M. (2013). Axial compressive capacity of helical piles from field tests and numerical study. *Canadian Geotechnical Journal*, *50*. https://doi.org/10.1139/cgj-2012-0487

20 Fattah, M., Salim, N., & M.B.Al-Gharrawi, A. (2019). Effect of soil plug removal on the load-carrying capacity of symmetric and non-symmetric pile groups. *Ships and Offshore Structures*, *15*, 1–23. https://doi.org/10.1080/17445302.2019.1694298

21 Fenton, J. D. (1985). A fifth-order stokes theory for steady waves. *Journal of waterway, port, coastal, and ocean engineering*, *111*(2), 216–234.

22 Fenton, J. D. (1988). The numerical solution of steady water wave problems. *Computers & Geosciences*, *14*(3), 357–368.

23 Fernandez, I. (2023). Most Common Offshore Substructures for Wind Turbines in Europe 2020. *Statista*.

24 Fugro and Netherlands Enterprise Agency. (2016). *Geotechnical Report / Investigation Data Seafloor In Situ Test Locations Borssele Wind Farm Site IV* (tech. rep.). https://offshorewind.rvo.nl/file/download/33ab9b2d-9d72-45f1-80f5-cfe5f3768be7/1456928630sdb_report_data_seafloor%20in%20situ%20test%20locations_wfs%20iv_160302_fugro.pdf

25 Geene, P. (2023). *Expert interview: Intellectual properties & helical piles for templates*.

26 Giampa, J. R., Bradshaw, A. S., & Schneider, J. A. (2017). Influence of dilation angle on drained shallow circular anchor uplift capacity. *International Journal of Geomechanics*, *17*(2), 04016056.

27 Hagenaar, P. (2023). *Expert interview: Template design and helical piles*.

28 Han, F., Ganju, E., Salgado, R., & Prezzi, M. (2018). Effects of interface roughness, particle geometry, and gradation on the sand–steel interface friction angle. *Journal of Geotechnical and Geoenvironmental Engineering*, *144*(12), 04018096.

29 Han, F., Ganju, E., Salgado, R., & Prezzi, M. (2019). Comparison of the load response of closed-ended and open-ended pipe piles driven in gravelly sand. *Acta Geotechnica*, *14*, 1785–1803.

30 Hansen, J. B. (1970). A revised and extended formula for bearing capacity.

31 Hao, D., Wang, D., O'Loughlin, C. D., & Gaudin, C. (2019). Tensile monotonic capacity of helical anchors in sand: Interaction between helices. *Canadian Geotechnical Journal*, *56*(10), 1534–1543. https://doi.org/10.1139/cgj-2018-0202

32 International Organisation for Standardization (ISO). (2017). *Geotechnical investigation and testing — Identification and classification of soil — Part 1: Identification and description* (tech. rep. ISO 14688). https://www.iso.org/standard/66345.html

33 International Organization for Standardization. (2016). *Petroleum and Natural Gas Industries — Specific Requirements for offshore structures — Part 4: Geotechnical and Foundation Design Considerations* (tech. rep. ISO 19901-4).

34 Jiang, Z. (2021). Installation of offshore wind turbines: A technical review. *Renewable and Sustainable Energy Reviews*, *139*, 110576. https://doi.org/https://doi.org/10.1016/j.rser.2020.110576

35 Lanyi-Bennett, S., & Deng, L. (2019). Effects of inter-helix spacing and short-term soil setup on the behaviour of axially loaded helical piles in cohesive soil. *Soils and Foundations*, *59*. https://doi.org/10.1016/j.sandf.2018.12.002

36 Lehane, B. M., Gaudin, C., & Schneider, J. A. (2005). Scale effects on tension capacity for rough piles buried in dense sand. *Géotechnique*, *55*(10), 709–719. https://doi.org/10.1680/geot.2005.55.10.709

37 Liebherr. (n.d.). *Liebherr Casing Oscillator*. https://www.liebherr.com/shared/media/construction-machinery/deep-foundation/pdf/flyer/liebherr-casing-oscillator-deep-foundation-en

38 Liu, B., Wang, X., Liu, C., & Kong, J. (2023). Effect of relative stiffness of pile and soil on pile group effect. *Journal of Marine Science and Engineering*, *11*(1). https://doi.org/10.3390/jmse11010192

39 MacCamy, R. C., & Fuchs, R. A. (1954). *Wave Forces on Piles*.

40 Meijer, P. H. N. (2023). Helical Piles as Foundation Technique for Offshore Wind Turbine Templates: A Literature Review.

41 Mitchell, J. K., Soga, K., et al. (2005). *Fundamentals of soil behavior* (Vol. 3). John Wiley & Sons New York.

42 Mohajerani, A., Bosnjak, D., & Bromwich, D. (2016). Analysis and design methods of screw piles: A review. *Soils and Foundations*, *56*(1), 115–128.

43 Noorzaei, J., Bahrom, S., Jaafar, M., Abdul, W., Thanoon, M., & Mohammad, S. (2005). Simulation of wave and current forces on template offshore structures.

44 Ochshorn, J. (2010). Chapter 1 - statics. In J. Ochshorn (Ed.), *Structural elements for architects and builders* (pp. 1–37). Butterworth-Heinemann. https://doi.org/https://doi.org/10.1016/B978-1-85617-771-9.00001-5

45 Paik, K., Salgado, R., Lee, J., & Kim, B. (2003). Behavior of open-and closed-ended piles driven into sands. *Journal of Geotechnical and Geoenvironmental Engineering*, *129*(4), 296–306.

46 Pisano, F., & Technical University of Delft. (2022). Offshore Geotechnical Engineering - Lecture: Offshore Piled Foundations.

47 Quinteros, S., Dyvik, R., & Mortensen, N. (2017). Interface friction angle soil-on-steel from ring shear tests on offshore north sea sands. https://doi.org/10.1061/9780784480472.038

48 Randolph, M., & Gourvenec, S. (2017). *Offshore Geotechnical Engineering*. https://doi.org/10.1201/9781315272474

49 Remmers, J. (2023). *Expert interview: Template design and helical piles*.

50 Rietema, B. (2022). Uplift behavior of offshore shallow foundations during retrieval. http://resolver.tudelft.nl/uuid:c911b76e-6774-4afb-9674-e229d19236c6

51 Schanz, T., & Vermeer, P. A. (1996). Angles of friction and dilatancy of sand. *Géotechnique*, *46*(1), 145–151. https://doi.org/10.1680/geot.1996.46.1.145

52 Sonnema, W. (2022). *Expert interview: Helical piles as foundation*.

53 Sunday, K., & Brennan, F. (2021). A review of offshore wind monopiles structural design achievements and challenges. *Ocean Engineering*, *235*, 109409. https://doi.org/https://doi.org/10.1016/j.oceaneng.2021.109409

54 Timoshenko, S., Woinowsky-Krieger, S., et al. (1959). *Theory of plates and shells* (Vol. 2). McGraw-hill New York.

55 Van Der Tempel, J., Diepeveen, N., De Vries, W., & Cerda Salzmann, D. (2011). 15 - offshore environmental loads and wind turbine design: Impact of wind, wave, currents and ice. In J. D. Sørensen & J. N. Sørensen (Eds.), *Wind energy systems* (pp. 463–478). Woodhead Publishing. https://doi.org/https://doi.org/10.1533/9780857090638.4.463

56 Venkatesan, V., & Mayakrishnan, M. (2023). Experimental and numerical study of group effect on the behavior of helical piles in soft clays under uplift and lateral loading. *Ocean Engineering*, *268*, 113500. https://doi.org/https://doi.org/10.1016/j.oceaneng.2022.113500

57 Vugts, J. (2016). *Handbook of Bottom Founded Offshore Structures Part II*. Eburon.

A

Heerema Marine Contractors

A.1. History

Heerema has been installing, fabricating, and providing unique engineering solutions over the past sixty years. Heerema Group consists of three companies: Heerema Marine Contractors (HMC), Heerema Fabrication Group (HFG), and Heerema Engineering Solutions (HES). Heerema Group was established in 1948, and was specialised in the construction and installation of drilling platforms for oil companies in Venezuela. The shift towards the North Sea started from 1962, when HES was founded. Also, the first crane vessel was introduced in this year. Later, in 1978, world's first semi-submersible crane vessels (SSCVs) were commissioned, called Balder and Hermod. These vessels brought an innovative dual-crane feature to the market, leading to a significant reduction in installation time of projects in the oil and gas industry. Thereafter, another SSCV, the Thialf, was added to Heerema's fleet in 1985. Consequently, in 2013, a monohull crane vessel was christened, called Aegir. Finally, the Sleipnir was added to the fleet, being world's largest SSCV. A description of the vessels is located in Section A.2.

A.2. Fleet

Sleipnir

The newest vessel of HMC's fleet is the semi-submersible crane vessel *Sleipnir*, which was christened in 2019. The vessel is equipped with two cranes of 10,000 tonnes lifting capacity each. The deck area is large, and its configuration has been optimised to transport as many jackets, topsides or modules as possible. The transit speed is over 10 knots, and the vessel is powered by LNG. The vessel and its main dimensions, deck load, crane specifications and other information are shown in Figure A.1.

(a) SSCV Sleipnir

Main data

Construction Year	2019
Lift Capacity	20,000 metric tons
Dimensions	
Length	220 m
Width	102 m
Draft	12 - 32 m

(b) Sleipnir specifications

Figure A.1: Vessel overview Sleipnir

Thialf

The second largest semi-submersible crane vessel *Thialf* was constructed in 1985, and is capable of a tandem lift of 14,200 tonnes. The transit speed is around 7 knots, and the vessel is powered by diesel engines. The vessel and its dimensions and crane specifications are illustrated in Figure A.2.

(a) SSCV Thialf

Main data

Construction Year	1985
Lift Capacity	14,200 metric tons
Dimensions	
Length	201.6 m
Width	88.4 m
Depth to work deck	49.5 m
Draft	11.9 - 31.6 m

(b) Thialf specifications

Figure A.2: Vessel overview Thialf

Balder

The *Balder* is also a semi-submersible crane vessel and is the oldest SSCV that is still in operation. The SSCV was commissioned in 1978, and got a makeover to extend its lifetime in 2001. The vessel is capable of a tandem lift of 6,300 tonnes. The vessel and its dimensions and crane specifications are illustrated in Figure A.3.

(a) SSCV Balder

Main data

Construction Year	1978
Lift Capacity	6,300 metric tons
Dimensions	
Length	154 m
Width	86 m
Width of Deck	105 m
Draft	
Draft	14 m and deeper
Draft incl. thrusters	4.5 m under hull

(b) Balder specifications

Figure A.3: Vessel overview Balder

Aegir

The *Aegir* is a fast-moving heavy-lift vessel, and was introduced to the fleet in 2013. The vessel is one of the world's largest monohull crane vessels and has a single crane with a lifting capacity of 5,000 tonnes. The Aegir and its dimensions and crane specifications are illustrated in Figure A.4.

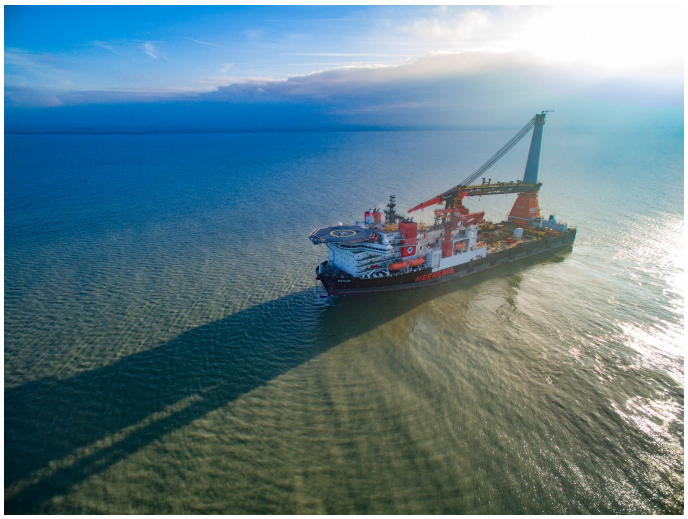

(a) Monohul vessel Aegir

Main data

Construction Year	2012
Lift Capacity	5,000 metric tons
Dimensions	
Length	211 m
Width	46 m
Draft	
Operating draft	9 - 11 m
Transit draft	8 m

(b) Aegir specifications

Figure A.4: Vessel overview Aegir

Bylgia and Kolga

HMCs fleet also consists of two support vessels, anchor handling tugs Bylgia and Kolga. Its dimensions and pulling capacity are shown in Figure A.5b.

(a) Anchor handling tugs Bylgia and Kolga

Main data

Construction Year	2013
Summer draft	7.37 m
Dimensions	
Length	72 m
Width	18 m
Bollard pull	
Bylgia	200 t
Kolga	212 t

(b) Bylgia and Kolga specifications

Figure A.5: Vessel overview Bylgia and Kolga

A.3. Crane capability curves & deck lay-out

The crane load and clearance curves for all crane vessels are shown below. Additionally, the deck lay-out of each vessel is shown. This lay-out is used to determine if the template fits on the available deck space without interfering with cranes or other equipment.

Sleipnir

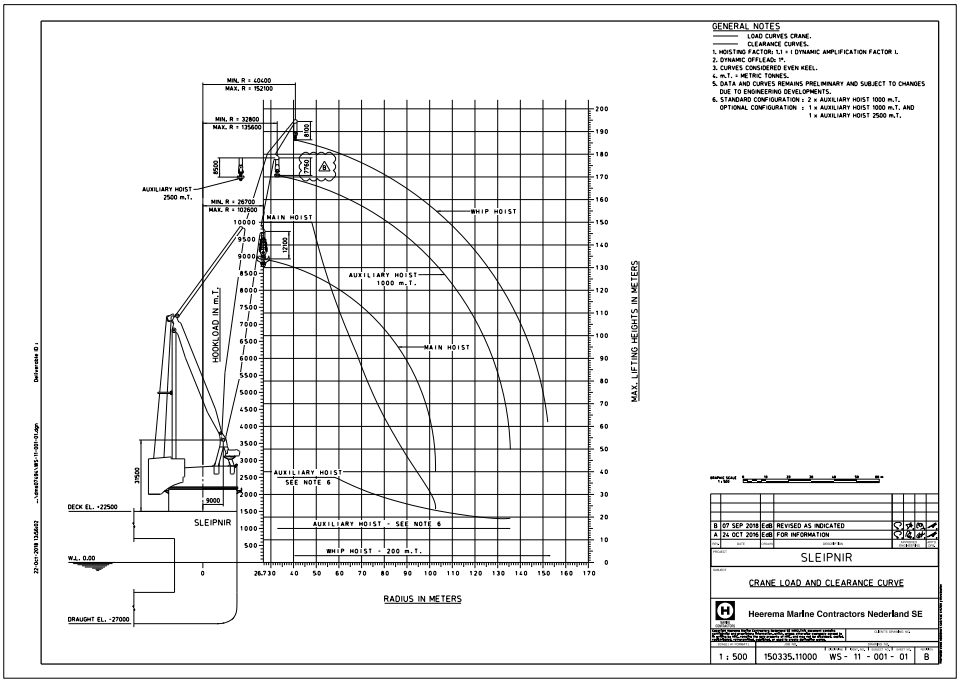

Figure A.6: Crane capability curve Sleipnir

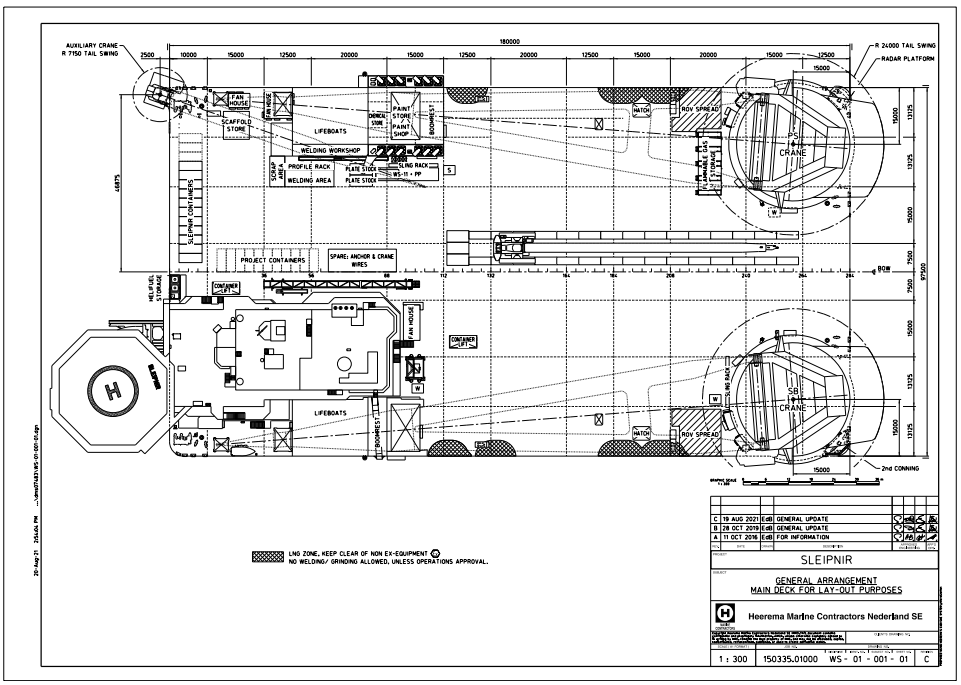

Figure A.7: Deck lay-out Sleipnir

Thialf

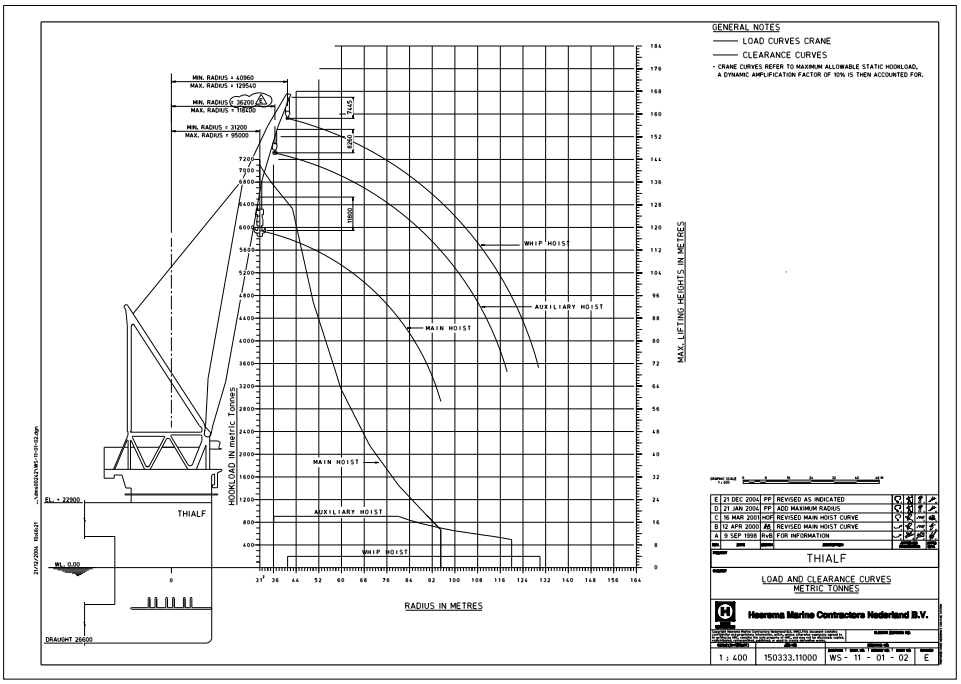

Figure A.8: Crane capability curve Thialf

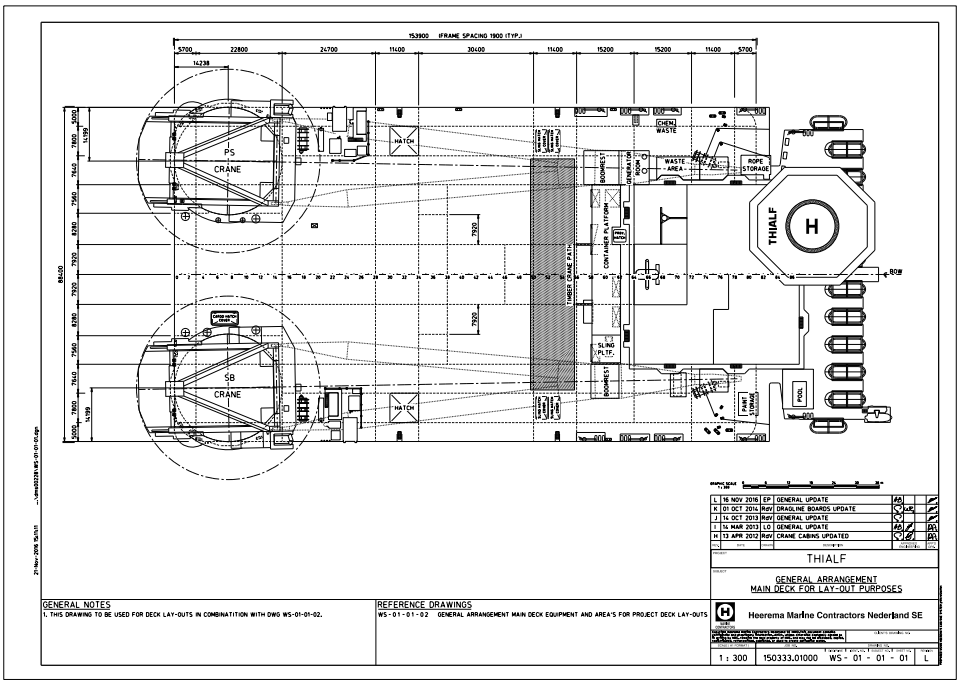

Figure A.9: Deck lay-out Thialf

Balder

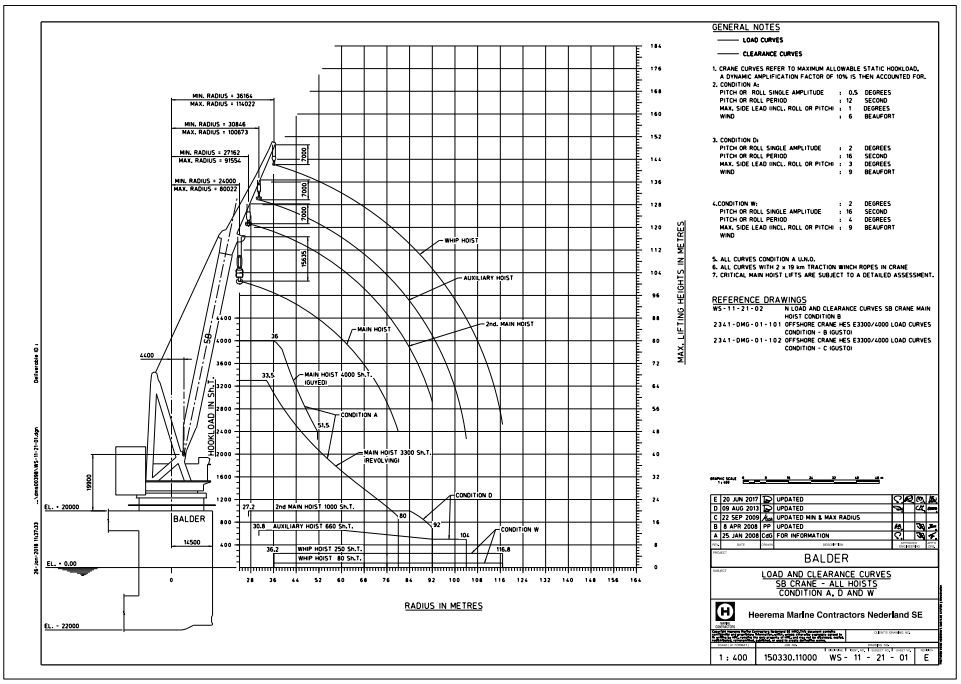

Figure A.10: Crane capability curve Balder

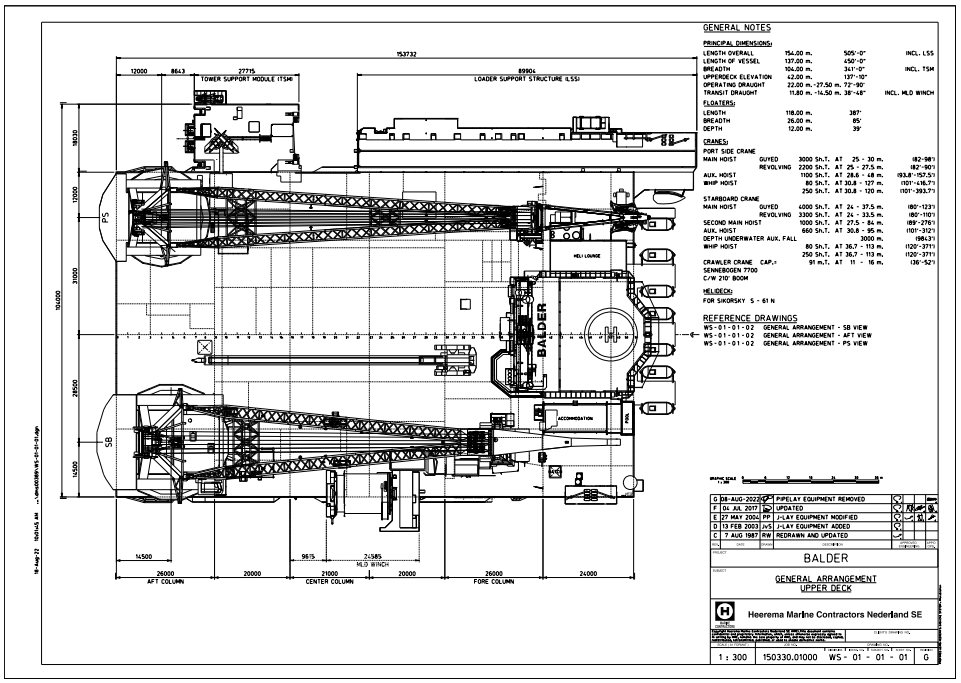

Figure A.11: Deck lay-out Balder

Aegir

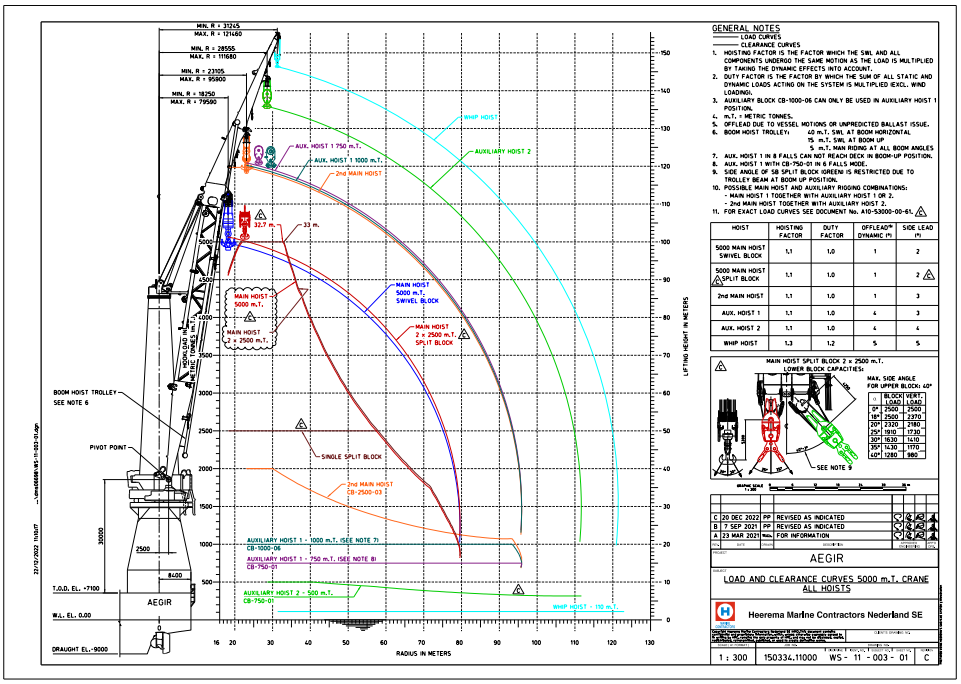

Figure A.12: Crane capability curve Aegir

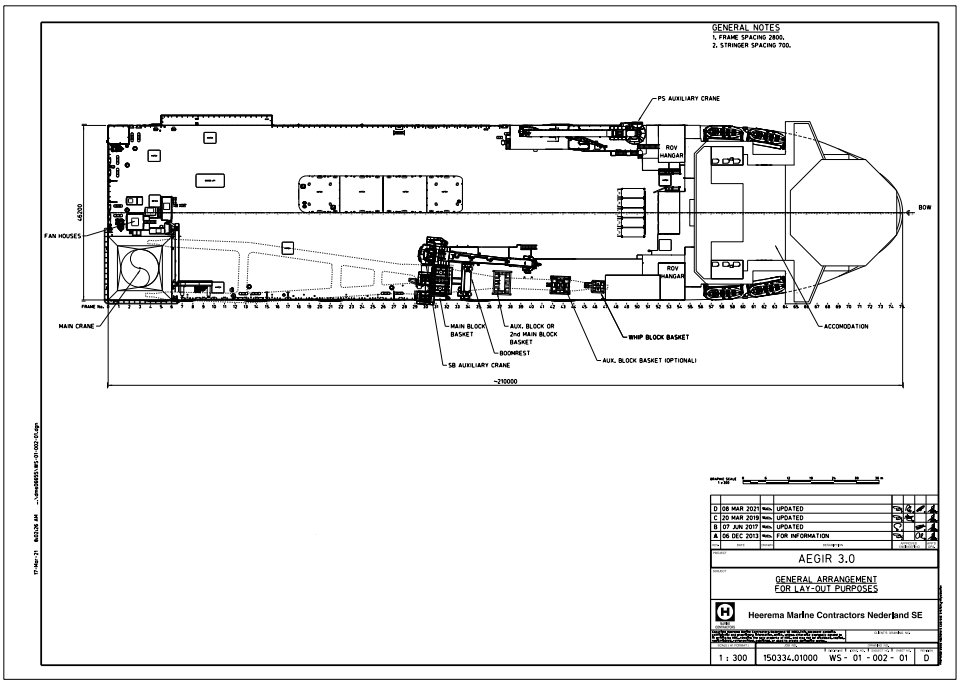

Figure A.13: Deck lay-out Aegir

B

Environmental Loading

Below the output of the Fenton tool is presented for the range of considered peak periods. The output of the Fenton tool is partly utilised, as shown on the two leftmost columns. These values are used to determine the kinematics of the wave particles. The average of the acceleration and speed is taken per section, to determine the horizontal load and the moment. This output is used for the determination of the wave loading on the monopile as well as on the template. Thereafter, the finding of this Morison method is compared to the results of the software models WAMIT and CFD. The results are shown in Figure B.1.

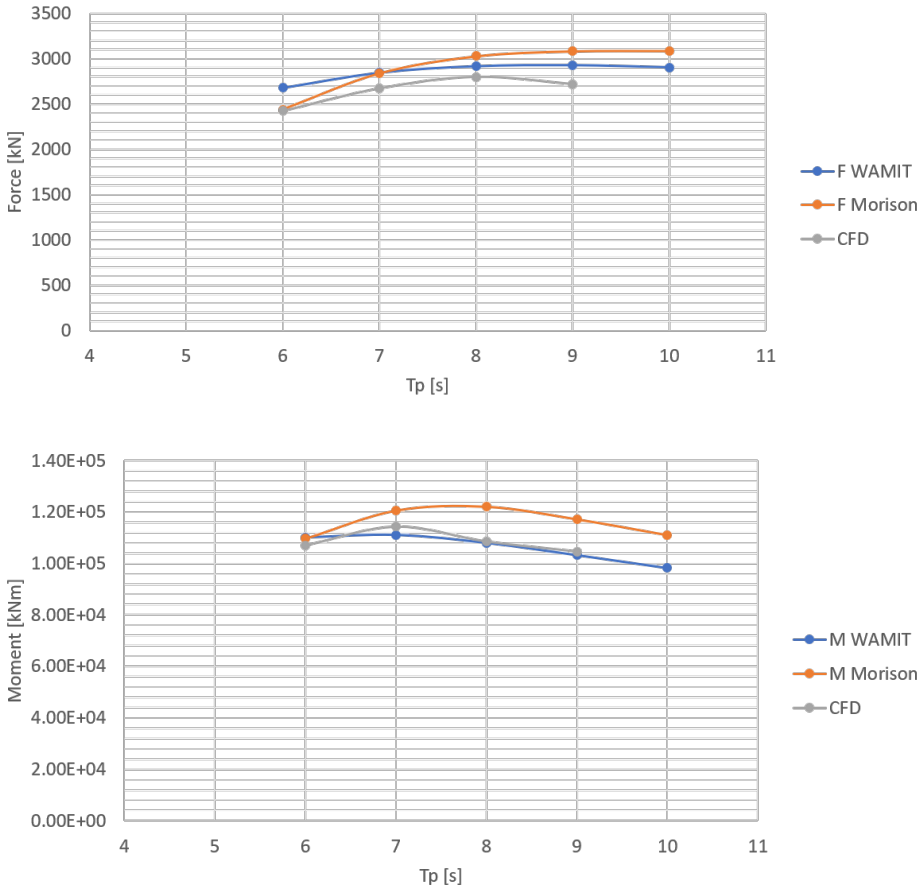

Figure B.1: Hydrodynamics approach comparison (WAMIT, CFD and Morison)

Tp 6 seconds

Inertia Load

X/d	acc/g
0.00	0.00
0.05	0.00
0.10	0.00
0.15	0.00
0.20	0.00
0.26	0.00
0.31	0.00
0.36	0.00
0.41	0.00
0.46	0.00
0.51	0.01
0.56	0.01
0.61	0.01
0.66	0.02
0.72	0.03
0.77	0.04
0.82	0.07
0.87	0.10
0.92	0.16
0.97	0.25
1.02	0.41

Inertia Load						
h [m]	**acc [m/s²]**	**acc_avr [m/s²]**	**arm [m]**	**δh [m]**	**Fhor [kN]**	**Mover [kNm]**
0.000	0.002					
2.555	0.002	0.002	1.3	2.555	1	1
5.110	0.003	0.002	3.8	2.555	1	3
7.665	0.003	0.003	6.4	2.555	1	6
10.220	0.005	0.004	8.9	2.555	1	11
12.775	0.007	0.006	11.5	2.555	2	22
15.330	0.011	0.009	14.1	2.555	3	40
17.885	0.016	0.013	16.6	2.555	4	72
20.440	0.025	0.020	19.2	2.555	7	126
22.995	0.036	0.030	21.7	2.555	10	215
25.550	0.055	0.046	24.3	2.555	15	361
28.105	0.083	0.069	26.8	2.555	23	605
30.660	0.126	0.104	29.4	2.555	34	1000
33.215	0.190	0.158	31.9	2.555	51	1644
35.770	0.288	0.239	34.5	2.555	78	2690
38.325	0.439	0.363	37.0	2.555	118	4388
40.880	0.669	0.554	39.6	2.555	180	7146
43.435	1.026	0.848	42.2	2.555	276	11643
45.990	1.590	1.308	44.7	2.555	426	19059
48.545	2.499	2.044	47.3	2.555	666	31488
51.100	4.005	3.252	49.8	2.555	1060	52795

Σ w/o corr.	2957	133315	kNm
Σ with corr.	2410	108652	

X/d	u/sqrt(gd)
0	0.0001
0.0511	0.0001
0.1022	0.0001
0.1533	0.0001
0.2044	0.0001
0.2555	0.0002
0.3066	0.0003
0.3577	0.0004
0.4088	0.0007
0.4599	0.001
0.511	0.0015
0.5621	0.0023
0.6132	0.0034
0.6643	0.0052
0.7154	0.0078
0.7665	0.0117
0.8176	0.0176
0.8687	0.0265
0.9198	0.0397
0.9709	0.0593
1.022	0.0881

Drag Load							
h [m]	**u [m/s]**	**u_avr [m/s]**	**arm [m]**	**δh [m]**	**Cd* [-]**	**Fhor [kN]**	**Mover [kNm]**
0.000	0.002						
2.555	0.002	0.002	1.3	2.555	1.02	1	1
5.110	0.002	0.002	3.8	2.555	1.02	1	2
7.665	0.002	0.002	6.4	2.555	1.02	1	4
10.220	0.002	0.002	8.9	2.555	1.02	1	5
12.775	0.004	0.003	11.5	2.555	1.01	1	7
15.330	0.007	0.006	14.1	2.555	1.01	1	8
17.885	0.009	0.008	16.6	2.555	1.01	1	10
20.440	0.016	0.012	19.2	2.555	1.00	1	12
22.995	0.022	0.019	21.7	2.555	1.00	1	14
25.550	0.033	0.028	24.3	2.555	0.98	1	17
28.105	0.051	0.042	26.8	2.555	0.97	1	21
30.660	0.075	0.063	29.4	2.555	0.94	1	26
33.215	0.115	0.095	31.9	2.555	0.89	1	33
35.770	0.173	0.144	34.5	2.555	0.83	1	44
38.325	0.259	0.216	37.0	2.555	0.73	2	60
40.880	0.390	0.324	39.6	2.555	0.57	2	78
43.435	0.587	0.488	42.2	2.555	0.33	2	81
45.990	0.879	0.733	44.7	2.555	0.19	2	91
48.545	1.313	1.096	47.3	2.555	0.19	4	184
51.100	1.951	1.632	49.8	2.555	0.20	8	403

Σ	30	1102

Tp 7 seconds

inertia

X/d	acc/g
0	0.0011
0.0505	0.0011
0.1011	0.0013
0.1516	0.0016
0.2021	0.002
0.2526	0.0027
0.3032	0.0036
0.3537	0.0049
0.4042	0.0066
0.4547	0.0091
0.5053	0.0124
0.5558	0.017
0.6063	0.0234
0.6568	0.032
0.7074	0.0439
0.7579	0.0604
0.8084	0.083
0.8589	0.1142
0.9095	0.1574
0.96	0.2173
1.0105	0.3008

Inertia Load

h [m]	acc [m/s²]	acc_avr [m/s²]	arm [m]	δh [m]	Fhor [kN]	Mover [kNm]
0.000	0.011					
2.525	0.011	0.011	1.3	2.525	3	4
5.055	0.013	0.012	3.8	2.53	4	14
7.580	0.016	0.014	6.3	2.525	5	29
10.105	0.020	0.018	8.8	2.525	6	50
12.630	0.026	0.023	11.4	2.525	7	84
15.160	0.035	0.031	13.9	2.53	10	139
17.685	0.048	0.042	16.4	2.525	13	220
20.210	0.065	0.056	18.9	2.525	18	344
22.735	0.089	0.077	21.5	2.525	25	532
25.265	0.122	0.105	24.0	2.53	34	817
27.790	0.167	0.144	26.5	2.525	46	1232
30.315	0.230	0.198	29.1	2.525	64	1854
32.840	0.314	0.272	31.6	2.525	88	2763
35.370	0.431	0.372	34.1	2.53	120	4097
37.895	0.593	0.512	36.6	2.525	165	6035
40.420	0.814	0.703	39.2	2.525	227	8869
42.945	1.120	0.967	41.7	2.525	311	12983
45.475	1.544	1.332	44.2	2.53	430	19003
48.000	2.132	1.838	46.7	2.525	592	27661
50.525	2.951	2.541	49.3	2.525	818	40314

Σ w/o corr.	2986	127047	kNm
Σ with corr.	2822	120059	

drag

X/d	u/sqrt(gd)
0	0.0002
0.0505	0.0002
0.1011	0.0002
0.1516	0.0002
0.2021	0.0003
0.2526	0.0004
0.3032	0.0006
0.3537	0.0008
0.4042	0.0011
0.4547	0.0014
0.5053	0.002
0.5558	0.0027
0.6063	0.0037
0.6568	0.005
0.7074	0.0069
0.7579	0.0094
0.8084	0.0128
0.8589	0.0174
0.9095	0.0237
0.96	0.032
1.0105	0.0431

Drag Load

h [m]	u [m/s]	u_avr [m/s]	arm [m]	δh [m]	Cd [-]	Fhor [kN]	Mover [kNm]
0.000	0.004						
2.525	0.004	0.004	1.3	2.525	0.96	1	1
5.055	0.004	0.004	3.8	2.53	0.96	1	2
7.580	0.004	0.004	6.3	2.525	0.96	1	4
10.105	0.007	0.006	8.8	2.525	0.96	1	5
12.630	0.009	0.008	11.4	2.525	0.95	1	7
15.160	0.013	0.011	13.9	2.53	0.94	1	8
17.685	0.018	0.016	16.4	2.525	0.94	1	10
20.210	0.024	0.021	18.9	2.525	0.92	1	12
22.735	0.031	0.028	21.5	2.525	0.90	1	14
25.265	0.044	0.038	24.0	2.53	0.88	1	17
27.790	0.060	0.052	26.5	2.525	0.85	1	20
30.315	0.082	0.071	29.1	2.525	0.80	1	23
32.840	0.111	0.096	31.6	2.525	0.73	1	27
35.370	0.153	0.132	34.1	2.53	0.63	1	32
37.895	0.208	0.180	36.6	2.525	0.50	1	36
40.420	0.283	0.246	39.2	2.525	0.32	1	34
42.945	0.385	0.334	41.7	2.525	0.19	1	28
45.475	0.525	0.455	44.2	2.53	0.19	1	45
48.000	0.709	0.617	46.7	2.525	0.19	2	73
50.525	0.955	0.832	49.3	2.525	0.20	2	123

Σ	17	520

Tp 8 seconds

inertia X/d	acc/g
0	0.0032
0.0504	0.0033
0.1008	0.0037
0.1512	0.0042
0.2016	0.005
0.252	0.0061
0.3024	0.0076
0.3528	0.0095
0.4032	0.012
0.4536	0.0153
0.504	0.0196
0.5544	0.025
0.6048	0.032
0.6552	0.041
0.7056	0.0526
0.756	0.0674
0.8063	0.0865
0.8567	0.111
0.9071	0.1426
0.9575	0.1831
1.0079	0.2354

Inertia Load						
h [m]	**acc [m/s²]**	**acc_avr [m/s²]**	**arm [m]**	**δh [m]**	**Fhor [kN]**	**Mover [kNm]**
0.000	0.031					
2.520	0.032	0.032	1.3	2.52	10	13
5.040	0.036	0.034	3.8	2.52	11	42
7.560	0.041	0.039	6.3	2.52	12	78
10.080	0.049	0.045	8.8	2.52	15	128
12.600	0.060	0.054	11.3	2.52	17	198
15.120	0.075	0.067	13.9	2.52	22	299
17.640	0.093	0.084	16.4	2.52	27	442
20.160	0.118	0.105	18.9	2.52	34	641
22.680	0.150	0.134	21.4	2.52	43	922
25.200	0.192	0.171	23.9	2.52	55	1317
27.720	0.245	0.219	26.5	2.52	70	1860
30.240	0.314	0.280	29.0	2.52	90	2604
32.760	0.402	0.358	31.5	2.52	115	3625
35.280	0.516	0.459	34.0	2.52	148	5020
37.800	0.661	0.589	36.5	2.52	189	6912
40.315	0.849	0.755	39.1	2.515	242	9457
42.835	1.089	0.969	41.6	2.52	311	12944
45.355	1.399	1.244	44.1	2.52	400	17628
47.875	1.796	1.598	46.6	2.52	513	23934
50.395	2.309	2.053	49.1	2.52	660	32415

Σ w/o corr.	2985	120478	kNm
Σ with corr.	3014	121683	

drag X/d	u/sqrt(gd)
0	0.0004
0.0504	0.0004
0.1008	0.0005
0.1512	0.0006
0.2016	0.0007
0.252	0.0008
0.3024	0.001
0.3528	0.0013
0.4032	0.0016
0.4536	0.002
0.504	0.0026
0.5544	0.0033
0.6048	0.0042
0.6552	0.0054
0.7056	0.0069
0.756	0.0088
0.8063	0.0113
0.8567	0.0144
0.9071	0.0183
0.9575	0.0233
1.0079	0.0296

Drag Load							
h [m]	**u [m/s]**	**u_avr [m/s]**	**arm [m]**	**δh [m]**	**Cd [-]**	**Fhor [kN]**	**Mover [kNm]**
0.000	0.009						
2.520	0.009	0.009	1.3	2.52	0.91	0.6	1
5.040	0.011	0.010	3.8	2.52	0.91	0.6	2
7.560	0.013	0.012	6.3	2.52	0.90	0.6	4
10.080	0.016	0.014	8.8	2.52	0.90	0.6	5
12.600	0.018	0.017	11.3	2.52	0.89	0.6	7
15.120	0.022	0.020	13.9	2.52	0.87	0.6	8
17.640	0.029	0.025	16.4	2.52	0.86	0.6	10
20.160	0.035	0.032	18.9	2.52	0.83	0.6	12
22.680	0.044	0.040	21.4	2.52	0.80	0.6	14
25.200	0.058	0.051	23.9	2.52	0.76	0.7	16
27.720	0.073	0.065	26.5	2.52	0.71	0.7	18
30.240	0.093	0.083	29.0	2.52	0.64	0.7	20
32.760	0.120	0.106	31.5	2.52	0.55	0.7	22
35.280	0.153	0.136	34.0	2.52	0.44	0.7	23
37.800	0.195	0.174	36.5	2.52	0.29	0.6	21
40.315	0.250	0.223	39.1	2.515	0.19	0.4	17
42.835	0.319	0.285	41.6	2.52	0.19	0.6	23
45.355	0.405	0.362	44.1	2.52	0.19	0.8	33
47.875	0.516	0.461	46.6	2.52	0.19	1.0	48
50.395	0.656	0.586	49.1	2.52	0.19	1.4	71

Σ	14	375

Tp 9 seconds

inertia

X/d	acc/g
0	0.007
0.0502	0.0071
0.1005	0.0076
0.1507	0.0083
0.2009	0.0093
0.2511	0.0108
0.3014	0.0126
0.3516	0.015
0.4018	0.0179
0.4521	0.0216
0.5023	0.0261
0.5525	0.0317
0.6028	0.0386
0.653	0.047
0.7032	0.0572
0.7534	0.0698
0.8037	0.0851
0.8539	0.1039
0.9041	0.1268
0.9544	0.1549
1.0046	0.1892

Inertia Load						
h [m]	**acc [m/s²]**	**acc_avr [m/s²]**	**arm [m]**	**δh [m]**	**Fhor [kN]**	**Mover [kNm]**
0.000	0.069					
2.510	0.070	0.069	1.3	2.51	22	28
5.025	0.075	0.072	3.8	2.515	23	87
7.535	0.081	0.078	6.3	2.51	25	157
10.045	0.091	0.086	8.8	2.51	28	243
12.555	0.106	0.099	11.3	2.51	32	357
15.070	0.124	0.115	13.8	2.515	37	508
17.580	0.147	0.135	16.3	2.51	43	707
20.090	0.176	0.161	18.8	2.51	52	973
22.605	0.212	0.194	21.3	2.515	62	1327
25.115	0.256	0.234	23.9	2.51	75	1787
27.625	0.311	0.284	26.4	2.51	91	2393
30.140	0.379	0.345	28.9	2.515	111	3194
32.650	0.461	0.420	31.4	2.51	134	4220
35.160	0.561	0.511	33.9	2.51	164	5547
37.670	0.685	0.623	36.4	2.51	199	7261
40.185	0.835	0.760	38.9	2.515	244	9487
42.695	1.019	0.927	41.4	2.51	297	12298
45.205	1.244	1.132	44.0	2.51	362	15920
47.720	1.520	1.382	46.5	2.515	443	20592
50.230	1.856	1.688	49.0	2.51	540	26460

Σ w/o corr.	2983	113546	kNm
Σ with corr.	3073	116952	

drag

X/d	u/sqrt(gd)
0	0.0007
0.0502	0.0007
0.1005	0.0007
0.1507	0.0008
0.2009	0.0009
0.2511	0.0011
0.3014	0.0012
0.3516	0.0015
0.4018	0.0018
0.4521	0.0021
0.5023	0.0026
0.5525	0.0031
0.6028	0.0038
0.653	0.0046
0.7032	0.0055
0.7534	0.0067
0.8037	0.0082
0.8539	0.01
0.9041	0.0121
0.9544	0.0147
1.0046	0.0178

Drag Load							
h [m]	**u [m/s]**	**u_avr [m/s]**	**arm [m]**	**δh [m]**	**Cd [-]**	**Fhor [kN]**	**Mover [kNm]**
0.000	0.016						
2.510	0.016	0.016	1.3	2.51	0.87	1	1
5.025	0.016	0.016	3.8	2.515	0.87	1	2
7.535	0.018	0.017	6.3	2.51	0.86	1	3
10.045	0.020	0.019	8.8	2.51	0.85	1	5
12.555	0.024	0.022	11.3	2.51	0.84	1	6
15.070	0.027	0.025	13.8	2.515	0.82	1	8
17.580	0.033	0.030	16.3	2.51	0.79	1	9
20.090	0.040	0.037	18.8	2.51	0.76	1	11
22.605	0.047	0.043	21.3	2.515	0.72	1	12
25.115	0.058	0.052	23.9	2.51	0.68	1	13
27.625	0.069	0.063	26.4	2.51	0.62	1	14
30.140	0.084	0.076	28.9	2.515	0.54	1	14
32.650	0.102	0.093	31.4	2.51	0.45	0	14
35.160	0.122	0.112	33.9	2.51	0.34	0	11
37.670	0.148	0.135	36.4	2.51	0.20	0	10
40.185	0.182	0.165	38.9	2.515	0.19	0	13
42.695	0.221	0.202	41.4	2.51	0.19	0	16
45.205	0.268	0.245	44.0	2.51	0.19	0	21
47.720	0.326	0.297	46.5	2.515	0.19	1	27
50.230	0.394	0.360	49.0	2.51	0.19	1	36

Σ	10	247

Tp 10 seconds

inertia

X/d	acc/g
0	0.0117
0.0503	0.0118
0.1005	0.0123
0.1508	0.0131
0.2011	0.0143
0.2514	0.0158
0.3016	0.0178
0.3519	0.0202
0.4022	0.0232
0.4525	0.0268
0.5027	0.0312
0.553	0.0364
0.6033	0.0425
0.6536	0.0498
0.7038	0.0585
0.7541	0.0687
0.8044	0.0808
0.8547	0.0951
0.9049	0.1119
0.9552	0.1318
1.0055	0.1552

Inertia Load

h [m]	acc [m/s²]	acc_avr [m/s²]	arm [m]	δh [m]	Fhor [kN]	Mover [kNm]
0.000	0.115					
2.515	0.116	0.115	1.3	2.515	37	46
5.025	0.121	0.118	3.8	2.51	38	143
7.540	0.129	0.125	6.3	2.515	40	251
10.055	0.140	0.134	8.8	2.515	43	379
12.570	0.155	0.148	11.3	2.515	47	536
15.080	0.175	0.165	13.8	2.51	53	729
17.595	0.198	0.186	16.3	2.515	60	977
20.110	0.228	0.213	18.9	2.515	68	1287
22.625	0.263	0.245	21.4	2.515	79	1681
25.135	0.306	0.284	23.9	2.51	91	2175
27.650	0.357	0.332	26.4	2.515	106	2807
30.165	0.417	0.387	28.9	2.515	124	3588
32.680	0.489	0.453	31.4	2.515	145	4563
35.190	0.574	0.531	33.9	2.51	170	5770
37.705	0.674	0.624	36.4	2.515	200	7294
40.220	0.793	0.733	39.0	2.515	235	9164
42.735	0.933	0.863	41.5	2.515	277	11478
45.245	1.098	1.015	44.0	2.51	325	14298
47.760	1.293	1.195	46.5	2.515	383	17829
50.275	1.523	1.408	49.0	2.515	452	22133

Σ w/o corr.	2974	107128	kNm
Σ with corr.	3078	110878	

drag

X/d	u/sqrt(gd)
0	0.0013
0.0503	0.0013
0.1005	0.0013
0.1508	0.0014
0.2011	0.0016
0.2514	0.0017
0.3016	0.0019
0.3519	0.0022
0.4022	0.0025
0.4525	0.0029
0.5027	0.0034
0.553	0.0039
0.6033	0.0046
0.6536	0.0054
0.7038	0.0063
0.7541	0.0074
0.8044	0.0087
0.8547	0.0102
0.9049	0.0119
0.9552	0.014
1.0055	0.0164

Drag Load

h [m]	u [m/s]	u_avr [m/s]	arm [m]	δh [m]	Cd [-]	Fhor [kN]	Mover [kNm]
0.000	0.029						
2.515	0.029	0.029	1.3	2.515	0.81	1	1
5.025	0.029	0.029	3.8	2.51	0.80	1	2
7.540	0.031	0.030	6.3	2.515	0.80	1	3
10.055	0.035	0.033	8.8	2.515	0.78	1	5
12.570	0.038	0.037	11.3	2.515	0.77	1	6
15.080	0.042	0.040	13.8	2.51	0.75	1	7
17.595	0.049	0.045	16.3	2.515	0.72	1	8
20.110	0.055	0.052	18.9	2.515	0.68	1	10
22.625	0.064	0.060	21.4	2.515	0.64	0	10
25.135	0.075	0.070	23.9	2.51	0.59	0	11
27.650	0.086	0.081	26.4	2.515	0.53	0	11
30.165	0.102	0.094	28.9	2.515	0.46	0	10
32.680	0.120	0.111	31.4	2.515	0.37	0	8
35.190	0.140	0.130	33.9	2.51	0.27	0	9
37.705	0.164	0.152	36.4	2.515	0.19	0	11
40.220	0.193	0.178	39.0	2.515	0.19	0	14
42.735	0.226	0.209	41.5	2.515	0.19	0	17
45.245	0.264	0.245	44.0	2.51	0.19	0	21
47.760	0.310	0.287	46.5	2.515	0.19	1	26
50.275	0.363	0.337	49.0	2.515	0.19	1	34

Σ	9	225

C

Mud-Mat Calculations

This section provides additional information for the derivation of the mud-mat capacity. All equations are based on ISO 19901, for drained conditions [33].

Bearing capacity

The bearing capacity can be calculated using the following equations.

$$Q_v = q_v A' \tag{C.1}$$

Where

q_v is the unit bearing capacity
A' is effective area of the mud-mat

$$q_\mathsf{v} = 0.5\gamma' B' N_\gamma K_\gamma + \sigma'_{v0} \left(N_\mathsf{q} - 1\right) K_\mathsf{q} \tag{C.2}$$

Where

q_v is the design vertical bearing resistance
N_Y, N_q are drained bearing capacity factors, as a function of φ'
$K_\mathsf{q}, K_\mathsf{q}$ are correction factors that account for inclined actions, foundation shape, depth of embedment, inclination of base, and inclination of the seafloor
φ' is the effective friction angle
γ' is the characteristic value of submerged unit weight of soil
$\sigma'_{\mathsf{v}0}$ is the in situ effective overburden stress at foundation base level
B' is the minimum effective lateral foundation dimension, also referred to as effective foundation width

The eccentricity is determined with Figure C.1 and the following equations:

$$e_1 = \frac{M_1}{F_v} \tag{C.3}$$

$$e_2 = \frac{M_2}{F_v} \tag{C.4}$$

Where

H_{joint} is the ball joint height
F_h is the factored horizontal load
F_v is the factored vertical load

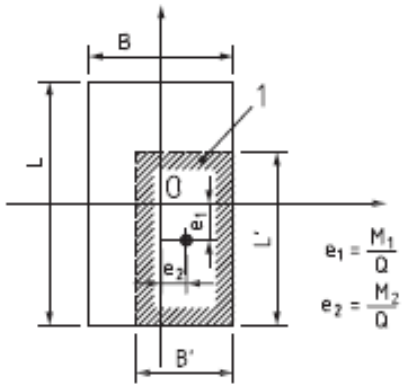

Figure C.1: Eccentricity mud-mats

The mud-mats are schematised as squared foundation elements, with a surface equal to the actual mud-mats. The length of the equivalent foundation element is therefore determined as follows.

$$L = B = \sqrt{A} \tag{C.5}$$

The effective area of the foundation element is reduced due to the eccentricity, and can be obtained by the following equations.

$$L' = L - 2e_1 \tag{C.6}$$

$$B' = B - 2e_2 \tag{C.7}$$

$$A_{eff} = L' \cdot B' \tag{C.8}$$

The bearing capacity factors given in DVNGL [17] and ISO [33] are recommended for pure vertical action on a strip foundation with no embedment, shown in the following equations:

$$N_{\mathsf{q}} = \left[\tan\left[\frac{\pi}{4} + 0.5\tan^{-1}\left(\frac{\tan\varphi'}{\gamma_{\mathsf{m}}}\right)\right]\right]^2 \left[\exp\left(\pi\frac{\tan\varphi'}{\gamma_{\mathsf{m}}}\right)\right] \tag{C.9}$$

$$N_\gamma = 1.5\left(N_{\mathsf{q}} - 1\right)\left(\frac{\tan\varphi'}{\gamma_{\mathsf{m}}}\right) \tag{C.10}$$

The bearing capacity correction factors are shown below, for drained conditions. The subscripts identify the bearing capacity factor with which the correction term is associated.

$$K_q = s_q d_q i_q b_q g_q \tag{C.11}$$

$$K_\gamma = s_\gamma d_\gamma i_\gamma b_\gamma g_\gamma \tag{C.12}$$

Where

s is the factor related to foundation shape
d is related to foundation depth
i is related to action inclination
b is related to base inclination
g is related to seafloor surface inclination

These factors are calculated using the following equations:

$$s_\gamma = 1 - 0.4 i_\gamma \left(\frac{B'}{L'}\right) \tag{C.13}$$

$$s_\mathsf{q} = 1 + i_\mathsf{q} \left(\frac{B'}{L'}\right) \sin\left[\tan^{-1}\left(\frac{\tan\varphi'}{\gamma_\mathsf{m}}\right)\right] \tag{C.14}$$

$$d_\gamma = 1 \tag{C.15}$$

$$d_\mathsf{q} = 1 + 1.2\left(\frac{D_\mathsf{b}}{B'}\right)\left(\frac{\tan\varphi'}{\gamma_\mathsf{m}}\right)\left[1 - \sin\left[\tan^{-1}\left(\frac{\tan\varphi'}{\gamma_\mathsf{m}}\right)\right]\right]^2 \tag{C.16}$$

$$i_\gamma = \left[1 - 0.7\left(\frac{H_b}{V_b}\right)\right]^5 \tag{C.17}$$

$$i_q = \left[1 - 0.5\left(\frac{H_b}{V_b}\right)\right]^5 \tag{C.18}$$

$$b_\gamma = e^{-2.7\nu\left(\frac{\tan\varphi'}{\gamma_\mathsf{m}}\right)} \tag{C.19}$$

$$b_\mathsf{q} = e^{-2\nu\left(\frac{\tan\varphi'}{\gamma_\mathsf{m}}\right)} \tag{C.20}$$

$$g_\gamma = (1 - 0.5\tan\beta)^5 \tag{C.21}$$

$$g_\mathsf{q} = (1 - 0.5\tan\beta)^5 \tag{C.22}$$

Figure C.2 shows the definitions for the inclined base and seafloor surface which can be used for the correction factors. The seabed inclination ν is set to its maximum of 3°. Furthermore, as no skirts are present, and thus there is no penetration, D is assumed to be zero. Similarly, β is assumed to be zero as the maximum seabed inclination is already taken into account.

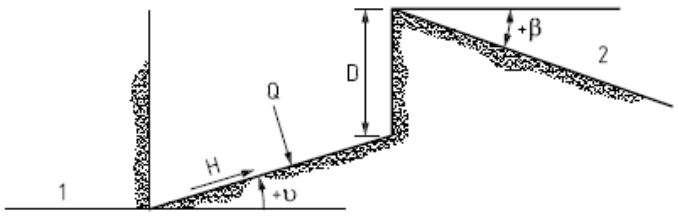

Key

1 horizontal surface

2 ground surface

Figure C.2: Definitions for inclined base and sea floor surface [30]

D

Helical Pile Calculations

This section provides additional information about the calculations on the helical piles. Calculations are shown for the mass derivation, installation requirements, and capacities. Moreover, the structural requirements of the helical pile is discussed in detail. Finally, the determination of the mass of the installation tools is presented.

D.1. Mass

First, the volume of the shaft and the helix is derived and thereafter multiplied with the steel density. The steel density of offshore steel is, generally, 7850 kg/m^3. The geometry of the helical and the shaft are shown in Table 9.1. The area of the plate is multiplied with the plate thickness to derive the volume of the helix plate, as shown in the following equation. The volume of the shaft is derived using the equation shown below. It is assumed that the helix plate and the shaft is made out of the same steel and therefore share the same properties. Furthermore, the mass of the weld is neglected in this derivation.

$$V_{helix} = A_{helix} \cdot t_{helix} = \pi \cdot \left(r_{plate}^2 - r_{shaft}^2\right) \cdot t_{helix} \tag{D.1}$$

$$V_{shaft} = A_{shaft} \cdot L_{shaft} = \pi \cdot \left(r_{shaft}^2 - r_{inner}^2\right) \cdot L_{shaft} \tag{D.2}$$

D.2. Installation requirements

In this section, the method for the estimation of the required installation force and torque is described. Different components are calculated as per [13]. The shaft torque and vertical forces are calculated incrementally by summing up elementary pile core height (dH).

$$T(H) = T_c(D_c^2, \overline{q}_c(H), a, H) + T_b(D_c^3, \overline{q}_c(H), \delta) + T_h(D_h^3, D_c^3, \overline{q}_c(H), a, t_h, K_0) \tag{D.3}$$

$$F_{y,c}(H) = F_c(D_c, \overline{q}_c(H), \delta, H) + F_b(D_c^2, \overline{q}_c(H)) + F_h(D_h^2, D_c^2, \overline{q}_c(H), a, t_h, K_0) \tag{D.4}$$

Where,

T_c, T_b and T_h are the torque related to the shaft, base and helix respectively
F_c, F_b and F_h are the forces related to the shaft, base and helix respectively
$\overline{q}_c(H)$ is the averaged cone resistance (CPT data)
δ is the sand-steel interface friction angle
K_0 is the coefficient of lateral earth pressure ($= 1 - sin\ \varphi$)
a is the stress drop index [36]
t_h is the plate thickness
D_c and D_h are the shaft diameter and helix diameter respectively

H is the depth to the helix

The following equations are used in the method to derive the installation torque and force. The torque is calculated per section using:

$$T_c = \sum a\overline{q}_c(H)\tan(\delta)dH\frac{D_c^2}{2} \tag{D.5}$$

$$T_b = \overline{q}_c(H)\pi\frac{D_c^3}{12}\tan(\delta) \tag{D.6}$$

$$T_h = a\overline{q}_c(H)\frac{\tan(\delta+\theta)\pi(D_h^3-D_c^3)}{12K_0} + a\overline{q}_c(H)\frac{t_h\tan(\delta)\pi D_h^2}{2} + a\overline{q}_c(H)t_h\frac{D_h^2-D_c^2}{8} \tag{D.7}$$

The stress drop index is determined with Lehane et al., 2005 [36]. F_r is the friction ratio of the CPT cone [1], and is generally 0.01.

$$a = \frac{F_r}{\tan(\delta)} \tag{D.8}$$

The earth pressure coefficient (at rest) is calculated as follows, in normally-consolidated soil.

$$K_0 = 1 - \sin(\varphi) \tag{D.9}$$

The helix angle is given by the following equation, using the helix pitch and helix diameter.

$$\theta = \tan^{-1}(\frac{p_h}{\pi D_h}) \tag{D.10}$$

For close-ended piles, the pile-end bearing resistance is equal to 0.6, the installation forces can be calculated using:

$$F_c = \sum 0.6a\overline{q}_c(H)\tan(\delta)dH\pi D_c \tag{D.11}$$

$$F_b = 0.6\overline{q}_c(H)\pi\frac{D_c^2}{4} \tag{D.12}$$

$$F_h = a\overline{q}_c(H)\frac{\pi(D_h^2-D_c^2)}{4K_0} + a\overline{q}_c(H)\frac{t_h\pi D_h}{K_0} + \overline{q}_c(H)t_h\frac{D_h-D_c}{2} \tag{D.13}$$

D.3. Capacity

Uplift capacity

The uplift capacity can be determined by using the following equations, which assumes a shallow failure mechanism in sand:

$$F_u = \left[1 + F_{s1}\frac{H}{D_h} + F_{s2}(\frac{H}{Dh})^2\right]\cdot\gamma'\frac{\pi}{4}D_h^2H \tag{D.14}$$

$$F_{s1} = 2F_{ps} \tag{D.15}$$

$$F_{s2} = \frac{4}{3}F_{ps}\cdot\tan\psi \tag{D.16}$$

$$F_{ps} = \tan\psi + \cos(\varphi_p-\psi)(\tan\varphi_p - \tan\psi) \tag{D.17}$$

Where

H is the embedment depth
D_h is the diameter of the helix
F_{s1}, F_{s2} and F_{ps} are the uplift factors
φ_p is the sand peak friction angle
ψ is the dilatancy angle

Results

The uplift capacity is determined for a range of maximum installation torques, from 6 MNm to 8 MNm, with steps of 0.5 MNm. It can be concluded that the largest uplift capacity is found when the maximum available installation torque is utilised, hence 8 MNm.

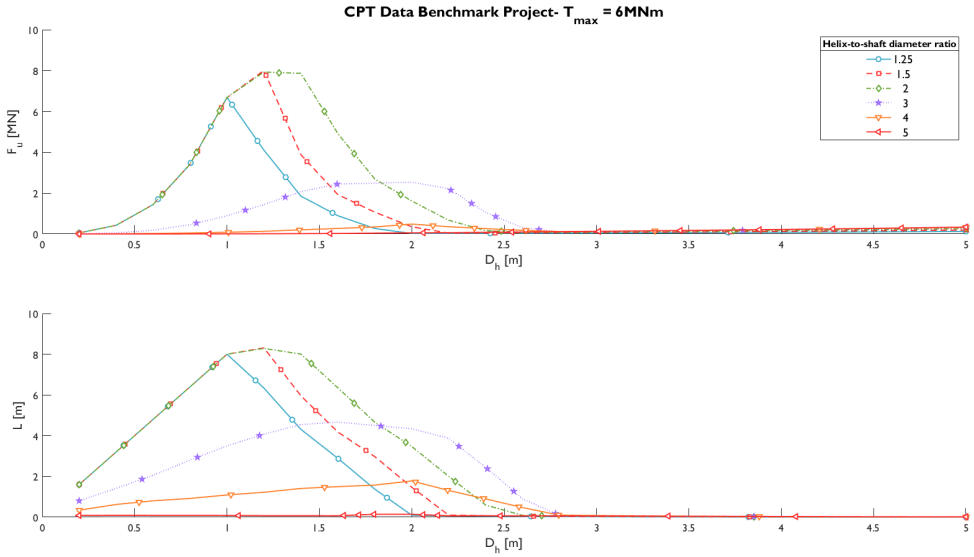

(a) Uplift capacity and installation depth for a maximum installation torque of 6 MNm

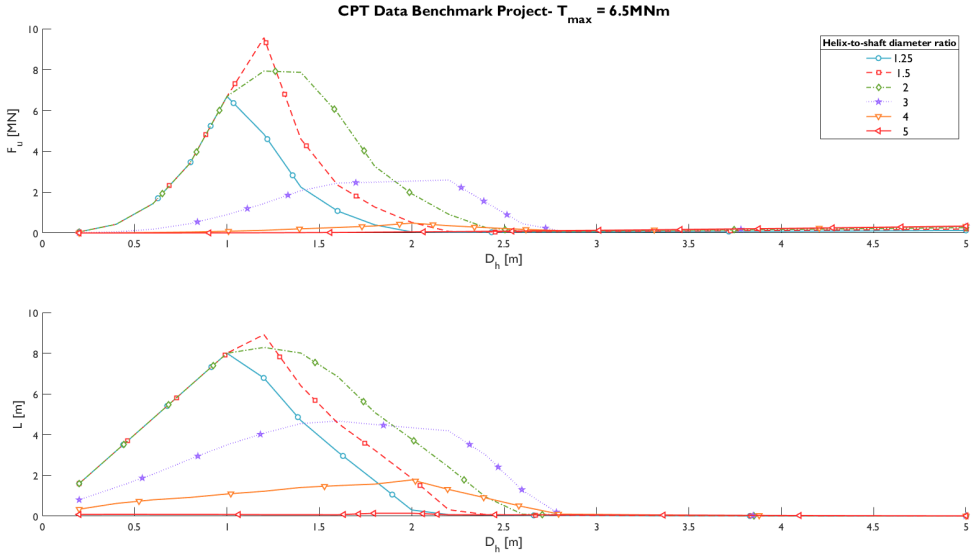

(b) Uplift capacity and installation depth for a maximum installation torque of 6.5 MNm

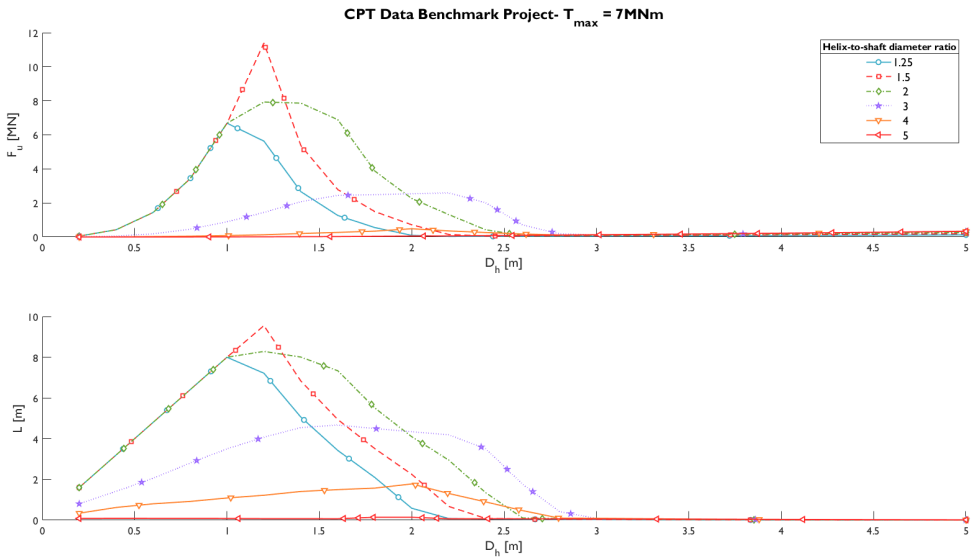

(c) Uplift capacity and installation depth for a maximum installation torque of 7 MNm

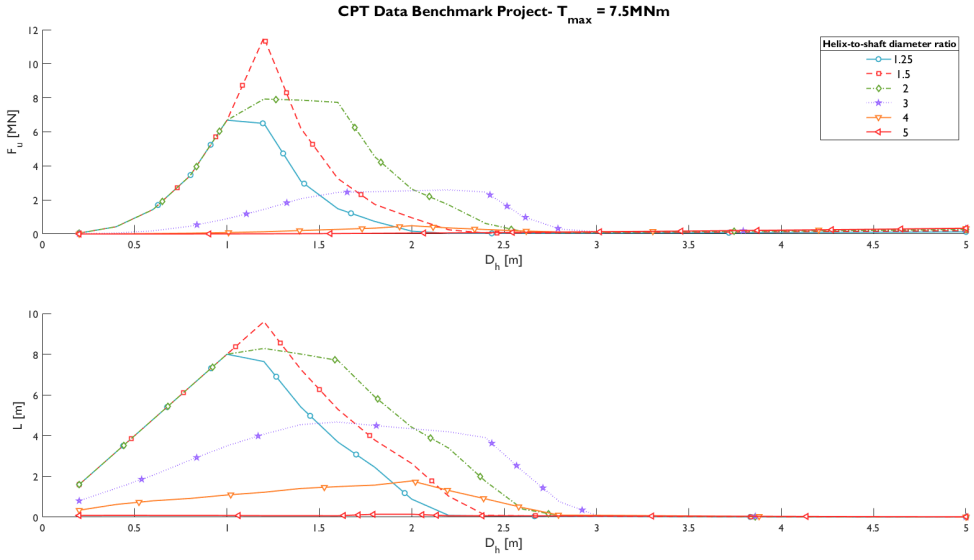

(d) Uplift capacity and installation depth for a maximum installation torque of 7.5 MNm

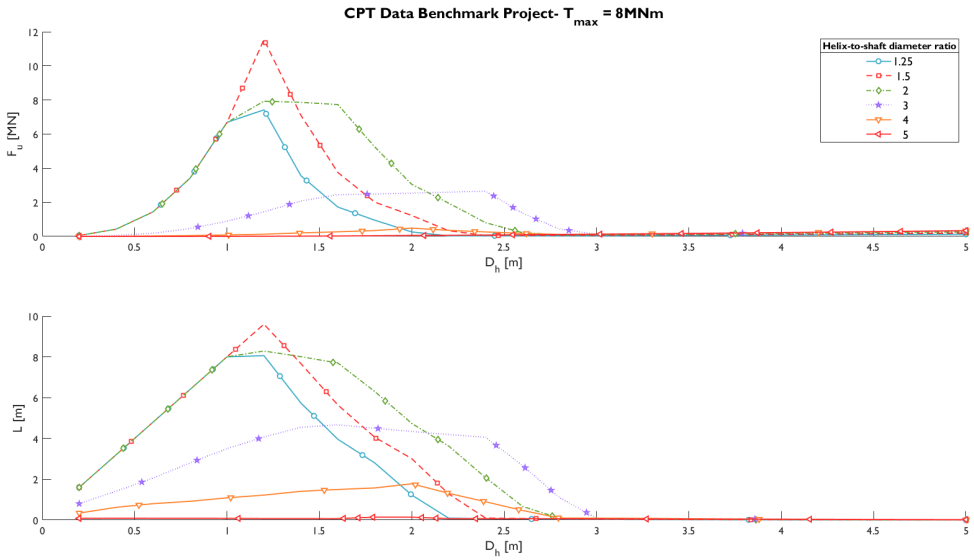

(e) Uplift capacity and installation depth for a maximum installation torque of 8 MNm

Figure D.1: Uplift capacity and installation depth as a function of helix diameter and depth-to-diameter ratio

Lateral capacity

The lateral capacity is determined using API-RP-2GEO [4]. It is assumed that the piles remain in shallow depths, and therefore only the ultimate lateral capacity for shallow depths is determined as shown in the equations below.

$$p_{us} = (C_1 z + C_2 D)\,\gamma' z \tag{D.18}$$

Where

C_1 and C_2 are the coefficients, determined as shown below
γ' is the effective soil unit weight of sand
z is the depth below the seabed
D is the pile outside diameter

$$C_1 = \frac{(\tan\beta)^2 \tan\alpha}{\tan(\beta-\varphi)} + K_o \times \left[\frac{\tan\varphi \times \sin\beta}{\cos\alpha \times \tan(\beta-\varphi)} + \tan\beta \times (\tan\varphi \times \sin\beta - \tan\alpha)\right] \tag{D.19}$$

$$C_2 = \frac{\tan\beta}{\tan(\beta-\varphi)} - K_a \tag{D.20}$$

The coefficients are validated with graphs shown in API RP 2GEO [4].

$$\alpha = \frac{\varphi}{2} \tag{D.21}$$

$$\beta = 45 + \frac{\varphi}{2} \tag{D.22}$$

$$K_0 = 0.4 \tag{D.23}$$

$$K_a = \frac{1-\sin\varphi}{1+\sin\varphi} \tag{D.24}$$

D.4. Structural checks lateral loading

The ultimate lateral resistance calculated in Equation 6.14 is used to determine the maximum deformation (w) due to this loading, see equations below. This resistance is used as force, but translated to the end of the pile at 9.6 meters. The elastic modulus of steel is 210 GPa, and the moment of inertia can be determined using the inner and outer diameter. This results in a deformation of 0.244 meters. This is around 2.54% of the embedment length of the pile.

$$w = \frac{FL^3}{3EI} \tag{D.25}$$

$$I = \frac{\pi(D_o^4 - D_i^4)}{64} \tag{D.26}$$

The maximum bending stress is determined using the same input as for the deformation check. The stress can be determined using the following equation. The moment M is calculated by multiplying F with the length L. The maximum bending stress is located at the outside of the pile, where y is the distance from the centre-line to the outside of the pile ($D_o/2$). The moment of inertia is described above, and this leads to a maximum bending stress of 667.7 MPa. The yield strenght of steel is 350 MPa.

$$\sigma_{max} = \frac{My}{I} \tag{D.27}$$

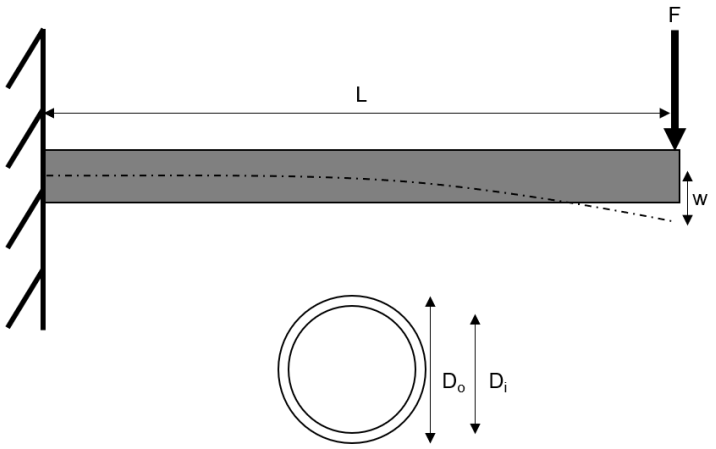

Figure D.2: Lateral deformation of inclined beam

D.5. Weld joint

The maximum stress in the helix can be derived using the following equation, and using the uniformly distributed surface load q.

$$q = \frac{4F_{y,max}}{\pi(D_h^2 - D_c^2)} \tag{D.28}$$

$$\sigma_x = k\frac{qD_h^2}{4t_h^2} \leq f_{y,max} \tag{D.29}$$

The bending moment can be obtained using the following equation:

$$M = \sigma_x W_{el} \tag{D.30}$$

Where W_{el} is the elastic section modulus, which is equal to $t_h^2/6$ in this case [44]. So the shear force at the connection can be obtained using the following equation.

$$Q = \frac{q\frac{\pi}{4}(D_h^2 - D_c^2)}{\pi D_c} = \frac{qD_c}{4}\left[(R_{hc}^2 - 1)\right] \tag{D.31}$$

Where R_{hc} is the ratio between the helix diameter and the shaft diameter. The bending moment in the helix can be converted into two point forces F. This force is applied to the upper and lower weld joint, have equal magnitude but opposite direction.

$$M = Ft_h \tag{D.32}$$

This leads to the normal stress and shear stress, which can be derived using the following equations.

$$\sigma_w = \frac{[F \pm \frac{Q}{2}\cos(45)]}{a_w} \tag{D.33}$$

$$\tau_w = \frac{[F \pm \frac{Q}{2}\cos(45)]}{a_w} \tag{D.34}$$

Where a_w is the weld throat. The $\pm$ refers to the upper or lower wedge joint, and depends whether the joint is in compression or tension due to the bending moment. Furthermore, it is assumed that the material obeys the Von Mises criterion, therefore the equivalent stress should be equal to the following equation.

$$\sigma_{eq,w} = \sqrt{\sigma_w^2 + 3\tau_w^2} \leq f_y \tag{D.35}$$

D.6. Installation tools

The mass of onshore helical pile installation tools and the torque they deliver exhibit a positive correlation, indicating that as the mass of the tool increases, the torque output tends to rise as well. This relationship is used to estimate the mass of the tool that is required to deliver the desired torque output, as shown in Figure D.3 [7, 18, 37]. The installation tool mass is estimated with experts at HMC, and is assumed to be 50000 kg (50 mT) per tool.

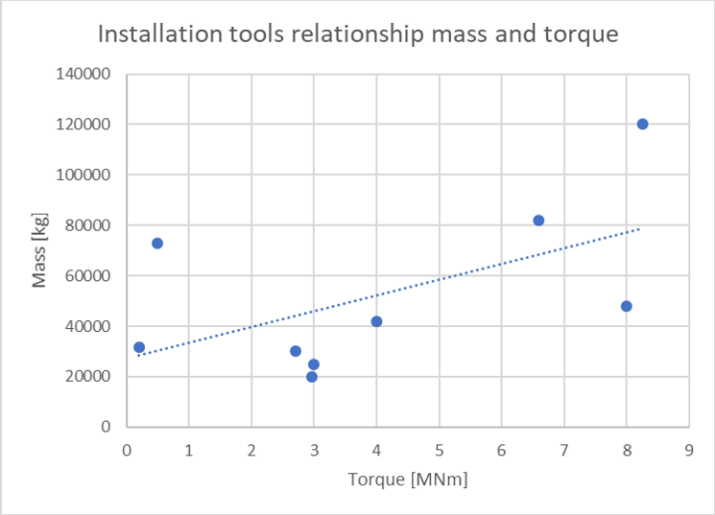

Figure D.3: Installation equipment mass related to delivered torque for helical pile installation

E

Load Determination - Coupled Method

The output of the coupled method for load determination is shown, using the internal software application of HMC. On the first page the input is summarised, the following pages provide the output results. It is important to note that this is the derivation load case 2.3 and 3.3, with no reduction in mud-mat size or template size/mass.

```
+-------------------------------------------------------------------------------------------
-----------------------------------------+
|                                                    HEEREMA MARINE CONTRACTORS
                                page:   1 |
|  Software release : 1.4.19269.5                              mudmat.exe
          Date :     06-Jul-2023 11:19:32 |
|                        Z:\Helical Pile Template\Vineyard\Soil\Mud-mat orientation and
displacement.mud_rpt                      |
+-------------------------------------------------------------------------------------------
-----------------------------------------+
|                                             Mud-mat orientation and displacement
                                          |
|                                                    Geometry Data
                                          |
+-------------------------------------------------------------------------------------------
-----------------------------------------+

Geometry : (no symmetry)
        ID                  x        y        x        y        x        y        x
   y     mesh
        A1 : Rectangle   -14.00    +8.77    -4.75    +8.77    -4.75   +18.02   -14.00
+18.02   5   5

        A2 : Rectangle    +4.75    +8.77   +14.00    +8.77   +14.00   +18.02    +4.75
+18.02   5   5

        A3 : Rectangle   +11.15    -5.20   +21.55    -5.20   +21.55    +5.20   +11.15
 +5.20   5   5

        A4 : Rectangle    +2.98   -19.36   +13.38   -19.36   +13.38    -8.96    +2.98
 -8.96   5   5

        A5 : Rectangle   -13.38   -19.36    -2.98   -19.36    -2.98    -8.96   -13.38
 -8.96   5   5

        A6 : Rectangle   -21.55    -5.20   -11.15    -5.20   -11.15    +5.20   -21.55
 +5.20   5   5

Springs :
Lateral spring (linear) Kx     = +1.000e+03    Ky     = +1.000e+03
Axial spring  (non-lin) Kzcomp = +3.000e+03    Kztens = +1.000e-04
                        dzcomp =        +0.1    dztens =          +0

Mudmat properties :
Area        =       +603.7650
cog         =         +0.0000         -1.2771
Ix          =     +78201.0447
Iy          =     +92453.5189
+-------------------------------------------------------------------------------------------
-----------------------------------------+
|                                                    HEEREMA MARINE CONTRACTORS
                                page:   2 |
|  Software release : 1.4.19269.5                              mudmat.exe
          Date :     06-Jul-2023 11:19:32 |
|                        Z:\Helical Pile Template\Vineyard\Soil\Mud-mat orientation and
displacement.mud_rpt                      |
+-------------------------------------------------------------------------------------------
```

```
-----------------------------------------+
|                                                Mud-mat orientation and displacement
                                         |
|                                                          Loading Data
                                         |
+-----------------------------------------------------------------------------------
-----------------------------------------+

Loadcase :    2.3 x
==========

Toppling :
   Angle    Load dir.      Moment     Extr. Moment   Restoring Arm    factor
    0.00       90.00    274697.26        294371.11       18.07          0.933

                                Fx          Fy          Fz          Mx          My
Mz       origx      origy      origz
                           +4471.00      +0.00  -15205.50      +0.00      +0.00
+0.00      +0.000     +0.000    +15.000

-------------------------------------------------------------------
At geometry origin    :    +4471.00      +0.00  -15205.50      +0.00  +67065.00
+0.00

                                  dx          dy          dz          rx          ry
rz
At geometry origin    :     +0.0074    +0.0000    -0.0085  -0.000083  +0.000242
-0.000034

 Axial Result
 Segment        fmin     fmax        Fcomp      FcompArea      Ftens      FtensArea
   ID         [kN/m2]  [kN/m2]        [kN]        [m2]         [kN]        [m2]
        A1 :   -26.52   -17.51     -1883.53       +85.56        -0.00        +0.00
        A2 :   -40.14   -31.13     -3049.07       +85.56        -0.00        +0.00
        A3 :   -42.44   -32.31     -4042.59      +108.16        -0.00        +0.00
        A4 :   -32.99   -22.86     -3020.41      +108.16        -0.00        +0.00
        A5 :   -21.12   -10.98     -1736.04      +108.16        -0.00        +0.00
        A6 :   -18.69    -8.56     -1473.86      +108.16        -0.00        +0.00
                                   ---------    ---------     --------    ---------
 Totals :                         -15205.50      +603.77        -0.00        +0.00
                                   =========    =========     ========    =========
Lateral Result
 Segment         Fx       Fy         Fres
   ID           [kN]     [kN]        [kN]
        A1 :  +675.67   +26.89      +676.21
        A2 :  +675.67   -26.89      +676.21
        A3 :  +805.58   -59.27      +807.75
        A4 :  +754.25   -29.63      +754.83
        A5 :  +754.25   +29.63      +754.83
        A6 :  +805.58   +59.27      +807.75
             --------- ---------
 Totals :    +4471.00    +0.00
             ========= =========
♠
+-----------------------------------------------------------------------------------
-----------------------------------------+
|                                                    HEEREMA MARINE CONTRACTORS
                                  page:   3 |
|  Software release : 1.4.19269.5                          mudmat.exe
```

| Z:\Helical Pile Template\Vineyard\Soil\Mud-mat orientation and displacement.mud_rpt |

Mud-mat orientation and displacement

Loading Data

Loadcase : 2.3 y

Toppling :

Angle	Load dir.	Moment	Extr. Moment	Restoring Arm	factor
0.00	90.00	274697.26	294371.11	18.07	0.933

	Fx	Fy	Fz	Mx	My	Mz	origx	origy	origz
	+0.00	+4471.00	-15205.50	+0.00	+0.00	+0.00	+0.000	+0.000	+15.000
At geometry origin :	+0.00	+4471.00	-15205.50	-67065.00	+0.00	+0.00			

	dx	dy	dz	rx	ry	rz
At geometry origin :	+0.0000	+0.0074	-0.0089	-0.000369	-0.000000	-0.000000

Axial Result

Segment ID	fmin [kN/m2]	fmax [kN/m2]	Fcomp [kN]	FcompArea [m2]	Ftens [kN]	FtensArea [m2]
A1 :	-46.57	-36.32	-3546.11	+85.56	-0.00	+0.00
A2 :	-46.56	-36.30	-3544.80	+85.56	-0.00	+0.00
A3 :	-32.35	-20.82	-2875.54	+108.16	-0.00	+0.00
A4 :	-16.67	-5.14	-1179.58	+108.16	-0.00	+0.00
A5 :	-16.68	-5.15	-1181.03	+108.16	-0.00	+0.00
A6 :	-32.38	-20.85	-2878.43	+108.16	-0.00	+0.00
Totals :			-15205.50	+603.77	-0.00	+0.00

Lateral Result

Segment ID	Fx [kN]	Fy [kN]	Fres [kN]
A1 :	+0.00	+633.61	+633.61
A2 :	+0.00	+633.61	+633.61
A3 :	+0.00	+800.95	+800.95
A4 :	-0.00	+800.95	+800.95
A5 :	-0.00	+800.95	+800.95
A6 :	+0.00	+800.95	+800.95
Totals :	+0.00	+4471.00	

```
-----------------------------------------+
|                                                                    HEEREMA MARINE CONTRACTORS
                                page:   4 |
|  Software release : 1.4.19269.5                                          mudmat.exe
          Date :     06-Jul-2023 11:19:32 |
|                        Z:\Helical Pile Template\Vineyard\Soil\Mud-mat orientation and
displacement.mud_rpt                      |
+-------------------------------------------------------------------------------------
-----------------------------------------+
|                                              Mud-mat orientation and displacement
                                            |
|                                                                  Loading Data
                                            |
+-------------------------------------------------------------------------------------
-----------------------------------------+

Loadcase :    2.3 -y
==========

Toppling :
   Angle    Load dir.      Moment     Extr. Moment   Restoring Arm    factor
    0.00       90.00    274697.26        294371.11       18.07         0.933

                                Fx         Fy         Fz         Mx         My
Mz       origx      origy      origz
                               +0.00   -4471.00  -15205.50      +0.00      +0.00
+0.00      +0.000     +0.000    +15.000

-------------------------------------------------------------------
At geometry origin    :       +0.00   -4471.00  -15205.50  +67065.00      +0.00
+0.00

                                  dx         dy         dz         rx         ry
rz
At geometry origin    :     -0.0000    -0.0074    -0.0081  +0.000203  +0.000000
+0.000000

 Axial Result
 Segment        fmin     fmax        Fcomp      FcompArea      Ftens      FtensArea
   ID         [kN/m2]  [kN/m2]        [kN]        [m2]         [kN]        [m2]
        A1 :   -19.05   -13.40     -1388.37       +85.56        -0.00        +0.00
        A2 :   -19.06   -13.41     -1389.10       +85.56        -0.00        +0.00
        A3 :   -27.59   -21.24     -2640.44      +108.16        -0.00        +0.00
        A4 :   -36.23   -29.87     -3574.77      +108.16        -0.00        +0.00
        A5 :   -36.22   -29.87     -3573.97      +108.16        -0.00        +0.00
        A6 :   -27.57   -21.22     -2638.85      +108.16        -0.00        +0.00
                                   ---------    ---------     --------    ---------
 Totals :                         -15205.50      +603.77        -0.00        +0.00
                                   =========    =========     ========    =========
Lateral Result
 Segment         Fx       Fy         Fres
   ID          [kN]     [kN]        [kN]
        A1 :    -0.00  -633.61      +633.61
        A2 :    -0.00  -633.61      +633.61
        A3 :    -0.00  -800.95      +800.95
        A4 :    +0.00  -800.95      +800.95
        A5 :    +0.00  -800.95      +800.95
        A6 :    -0.00  -800.95      +800.95
             --------- ---------
```

```
 Totals :       -0.00 -4471.00
           ========= =========
```

```
+-----------------------------------------------------------------------------
-----------------------------------------+
|                                                  HEEREMA MARINE CONTRACTORS
                                page:   5 |
|  Software release : 1.4.19269.5                            mudmat.exe
          Date :     06-Jul-2023 11:19:32 |
|                      Z:\Helical Pile Template\Vineyard\Soil\Mud-mat orientation and
displacement.mud_rpt                      |
+-----------------------------------------------------------------------------
-----------------------------------------+
|                                          Mud-mat orientation and displacement
                                          |
|                                                      Loading Data
                                          |
+-----------------------------------------------------------------------------
-----------------------------------------+
```

Loadcase : 2.3 xy
==========

Toppling :

Angle	Load dir.	Moment	Extr. Moment	Restoring Arm	factor
0.00	90.00	274697.26	294371.11	18.07	0.933

	Fx	Fy	Fz	Mx	My	Mz	origx	origy	origz
	+3161.47	+3161.47	-15205.50	+0.00	+0.00	+0.00	+0.000	+0.000	+15.000
At geometry origin :	+3161.47	+3161.47	-15205.50	-47422.12	+47422.12	+0.00			

	dx	dy	dz	rx	ry	rz
At geometry origin :	+0.0053	+0.0052	-0.0088	-0.000285	+0.000171	-0.000024

Axial Result

Segment ID	fmin [kN/m2]	fmax [kN/m2]	Fcomp [kN]	FcompArea [m2]	Ftens [kN]	FtensArea [m2]
A1 :	-39.26	-26.60	-2817.37	+85.56	-0.00	+0.00
A2 :	-48.88	-36.22	-3640.73	+85.56	-0.00	+0.00
A3 :	-41.78	-27.55	-3749.46	+108.16	-0.00	+0.00
A4 :	-25.47	-11.24	-1985.18	+108.16	-0.00	+0.00
A5 :	-17.08	-2.85	-1077.89	+108.16	-0.00	+0.00
A6 :	-25.01	-10.77	-1934.87	+108.16	-0.00	+0.00
Totals :			-15205.50	+603.77	-0.00	+0.00

Lateral Result

Segment ID	Fx [kN]	Fy [kN]	Fres [kN]
A1 :	+477.77	+467.04	+668.13
A2 :	+477.77	+429.01	+642.12
A3 :	+569.63	+524.45	+774.29

```
        A4 :  +533.34  +545.40      +762.83
        A5 :  +533.34  +587.31      +793.33
        A6 :  +569.63  +608.26      +833.34
              --------- ---------
 Totals :    +3161.47 +3161.47
              ========= =========
```



```
+-------------------------------------------------------------------------------------------
-----------------------------------------+
|                                                    HEEREMA MARINE CONTRACTORS
                                page:   6 |
|  Software release : 1.4.19269.5                            mudmat.exe
          Date :     06-Jul-2023 11:19:32 |
|                        Z:\Helical Pile Template\Vineyard\Soil\Mud-mat orientation and
displacement.mud_rpt                       |
+-------------------------------------------------------------------------------------------
-----------------------------------------+
|                                              Mud-mat orientation and displacement
                                            |
|                                                        Loading Data
                                            |
+-------------------------------------------------------------------------------------------
-----------------------------------------+

Loadcase :    2.3 -xy
==========

Toppling :
   Angle    Load dir.      Moment     Extr. Moment   Restoring Arm    factor
    0.00       90.00    274697.26        294371.11       18.07         0.933

                               Fx         Fy         Fz         Mx         My
Mz       origx      origy      origz
                          +3161.47   -3161.47  -15205.50      +0.00      +0.00
+0.00      +0.000     +0.000    +15.000

-----------------------------------------------------------------
At geometry origin    :    +3161.47   -3161.47  -15205.50  +47422.12  +47422.12
+0.00

                                dx         dy         dz         rx         ry
rz
At geometry origin    :     +0.0053    -0.0052    -0.0082  +0.000120  +0.000171
-0.000024

 Axial Result
 Segment        fmin     fmax        Fcomp      FcompArea      Ftens      FtensArea
   ID         [kN/m2]  [kN/m2]        [kN]        [m2]         [kN]        [m2]
        A1 :   -19.13   -11.06     -1291.62       +85.56        -0.00        +0.00
        A2 :   -28.77   -20.70     -2116.41       +85.56        -0.00        +0.00
        A3 :   -37.67   -28.59     -3583.22      +108.16        -0.00        +0.00
        A4 :   -38.55   -29.47     -3678.84      +108.16        -0.00        +0.00
        A5 :   -30.15   -21.07     -2769.95      +108.16        -0.00        +0.00
        A6 :   -20.86   -11.78     -1765.46      +108.16        -0.00        +0.00
                                   ---------    ---------     --------    ---------
 Totals :                         -15205.50      +603.77        -0.00        +0.00
                                   =========    =========     ========    =========
Lateral Result
 Segment         Fx       Fy          Fres
```

ID	[kN]	[kN]	[kN]
A1 :	+477.77	-429.01	+642.12
A2 :	+477.77	-467.04	+668.13
A3 :	+569.63	-608.26	+833.34
A4 :	+533.34	-587.31	+793.33
A5 :	+533.34	-545.40	+762.83
A6 :	+569.63	-524.45	+774.29
Totals :	+3161.47	-3161.47	

Mud-mat orientation and displacement

Loading Data

Loadcase : 3.3 x

Toppling :

Angle	Load dir.	Moment	Extr. Moment	Restoring Arm	factor
0.00	90.00	274697.26	294371.11	18.07	0.933

	Fx	Fy	Fz	Mx	My	Mz	origx	origy	origz
	+4347.29	+0.00	-15205.50	+0.00	+0.00	+0.00	+0.000	+0.000	+15.000
At geometry origin :	+4347.29	+0.00	-15205.50	+0.00	+65209.38	+0.00			

	dx	dy	dz	rx	ry	rz
At geometry origin :	+0.0072	+0.0000	-0.0085	-0.000083	+0.000235	-0.000033

Axial Result

Segment ID	fmin [kN/m2]	fmax [kN/m2]	Fcomp [kN]	FcompArea [m2]	Ftens [kN]	FtensArea [m2]
A1 :	-26.62	-17.79	-1899.68	+85.56	-0.00	+0.00
A2 :	-39.86	-31.03	-3032.96	+85.56	-0.00	+0.00
A3 :	-42.01	-32.08	-4007.05	+108.16	-0.00	+0.00
A4 :	-32.72	-22.80	-3002.61	+108.16	-0.00	+0.00
A5 :	-21.18	-11.25	-1753.79	+108.16	-0.00	+0.00
A6 :	-18.92	-8.99	-1509.41	+108.16	-0.00	+0.00

```
 Totals :                          -15205.50      +603.77        -0.00        +0.00
                                   =========    =========     ========    =========
Lateral Result
 Segment         Fx       Fy          Fres
   ID           [kN]     [kN]         [kN]
        A1 :  +656.98   +26.15      +657.50
        A2 :  +656.98   -26.15      +657.50
        A3 :  +783.29   -57.63      +785.40
        A4 :  +733.38   -28.81      +733.95
        A5 :  +733.38   +28.81      +733.95
        A6 :  +783.29   +57.63      +785.40
             --------- ---------
 Totals :    +4347.29    -0.00
             ========= =========
↟
+-------------------------------------------------------------------------------------
-----------------------------------------+
|                                                    HEEREMA MARINE CONTRACTORS
                                page:   8 |
|  Software release : 1.4.19269.5                            mudmat.exe
          Date :     06-Jul-2023 11:19:32 |
|                        Z:\Helical Pile Template\Vineyard\Soil\Mud-mat orientation and
displacement.mud_rpt                      |
+-------------------------------------------------------------------------------------
-----------------------------------------+
|                                          Mud-mat orientation and displacement
                                          |
|                                                    Loading Data
                                          |
+-------------------------------------------------------------------------------------
-----------------------------------------+

Loadcase :    3.3 y
==========

Toppling :
   Angle    Load dir.      Moment     Extr. Moment   Restoring Arm    factor
    0.00       90.00    274697.26        294371.11       18.07         0.933

                                Fx         Fy         Fz         Mx         My
Mz       origx      origy      origz
                               +0.00   +4347.29  -15205.50      +0.00      +0.00
+0.00      +0.000     +0.000    +15.000

-------------------------------------------------------------------
At geometry origin    :       +0.00   +4347.29  -15205.50  -65209.38      +0.00
+0.00

                                  dx         dy         dz         rx         ry
rz
At geometry origin    :     +0.0000    +0.0072    -0.0089  -0.000361  -0.000000
-0.000000

 Axial Result
 Segment        fmin     fmax        Fcomp      FcompArea      Ftens      FtensArea
   ID         [kN/m2]  [kN/m2]        [kN]        [m2]         [kN]        [m2]
        A1 :   -46.11   -36.08     -3516.26       +85.56        -0.00        +0.00
        A2 :   -46.10   -36.06     -3514.98       +85.56        -0.00        +0.00
        A3 :   -32.20   -20.91     -2872.28      +108.16        -0.00        +0.00
```

A4 :	-16.85	-5.57	-1212.72	+108.16	-0.00	+0.00
A5 :	-16.87	-5.58	-1214.14	+108.16	-0.00	+0.00
A6 :	-32.22	-20.94	-2875.12	+108.16	-0.00	+0.00
Totals :			-15205.50	+603.77	-0.00	+0.00

Lateral Result

Segment ID	Fx [kN]	Fy [kN]	Fres [kN]
A1 :	+0.00	+616.08	+616.08
A2 :	+0.00	+616.08	+616.08
A3 :	+0.00	+778.79	+778.79
A4 :	-0.00	+778.79	+778.79
A5 :	-0.00	+778.79	+778.79
A6 :	+0.00	+778.79	+778.79
Totals :	+0.00	+4347.29	

Loadcase : 3.3 -y

Toppling :

Angle	Load dir.	Moment	Extr. Moment	Restoring Arm	factor
0.00	90.00	274697.26	294371.11	18.07	0.933

	Fx	Fy	Fz	Mx	My	Mz	origx	origy	origz
	+0.00	-4347.29	-15205.50	+0.00	+0.00	+0.00	+0.000	+0.000	+15.000
At geometry origin :	+0.00	-4347.29	-15205.50	+65209.38	+0.00	+0.00			

	dx	dy	dz	rx	ry	rz
At geometry origin :	-0.0000	-0.0072	-0.0081	+0.000196	+0.000000	+0.000000

Axial Result

Segment	fmin	fmax	Fcomp	FcompArea	Ftens	FtensArea

ID	[kN/m2]	[kN/m2]	[kN]	[m2]	[kN]	[m2]
A1 :	-19.29	-13.86	-1418.23	+85.56	-0.00	+0.00
A2 :	-19.30	-13.87	-1418.92	+85.56	-0.00	+0.00
A3 :	-27.49	-21.39	-2643.69	+108.16	-0.00	+0.00
A4 :	-35.80	-29.69	-3541.63	+108.16	-0.00	+0.00
A5 :	-35.79	-29.68	-3540.87	+108.16	-0.00	+0.00
A6 :	-27.48	-21.38	-2642.16	+108.16	-0.00	+0.00
Totals :			-15205.50	+603.77	-0.00	+0.00

Lateral Result

Segment ID	Fx [kN]	Fy [kN]	Fres [kN]
A1 :	-0.00	-616.08	+616.08
A2 :	-0.00	-616.08	+616.08
A3 :	-0.00	-778.79	+778.79
A4 :	+0.00	-778.79	+778.79
A5 :	+0.00	-778.79	+778.79
A6 :	-0.00	-778.79	+778.79
Totals :	-0.00	-4347.29	

Mud-mat orientation and displacement

Loading Data

Loadcase : 3.3 xy

Toppling :

Angle	Load dir.	Moment	Extr. Moment	Restoring Arm	factor
0.00	90.00	274697.26	294371.11	18.07	0.933

	Fx	Fy	Fz	Mx	My	Mz	origx	origy	origz
	+3074.00	+3074.00	-15205.50	+0.00	+0.00	+0.00	+0.000	+0.000	+15.000
At geometry origin :	+3074.00	+3074.00	-15205.50	-46110.00	+46110.00	+0.00			

	dx	dy	dz	rx	ry	rz
At geometry origin :	+0.0051	+0.0051	-0.0088	-0.000280	+0.000166	

```
 Axial Result
 Segment        fmin     fmax        Fcomp      FcompArea      Ftens      FtensArea
   ID         [kN/m2]  [kN/m2]        [kN]        [m2]         [kN]        [m2]
        A1 :   -39.00   -26.63     -2807.68       +85.56        -0.00        +0.00
        A2 :   -48.36   -35.98     -3608.25       +85.56        -0.00        +0.00
        A3 :   -41.37   -27.46     -3722.03      +108.16        -0.00        +0.00
        A4 :   -25.41   -11.50     -1996.03      +108.16        -0.00        +0.00
        A5 :   -17.25    -3.34     -1113.85      +108.16        -0.00        +0.00
        A6 :   -25.06   -11.14     -1957.66      +108.16        -0.00        +0.00
                                   ---------    ---------     --------    ---------
 Totals :                         -15205.50      +603.77        -0.00        +0.00
                                   =========    =========     ========    =========
Lateral Result
 Segment         Fx       Fy          Fres
   ID          [kN]     [kN]         [kN]
        A1 :  +464.55  +454.12      +649.64
        A2 :  +464.55  +417.14      +624.35
        A3 :  +553.87  +509.94      +752.86
        A4 :  +518.58  +530.31      +741.72
        A5 :  +518.58  +571.06      +771.38
        A6 :  +553.87  +591.43      +810.28
             --------- ---------
 Totals :    +3074.00 +3074.00
             ========= =========
```



```
+-------------------------------------------------------------------------------------------
-----------------------------------------+
|                                                    HEEREMA MARINE CONTRACTORS
                                page:  11 |
|  Software release : 1.4.19269.5                          mudmat.exe
          Date :     06-Jul-2023 11:19:32 |
|                        Z:\Helical Pile Template\Vineyard\Soil\Mud-mat orientation and
displacement.mud_rpt                      |
+-------------------------------------------------------------------------------------------
-----------------------------------------+
|                                          Mud-mat orientation and displacement
                                          |
|                                                    Loading Data
                                          |
+-------------------------------------------------------------------------------------------
-----------------------------------------+

Loadcase :    3.3 -xy
==========

Toppling :
   Angle    Load dir.      Moment     Extr. Moment   Restoring Arm    factor
    0.00       90.00    274697.26        294371.11       18.07         0.933

                               Fx         Fy         Fz         Mx         My
Mz       origx      origy      origz
                          +3074.00   -3074.00  -15205.50      +0.00      +0.00
+0.00      +0.000     +0.000    +15.000

-----------------------------------------------------------------
At geometry origin    :    +3074.00   -3074.00  -15205.50  +46110.00  +46110.00
+0.00
```

	dx	dy	dz	rx	ry	rz
At geometry origin :	+0.0051	-0.0051	-0.0082	+0.000114	+0.000167	-0.000023

Axial Result

Segment ID	fmin [kN/m2]	fmax [kN/m2]	Fcomp [kN]	FcompArea [m2]	Ftens [kN]	FtensArea [m2]
A1 :	-19.37	-11.58	-1324.15	+85.56	-0.00	+0.00
A2 :	-28.74	-20.95	-2126.11	+85.56	-0.00	+0.00
A3 :	-37.30	-28.54	-3560.39	+108.16	-0.00	+0.00
A4 :	-38.06	-29.30	-3642.82	+108.16	-0.00	+0.00
A5 :	-29.89	-21.13	-2759.09	+108.16	-0.00	+0.00
A6 :	-20.96	-12.20	-1792.94	+108.16	-0.00	+0.00
Totals :			-15205.50	+603.77	-0.00	+0.00

Lateral Result

Segment ID	Fx [kN]	Fy [kN]	Fres [kN]
A1 :	+464.55	-417.14	+624.35
A2 :	+464.55	-454.12	+649.64
A3 :	+553.87	-591.43	+810.28
A4 :	+518.58	-571.06	+771.38
A5 :	+518.58	-530.31	+741.72
A6 :	+553.87	-509.94	+752.86
Totals :	+3074.00	-3074.00	